Investigation of neuronal manganese regulation in physiology and disease using high throughput screening,

induced pluripotent stem cells, and chemical biology approaches

By

Kevin Krishan Kumar

Dissertation

Submitted to the Faculty of the

Graduate School of Vanderbilt University

in partial fulfillment of the requirements

for the degree of

DOCTOR OF PHILOSOPHY

in

Neuroscience

December, 2014

Nashville, Tennessee

Approved:

Kevin C. Ess, M.D., Ph.D.

Michael Aschner, Ph.D.

Joseph S. Neimat, M.D., M.S.

Daniel O. Claassen, M.D., M.S.

C. David Weaver, Ph.D.

Aaron B. Bowman, Ph.D.

To my grandparents, parents, and family for their inspiration and support

ACKNOWLEDGEMENTS

TABLE OF CONTENTS

LIST OF TABLES

LIST OF FIGURES

MANGANESE AS A RISK FACTOR FOR NEURODEGENERATIVE DISEASE

Introduction

Neurodegenerative diseases are expected to be the second most common cause of death among the elderly by 2040 (Lilienfeld *et al.* 1993). Thus, it has become a priority to develop novel prevention strategies and treatments for these devastating illnesses. Despite identification of genetic and environmental factors that hasten degeneration, there is a dearth of information about the gene-environment interface that underlies selective neuronal vulnerability. One such environmental exposure, manganese (Mn), is neurotoxic and causes basal ganglia dysfunction and neurodegeneration. Specifically, Mn exposure is an environmental risk factor for parkinsonism and modulation of neuronal Mn status has been observed in the pathogenesis of Huntington's disease (HD) (Gorell *et al.* 1999, Kim *et al.* 1999, Gorell *et al.* 2004, Bowman *et al.* 2011). Given the known links of alterations in Mn biology with neurodegenerative disease, manipulation of neuronal Mn represents an attractive protective and therapeutic target for these disorders. However, the processes regulating intracellular Mn are poorly understood, hampering efforts to pharmacologically modify neuronal Mn handling.

Physiological role of Mn in the nervous system

Mn is required for several physiological processes vital for the nervous system function. These processes include its role as a co-factor for several metalloenzymes, including arginase, glutamine synthetase, phosphoenolpyruvate decarboxylase, serine threonine carboxylase, and Mn-superoxide dismutase (Mn-SOD) (Takeda 2003, Aschner *et al.* 2005). Maintenance of Mn levels in the nervous system is essential, as deviation from normal levels can cause neuronal dysfunction. Although tissue levels of Mn are highly regulated, acute

and chronic exposures can lead to CNS accumulation. For example, increased Mn levels are known to disrupt the levels of γ-aminobutyric acid (GABA), dopamine, and glutamate in the brain (Seth *et al.* 1984, Aschner *et al.* 2002, Takeda 2003). Mn preferentially accumulates in the substantia nigra *pars compacta* (SNpc), globus pallidus, and striatum; areas highly sensitive to oxidative injury and stress (Newland *et al.* 1989, Olanow 2004, Cersosimo *et al.* 2006, Guilarte 2010). Intracellular localized Mn predominantly accumulates in the mitochondria, where it interferes with cellular respiration and increases reactive oxygen species (ROS) production via inhibition of mitochondrial respiratory Complex I (Aschner *et al.* 2005, Bowman *et al.* 2011).

Parkinsonism, Parkinson's disease, and Huntington's disease: links to Mn

Parkinsonism and Parkinson's disease

Parkinson's disease (PD) is the second most common neurodegenerative disease. The prevalence of PD in the industrialized world is estimated at 0.3% of the general population and approximately 1% in individuals over the age of 60 (Nussbaum *et al.* 2003). Thus, PD is considered an age-related disease, with prevalence rising mainly after the age of 50 (Li *et al.* 1985, Schoenberg *et al.* 1988, Morgante *et al.* 1992, Tison *et al.* 1994, de Rijk *et al.* 1995, Mayeux *et al.* 1995, Fall *et al.* 1996, de Rijk *et al.* 1997, Claveria *et al.* 2002, Benito-Leon *et al.* 2003, de Lau *et al.* 2006). As the population ages, there is an increasing socioeconomic burden on society (de Lau *et al.* 2006). The incidence of PD is 8 to 18 per 100,000 person-years (de Rijk *et al.* 1995, de Lau *et al.* 2006). It has been noted that there is higher prevalence of PD in men than women, a finding hypothesized to be mediated by a neuroprotective role of estrogens (Morgante *et al.* 1992, Tison *et al.* 1994, de Rijk *et al.* 1995, de Rijk *et al.* 1997, de Lau *et al.* 2006).

PD diagnosis is contingent on presentation with at least two of the four cardinal symptoms of parkinsonism: resting tremor, bradykinesia, rigidity, and postural instability (de Lau *et al.* 2006). This clinical suspicion is

further supported by the patients' responsiveness to levodopa, asymmetry of symptoms, or SPECT imaging with DaTSCAN, although the latter is seldom used as a primary diagnostic procedure (Litvan *et al.* 2003, Tolosa *et al.* 2007). Furthermore, secondary causes of parkinsonism such as drug-induced parkinsonism must be excluded to achieve a diagnosis of PD. Interestingly, the course of PD is highly variable; studies analyzing PD progression suggest that functional deterioration is accelerated both early in the disease course and among patients presenting with postural instability gait difficulty (Jankovic *et al.* 2001, Lang 2007, Post *et al.* 2007, Jankovic 2008).

The majority (90%) of PD cases are sporadic in etiology with the remaining 10% of cases having known genetic causes. Furthermore, there is profound heterogeneity in age of onset, neuropathological findings, and characteristic symptoms even among the genetic forms of PD. Mn exposure is a major environmental risk factor for PD (Hudnell 1999). A national study revealed in urban areas incidence of PD is greater where emissions of Mn are highest (Weisskopf *et al.* 2010, Willis *et al.* 2012). Furthermore, long-term residence in areas with high cumulative industrial Mn release is associated with an increased PD incidence and risk (Willis *et al.* 2010). In particular, inhalational exposure has been well studied in welding, smelting, and mining (Schuler *et al.* 1957, Wang *et al.* 1989, Racette *et al.* 2001). In addition, excess Mn intake through drinking water and dietary sources has been associated with other neuropathologies suggesting potential application to parkinsonism and PD (Iwami *et al.* 1994, Iwami *et al.* 1994). Developmental exposure to Mn is also a concern because the organic compound methylcyclopentadienyl manganese tricarbonyl (MMT) is used as an anti-knock agent in petrol. Non-occupational exposures have had noted associations with Parkinsonian disorders in communities located in the vicinity of ferroalloy industries (Lucchini *et al.* 2007).

Notably, PD is distinct from the extrapyramidal motor syndrome manganism, which has similar clinical features including rigidity, bradykinesia, tremor, and dystonic movements (Newland *et al.* 1989, Calne *et al.* 1994,

Olanow 2004, Samii *et al.* 2004, Cersosimo *et al.* 2006, Guilarte 2010). PD differs profoundly from manganism in etiology; the latter is exclusively caused by excessive Mn deposition in the brain.

Although a complete understanding of the pathogenesis of PD remains elusive, current evidence suggests that PD results from a multitude of factors including: oxidative stress, protein aggregation, and mitochondrial dysfunction (Greenamyre *et al.* 2004). In addition, the study of the genetic forms of PD has offered insight regarding central mechanisms in PD pathogenesis. Defective proteins in familial PD result from mutations in genes that function in critical cellular processes such as the ubiquitin proteasome system (UPS), vesicle trafficking, mitochondrial function, and oxidative stress responses (Jakes *et al.* 1994, Mori *et al.* 2002, Nuytemans *et al.* 2010).

On a cellular level, PD is characterized by loss of dopaminergic neurons of the substantia nigra and the presence of intraneuronal protein aggregates composed of α-synuclein known as Lewy bodies (Wood-Kaczmar *et al.* 2006). Loss of dopamine levels in the striatum leads to downstream dysregulation of basal ganglia motor circuitry resulting in the motor symptoms observed in PD. While there is a common endpoint of decreased striatal dopamine levels, multiple pathways can influence an individual's pattern of neuronal cell death and the mechanism by which it occurs. For example, dysfunction in mitochondrial complex I results in upregulated free radical production causing protein damage. The damaged protein burden increases the stress on the UPS, leading to protein aggregation and subsequent neuronal death (Ali *et al.* 2011). However, this simple pathway could be influenced at any level by multiple inputs such as environmental toxins, genetic risk, and enhanced oxidative stress. Thus, an individual patient's history of environmental exposure and genetic risk are critical to their clinical manifestation of PD.

HD is an autosomal dominant, neurodegenerative disorder characterized by chorea, dystonia, cognitive decline, and behavioral abnormalities (Walker 2007). HD is caused by a CAG repeat expansion (with repeats of ~36 and higher being pathogenic) within the widely expressed *Huntingtin* (*HTT*) gene (Rubinsztein *et al.* 1996, McNeil *et al.* 1997, Rubinsztein *et al.* 2003, Walker 2007). HTT is expressed in all mammalian cells with highest concentrations in the brain and testes, followed by liver, heart, and lungs (DiFiglia *et al.* 1995). CAG repeat length in HTT is inversely correlated with time to diagnosis for HD, accounting for 44% of variation in age of onset (Brinkman *et al.* 1997, Wexler *et al.* 2004). Despite its wide expression pattern, the function of HTT and its role in HD pathogenesis is poorly understood.

HD has an overall prevalence of 0.38 per 100,000 per year (Pringsheim *et al.* 2012). The incidence varies by ethnicity, with 5-7 per 100,000 individuals in the white population and 0.5 per 10,000 in the Japanese population (Pridmore 1990, Takano *et al.* 1998, Walker 2007). Notably, HD has a lower incidence in other Asian and African populations (Hayden 1981, Wright *et al.* 1981, Bates *et al.* 2002). The prevalence of HD varies to 5.70 per 100,000 in Europe, North America, and Australia compared to 0.40 per 100,000 in Asia. The disparity in HD prevalence is attributed to difference in *HTT* gene haplotypes (Pringsheim *et al.* 2012).

HD diagnosis can be achieved anytime between the ages of 1 and 80 years of age, composed of a healthy period followed by a prediagnostic phase and final diagnostic phase. The prediagnostic phase is characterized by subtle change in motor control, cognition, and personality (Snowden *et al.* 1998, Walker 2007). Symptoms worsen until chorea, incoordination, motor impairment, and disruptions of saccadic eye movements are reported (Walker 2007).

Exhibiting some overlap with PD-neuroanatomical localization, typical adult-onset HD is characterized by degeneration of neurons within the corpus striatum, cortex, and hypothalamus (Cowan *et al.* 2006, Hult *et al.* 2010). Striatal medium spiny neurons (MSNs) are the most vulnerable cell type. Specifically, those neurons containing substance P and project to internal globus pallidus are more involved with disease pathology, while interneurons are generally spared (Walker 2007). The preferential dysfunction of thalamocortical circuitry generates chorea early in the course of HD given the involvement of the indirect pathway (Paulsen *et al.* 2005). There is also notable cell loss in the cortex, hippocampus, and parietal lobe, lateral tuberal nuclei of the hypothalamus, centromedial-parafasicular complex of the thalamus and Purkinje cells of the cerebellum (Jeste *et al.* 1984, Kremer *et al.* 1991, Kremer 1992, Spargo *et al.* 1993, Macdonald *et al.* 1997, Macdonald *et al.* 2002). These cells contain nuclear and cytoplasmic inclusions containing mutant huntingtin and polyglutamine (Davies *et al.* 1997). It is still unclear what role these inclusions play in HD pathogenesis, as they appear before symptom onset and fail to predict cellular dysfunction or disease activity (Gomez-Tortosa *et al.* 2001, Arrasate *et al.* 2004, Kaytor *et al.* 2004, Mukai *et al.* 2005, Van Raamsdonk *et al.* 2005).

Given the aforementioned finding that CAG repeat length accounts for less than half of variation in age of onset, there has been considerable interest in the role of environmental factors in modulation of disease progression in HD (Georgiou *et al.* 1999, Wexler *et al.* 2004, Friedman *et al.* 2005, van Dellen *et al.* 2005, Gomez-Esteban *et al.* 2007). In regards to Mn, changes in Mn dependent enzymatic activity have been observed that postmortem brains of HD patients (Butterworth 1986). Furthermore, expression of mutant *HTT* has been associated with decreased striatal Mn levels and alterations in the metabolism, transport, and/or toxicity of Mn (Williams *et al.* 2010, Williams *et al.* 2010). The lack of knowledge regarding the functional role of HTT has further complicated studies, since there are limited known targets and interacting proteins.

CHAPTER II

MANGANESE TRANSPORT IN NEURONS

Neuronal Mn transport: a black box of cell biology

Mn transport has been well described at the systemic level, including regulatory processes in the gut, blood brain barrier, and glia. For example, Mn is known to enter across cerebral capillaries at the blood brain barrier where it crosses the chorioid plexus in the cerebrospinal fluid (Aschner *et al.* 2005, Yokel 2009, Tuschl *et al.* 2013). However, the transport of Mn at the neuronal level remains poorly understood. The best-described processes for regulating neuronal Mn are those shared transporters used by other divalent metals such as iron (Fe) and calcium (Ca). These transporters include voltage regulated and ionotropic glutamate receptor Ca^{2+} channels, transient receptor potential cation channel, subfamily M, member 7 (TRPM7), store operated Ca^{2+} channel, and transferrin (Tf)-dependent and independent process via divalent metal transporter 1 (DMT1), and solute carrier (SLC) channels (including ZIP proteins) (**Figure 1**) (Kannurpatti *et al.* 2000, Riccio *et al.* 2002, Grimm *et al.* 2003, Roth *et al.* 2003, Aschner *et al.* 2006, Erikson *et al.* 2006, Garrick *et al.* 2006, He *et al.* 2006, Dean *et al.* 2009, Himeno *et al.* 2009, Yokel 2009, Fujishiro *et al.* 2011, Roth *et al.* 2013). These transport systems appear to only account for a proportion of total Mn, and are thought to be inadequate to handle acute and chronic exposures of Mn.
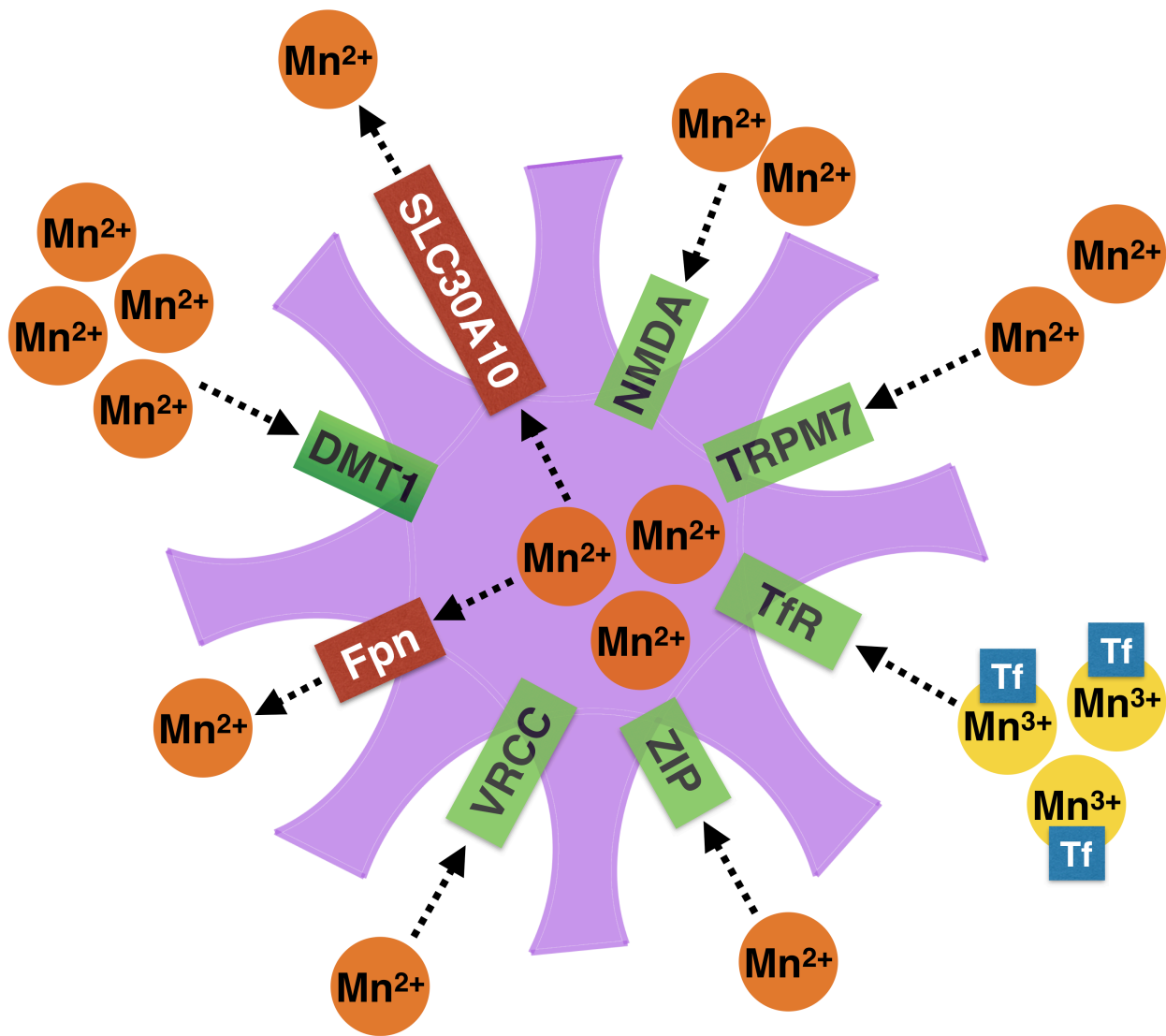
Figure 1 – Major neuronal Mn transporters. Representative Mn import (**green**) and efflux (**red**) transporters transport Mn along with other cations. Divalent metal transporter 1 (DMT1), ferroportin (Fpn), voltage regulated Ca^{2+} channel (VRCC), transient receptor potential cation channel, subfamily M, member 7 (TRPM7), solute carrier family 30, member 10 (SLC30A10), ionotropic glutamate receptor channel (NMDA), transferrin receptor (TfR) and ZIP8/14 (ZIP). Mn oxidation state is indicated as either Mn^{2+} or Mn^{3+}, which can be bound to transferrin (Tf).

Among these known transporters, DMT1 is one of the best studied, exhibiting specificity for a variety of

divalent cations included Fe^{2+}, Mn^{2+}, Cd^{2+}, Ni^{2+}, Co^{2+}, and Pb^{2+} (Gunshin *et al.* 1997, Mackenzie *et al.* 2007).

DMT1 primarily functions as a Fe transporter, but exhibits similar affinity for Mn. Both Mn and Fe can be

transported by both Tf-independent and dependent routes, processes well described in metal transport from the

apical surface of intestinal enterocytes. It is unclear what role DMT1 plays in neuronal Mn transport, but the

highest expression levels of DMT1 are found in the dopaminergic areas of the basal ganglia, areas of noted Mn

toxicity (Huang *et al.* 2004). One of the few areas of demonstrated DMT1-mediated transport on the neuronal level is in the presynaptic endings of olfactory bulb (Thompson *et al.* 2007). However, it is unknown if neurons in other regions of the brain utilize a similar transport mechanism, representing a major gap in the knowledge of neuronal Mn regulation. In addition, DMT1-mediated processes are likely not Mn-dependent, as expression of DMT1 isoforms is regulated by iron response elements (IREs), allowing Mn content to change based on *in vivo* Fe levels (Garcia *et al.* 2007, Fitsanakis *et al.* 2008, Hansen *et al.* 2009, Nunez *et al.* 2010). Consequently, DMT1-mediated transport has potential to contribute to disruption of Mn homeostasis in pathologies where Fe levels are impacted, such as hemochromatosis or anemia.

Alternatively, Tf-dependent transport mechanisms are known to traffic Mn when in its trivalent state Mn^{3+}. The trivalent state, normally found in the blood, permits access to binding sites on Tf. This Mn^{3+}-Tf complex is highly stable, and is slowly cleared by the hepatobiliary system (Roth *et al.* 2013). However compared to Mn, Tf has higher affinity for Fe and can carry other metals making it subject to disruptions in Fe levels. Furthermore, due to its pH and oxygen content, it is hypothesized that limited Mn^{3+} exists in the brain, limiting the ability of Tf-mediated routes to function as a major mechanism of neuronal Mn regulation (Roth *et al.* 2013). In addition, there exist alternate routes for non-protein-bound forms of Mn to cross the blood brain barrier, such as Mn citrate, but their role at the level of neurons is unknown (Crossgrove *et al.* 2003).

Another route of Mn transport is through the ZIP-family metal transporters. These proteins function as divalent cation/HCO_3^- symporters (He *et al.* 2006, Liuzzi *et al.* 2006, Girijashanker *et al.* 2008, Fujishiro *et al.* 2011). Two of the most well-studied ZIP proteins, ZIP8 and ZIP14, have a high degree of homology and share the ability to transport divalent metals including Mn^{2+} (Pinilla-Tenas *et al.* 2011). Unlike Tf-mediated transport, ZIP-mediated transport has the potential to transport a considerable proportion of Mn^{2+}, the predominant oxidation state found in the brain. However, this potential role in neurons is dubious given that ZIP-mediated

transport has only been established in the blood brain barrier, proximal convoluted tubule of the kidney, and in the liver (Girijashanker *et al.* 2008, Himeno *et al.* 2009, Fujishiro *et al.* 2012).

Similar to other routes, Mn can also be transported through Ca^{2+} channel-dependent transporters. There are several known types of transporters including voltage regulated, ionotropic glutamate receptor Ca^{2+} channels, TRPM7, and store operated Ca^{2+} channels (Lucaciu *et al.* 1997, Kannurpatti *et al.* 2000, Loutzenhiser *et al.* 2000, Riccio *et al.* 2002, Grimm *et al.* 2003, Yokel *et al.* 2004, Yokel 2009, Roth *et al.* 2013). Blockage of the voltage regulated Ca^{2+} channels, eliminates depolarization induced Mn uptake into cells (Lucaciu *et al.* 1997, Loutzenhiser *et al.* 2000). Similarly, inhibition of the ionotropic glutamate receptor Ca^{2+} channel has been shown to attenuate Mn induced toxicity while inhibitors of the sarcoplasmic reticulum Ca-ATPase induces Mn uptake (Jardin *et al.* 2009). It has also been demonstrated that modulation of expression of TRPM7 has been shown to change cellular Mn levels (Guilbert *et al.* 2009). Although each of these aforementioned characteristics of Ca^{2+} channel-dependent transporters has been studied in a diverse range of cell types found in the blood, kidney, and breast, the specific role of these transporters in neurons is undefined.

Notably, while there are several well-studied Mn transport routes that modulate uptake, modulators of Mn efflux could play a significant role in neuronal Mn homeostasis. One of these efflux mechanisms, Fpn, is widely expressed in all cell types including neurons (Moos *et al.* 2006). Induction of Fpn expression reduced Mn-induced toxicity and cellular Mn content (Yin *et al.* 2010). However, Fpn-mediated efflux is not Mn specific and is known to transport other divalent metals including Fe. Other routes of Mn efflux have pathological significance. Disruptions of neuronal Mn efflux have been reported in case of patients with Mn transporter deficiency due to mutations in *SLC30A10* (Gospe *et al.* 2000, Quadri *et al.* 2012, Stamelou *et al.* 2012, Tuschl *et al.* 2012, Lechpammer *et al.* 2014). Neuropathological findings in a patient with homozygous mutations in *SLC30A10* include neuronal loss, astrocytosis, myelin loss, and spongiosis in the basal ganglia (Lechpammer *et al.* 2014). In addition, depigmentation of the substantia nigra and a 16-fold increase in Mn content within the

basal ganglia was observed (Lechpammer *et al.* 2014). These patients also exhibited hepatic dysfunction, suggesting that SLC30A10 mediated transport is not neural specific, and its contribution relative to all routes of neuronal Mn homeostasis remains unknown.

In addition to transporters that exchange Mn between the extracellular milieu and the cytosol, Mn can also be regulated at the intracellular level. For example, SPCA1 and SPCA2, Ca^{2+}/Mn^{2+} ATPases, transport Mn^{2+} from the cytosol to the Golgi (Mukhopadhyay *et al.* 2011). These transporters are widely expressed and promote cell viability. The role of these transporters in neuronal Mn biology may have importance given that high Mn exposure mice accumulate Mn in brain regions with high SPCA1 expression (Sepulveda *et al.* 2007). Despite their therapeutic potential, the role of these intracellular regulators in neuronal Mn physiology remains a relatively unexplored scientific frontier.

A novel approach to understanding neuronal Mn regulation

Considered together, the known routes of cellular transport of Mn are neither metal nor neuronal-specific. Furthermore, there exists profound heterogeneity in the Mn concentrations in which the known transporters have been characterized, which include concentrations in excess of *in vivo* physiological relevance. The variation in the cell type and Mn exposure paradigm has made the development of a coherent model of neuronal Mn regulation difficult. The development of such a model is valuable given the critical role of Mn in neural development and function. We hypothesized that Mn-specific regulatory mechanisms exist in neurons, and perhaps other cells. These regulatory mechanisms should be pharmacologically targetable, allowing modulation of neuronal Mn content using small molecules. Thus, we developed an innovative approach using high throughput screening technology, permitting the interrogation of non-defined Mn homeostatic mechanisms to influence neuronal Mn biology.

In addition, we sought to explore Mn regulation in differentiating neurons given known Mn-related dysfunction in the developing brain. Blood Mn levels in schoolchildren have been significantly associated with environmental Mn levels (Rollin *et al.* 2005). Non-occupational childhood exposures are especially concerning, since they have been associated with lower cognitive performance (Wasserman *et al.* 2006, Bouchard *et al.* 2011, Menezes-Filho *et al.* 2011). Early Mn exposure in neonates, measured by cord blood Mn concentrations, were associated with impaired neurobehavioral development (Takser *et al.* 2003). The ability of early childhood exposure to Mn to lead to neurological impairment suggests a plausible mechanistic requirement for developing neurons to carefully regulate Mn.

We also sought to gain insight into the mechanisms through which modulation of an environmental stressor, such as Mn, alters neuronal function in the context of genotypic stressor, such as mutant *HTT*. The exploration of reduced Mn levels in striatal cells with mutant *HTT* has been difficult to study given the lack of knowledge regarding mechanisms linking HD and Mn at the neuronal level. Thus, we sought to employ an untargeted metabolomics to discover any Mn-specific, genotype-specific, and/or Mn-genotype changes in cellular metabolites in murine striatal cells.

This multidisciplinary approach allowed us to investigate the processes underlying Mn regulation and their implications for neurodegenerative pathologies (**Figure 2**).
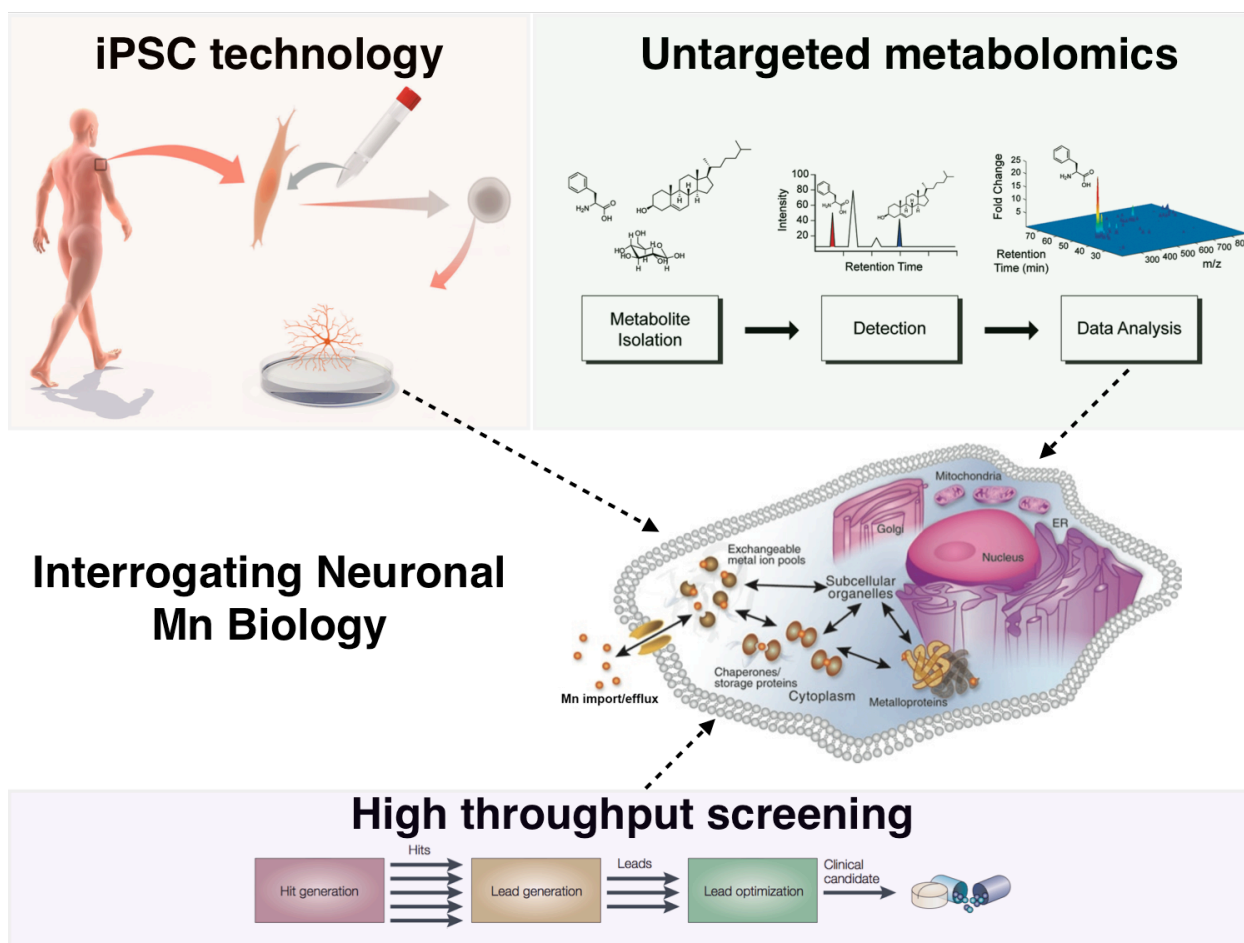
Figure 2 – Summary schematic of approach to studying neuronal Mn biology. The use of high throughput screening, induced pluripotent stem cell (iPSC) technology, and untargeted metabolomics can lend insight into the processes underlying neuronal Mn handling. Figure adapted from (Bleicher *et al.* 2003, Domaille *et al.* 2008, Vinayavekhin *et al.* 2010) and <http://www.nobelprize.org/nobel_prizes/medicine/laureates/2012/ med_image_press_eng.pdf>.

In subsequent chapters, the findings from three major studies: (1) a high throughput screen for novel modulators of Mn content, (2) examination of regulation of cellular Mn content in human mesencephalic dopaminergic neural precursors, (3) untargeted metabolomics study of HD-Mn interactions will be discussed. The technical foundation of these studies will first be established, consisting of a comprehensive review of neurotoxicological applications of induced pluripotent stem cell technology (Chapter III) and optimization of the Cellular Fura2 Mn Extraction Assay (CFMEA) for HTS (Chapter IV). The results of the high throughput screen and application to human dopaminergic neurons will then be discussed (Chapter V) followed by the findings of the

untargeted metabolomic study of HD-Mn interactions in striatal cells (Chapter 6). The final portion of the dissertation, Chapter VII, is comprised of a discussion and summary of the findings and their translational applications for neurodegenerative disease.

THE POTENTIAL OF INDUCED PLURIPOTENT STEM CELLS AS A TRANSLATIONAL MODEL FOR NEUROTOXICOLOGICAL RISK[1]

Abstract

An important goal of neurotoxicological research is to provide relevant and accurate risk assessment of environmental and pharmacological agents for populations and individuals. Owing to the challenges of human subject research and the real possibility of species specific toxicological responses, neuronal lineages derived from human embryonic stem cells (hESCs) and human neuronal precursors have been offered as a potential solution for validation of neurotoxicological data from model organism systems in humans. More recently, with the advent of induced pluripotent stem cell (iPSC) technology, there is now the possibility of personalized toxicological risk assessment, the ability to predict individual susceptibility to specific environmental agents, by this approach. This critical advance is widely expected to facilitate analysis of cellular physiological pathways in the context of human neurons and the underlying genetic factors that lead to disease. Thus this technology opens the opportunity, for the first time, to characterize the physiological, toxicological, pharmacological and molecular properties of living human neurons with identical genetic determinants as human patients. Furthermore, armed with a complete clinical history of the patients, human iPSC (hiPSC) studies can theoretically compare patients and at risk groups with distinct sensitivities to particular environmental agents, divergent clinical outcomes, differing co-morbidities, and so forth. Thus iPSCs and neuronal lineages derived from them may reflect the unique genetic blueprint of the individuals from which they are generated. Indeed,

---

iPSC technology has the potential to revolutionize scientific approaches to human health. However, before this overarching goal can be reached a number of technical and theoretical challenges must be overcome. This review seeks to provide a realistic assessment of hiPSC technology and its application to risk assessment and mechanistic studies in the area of neurotoxicology. We seek to identify, prioritize, and detail the primary hurdles that need to be overcome if personalized toxicological risk assessment using patient-derived iPSCs is to succeed.

Introduction

The field of toxicology has seen rapid innovation in the past two decades by the advent of stem cell technology. Perhaps the first major successful use of stem cells for the study of toxicity was the Embryonic Stem Cell Test (EST) developed by Speilmann and colleagues (Heuer *et al.* 1993, Spielmann *et al.* 1997). This approach differentiates mouse embryonic stem cells (ESCs) into cardiomyocytes in the presence of potential developmentally toxic agents (Heuer *et al.* 1993, Seiler *et al.* 2011). Although this method utilizes mouse stem cells, and focuses on differentiation into beating cardiomyocytes, the method has been broadly hailed for its ingenuity (Scholz *et al.* 1999, Laustriat *et al.* 2010, Wobus *et al.* 2011). However, the method has notable shortcomings in its application to neurotoxicology. For example, although the EST correctly classified the majority of known embryotoxic chemicals tested, it is known that the EST in some cases failed to correctly classify methylmercury as a developmental toxicant (Genschow *et al.* 2004). There are several potential reasons for these shortcomings of the EST – including species-specific toxicities and tissue-type specific toxicities. Recently, Bremer *et al.* sought to address both of these issues by adapting the principles of the EST to toxicity testing in human ESCs (hESCs) undergoing neuronal differentiation (Stummann *et al.* 2009). Their study showed greater sensitivity of early-developing neural precursors over maturing neuronal cells to methylmercury toxicity (i.e. greater changes in expression of key early neurodevelopmental markers versus more mature neuronal markers) (Stummann *et al.* 2009). Other groups have also provided proof-of-principle experiments

16

demonstrating the potential of hESCs to evaluate developmental toxicity (Pal *et al.* 2011). However, ethical and regulatory concerns about the use of cells derived from human embryos have limited adoption of hESC based toxicity testing (Leist *et al.* 2008, Vojnits *et al.* 2010).

Pioneering studies have revealed both the feasibility as well as clear advantages for use of stem cell based approaches for neurotoxicological risk assessment. Although the fundamentals of stem cell culture are outside the scope of this review, a number of book chapters and review articles are available on this topic (Takahashi *et al.* 2007, Park *et al.* 2008, Neely *et al.* 2011).Studies using murine stem cells have identified mRNA based expression markers for assessment of neurodevelopmental toxicity (Kuegler *et al.* 2010, Theunissen *et al.* 2011). Comparative studies using hESC derived neurons versus rodent primary neuronal cultures have revealed important differences in sensitivity, reproducibility, and dynamic ranges by toxicity measures examining neurite outgrowth and cytotoxicity; suggesting further work is needed in developing and interpreting hESC-derived neurotoxicity tests (Harrill *et al.* 2011). Indeed, toxicogenomic approaches revealed key differences on the influence of a developmental neurotoxicant on expression profiles between *in vivo* models, stem-cell based *in vitro* models and primary tissue/cell culture based models – yet also identified examples of coherent responses from the *in vitro* ESC-based models and *in vivo* measures (Robinson *et al.* 2011). Furthermore, predictive neurotoxicity testing by hESC-based neuronal differentiation approaches has proven successful in discriminating chemicals and pharmaceuticals with known developmental neurotoxicity (Buzanska *et al.* 2009). A related approach to hESC-based neurotoxicology has been to start developmentally down-stream of the pluripotent state and utilize multipotent human neuroprogenitors as a starting point for developmental neurotoxicity testing (Breier *et al.* 2008, Moors *et al.* 2009, Harrill *et al.* 2010, Schreiber *et al.* 2010, Harrill *et al.* 2011, Tofighi *et al.* 2011, Tofighi *et al.* 2011). Neuralization of pluripotent stem cells or neuroprogenitors can be accomplished either by adherent culture-based neuronal differentiation or a neurosphere suspension culture, which may be followed by subsequent plating, differentiation and migration. A discussion of the

advantages and disadvantages of these two approaches has been recently reviewed by Breier and colleagues (Breier *et al.* 2010).

In this review, we seek to describe the methods of generating hiPSCs, explore the utility of this technology in the field of neurotoxicology, and discuss technical challenges for these applications. In addition, we will outline the process of generating and maintaining hiPSCs for toxicity testing, characterize multiple exposure paradigms, and attempt to predict the future of the field.

The promise of iPSC technology for neurotoxicology

A number of recent reviews have described potential applications of hESC and hiPSC technology to toxicology, pharmacology and the study of human diseases that have environmental contributions to their etiology (Heng *et al.* 2009, Saha *et al.* 2009, Winkler *et al.* 2009, Vojnits *et al.* 2010, Anson *et al.* 2011, Marchetto *et al.* 2011, Wobus *et al.* 2011). Here we focus on the promise and roadblocks specifically for neurotoxicological applications. An important advantage of a patient-specific iPSC approach to neurotoxicology is that environmental risk for an individual may be evaluated without *a priori* knowledge of the genetic risk factors. A complex relationship of environmental and genetic risk factors underlies many neurodevelopmental and neurodegenerative diseases – yet identification of causative factors has been severely hampered by the lack of suitable experimental models to account for the combinatorial influence of diverse toxicants and the inherent variation in human susceptibility and exposure. This complexity and variation of genetic and environmental influences between individuals also complicate epidemiological studies to identify contributors. For example, a link between pesticide exposure and Parkinson's disease (PD) became suspected in 1983 with the discovery that exposure to 1-methyl 4-phenyl 1,2,3,6-tetrahydropyridine (MPTP), a compound with structural similarity to the pesticide paraquat, causes a selective degeneration of dopaminergic neurons in the substantia nigra (Langston *et al.* 1983, Elbaz *et al.* 2008). Despite epidemiological evidence potentially linking pesticide use with risk for PD,

discerning the role of specific pesticides in human disease has been difficult (Frigerio *et al.* 2006, Dick *et al.* 2007, Dick *et al.* 2007, Kamel *et al.* 2007, Frigerio *et al.* 2009). Likewise, studies have found links between PD and exposure to Mn, Pb and other metals (Coon *et al.* 2006, Finkelstein *et al.* 2007). Interestingly, a recent study of a Chinese cohort found an association between blood Mn levels and PD, yet no differences in exposure were seen between control and disease groups (Fukushima *et al.* 2009). This raises the possibility that genetic risk factors may predispose some people to accumulate levels of this environmental toxicant thereby selectively increasing their risk for disease. The advent of hiPSC technology may provide researchers a method to test this and similar hypotheses, by allowing the evaluation of selective sensitivity to neurotoxicants across individual patients.

The utility of human pluripotent stem cell technology towards human toxicological risk assessment rests on the idea that cells differentiated from patient-derived stem cells can serve as a model system for understanding the role of human genetic factors in modulating the vulnerability of differentiated cells to specific toxicants. A number of technical as well as theoretical hurdles need to be overcome before the utility of this approach can be realized. For example, efficiency and consistency of stem cell derivation, contribution of epigenetic changes, protocols for differentiation, exposure paradigms, and assessment of toxicity need to be optimized. Perhaps, though, the most fundamental issue that must be addressed upfront is whether the methods for generating patient-derived pluripotent stem cells are capable of yielding a consistent model of sensitivity to environmental toxicants. Direct tests are needed for the hypothesis that iPSCs derived from distinct individuals can be differentiated into neurons that exhibit toxicological sensitivity profiles specific to the subject from which they are derived. In other words, it needs to be shown that neuronal cells from multiple iPSC lines made from the same patient show more similarity in their sensitivity to specific neurotoxicants than neuronal cells from hiPSC lines of different patients. This simple question is fundamental for the development of an iPSC-based personalized toxicological risk assessment.

Additional technical considerations for early experimental applications of iPSC technology to neurotoxicological research are necessary. These include the importance of studying cell autonomous mechanisms of neurotoxicity. Owing to challenges in differentiation of specific neuronal populations and the consequential challenge in developing models of human neuronal circuits, it is likely unfeasible to explore neuronal network based toxicity until a better understanding of cell-autonomous toxicity is examined. For example, direct toxicity due to impaired mitochondrial function or effects of toxicants on specific cell signaling cascades need to be examined before realization of the down-stream consequences to neuronal network activity or intercellular signaling can be understood. Prototypical bench assays of toxicological measures need to be developed before automation or high-throughput screening of toxicants can be performed. Detailed examination of differentiation methods and the developmental trajectories and marker expression, as well as method-based influences on neurological phenotypes, need to be established before the impact of neurotoxicants on differentiation and neuronal activity can be interpreted in the context of predicting human neurodevelopmental toxicity. Indeed, validation of toxicological outcomes in iPSC-based models might best begin with human subjects (individuals with known genetic risk factors) and toxicants for which clearly understood human gene-environment interactions exist to facilitate confidence in interpreting data for situations where risk factors are unknown.

The study of the interactions between neurotoxicants and neurological disorders is an especially exciting future application of hiPSC technology, given the complexities of the diverse and ill-defined environmental and genetic risk factors. Furthermore, the ability to differentiate neurons and glia from patient hiPSCs offers the potential to examine changes in both the development and maintenance of neural function resulting from complex genetic inheritance patterns and toxicant perturbation (Liu *et al.* 2011). The ability to expand, maintain, culture, and differentiate hiPSCs may enable utilization of this resource by a broad range of laboratories throughout the US, and around the world, expanding both the scope and depth of research into human disease.

Methods of hiPSC generation

In 2007 Yamanaka showed for the first time the possibility of transforming adult human fibroblasts to pluripotent stem cells using four defined transcription factors (Takahashi *et al.* 2007). This ground breaking discovery led the way to ample research in an attempt to both understand the molecular basis of stem cell induction and possible ways to improve it. Induced pluripotent stem cells (iPSCs) exhibit the typical characteristics of the inner mass-derived human embryonic stem cells, including self-renewal and the potential to differentiate to cell types of any of the three germ layers. In the original work by Yamanaka, after screening for 24 potential genetic targets, a set of four retrovirus-carried genes, namely *OCT4*, *SOX2*, *c-MYC*, and *KLF4*, were chosen to transduce human adult dermal fibroblasts. Further study of these factors revealed that except for *OCT4*, the requirement for these factors is not stringent. *c-MYC*, for example, was shown to be dispensable mainly for safety purposes, with a modest decrease in efficiency (Nakagawa *et al.* 2008). Similarly, *c-MYC* and *KLF-4* could be replaced with *NANOG* and *LIN28* with no significant effect on the outcome of stem cell induction (Yu *et al.* 2007).

Because of serious drawbacks associated with the use of retroviruses for transduction, including persistent expression and insertional mutagenesis, alternative methods have been developed to deliver genes into the target cells. One of the strategies employs a doxycyclin inducible expression of the transgenes (Brambrink *et al.* 2008). This diminishes the likelihood of constitutive transgene activation and could serve as an indicator of pluripotency since fully reprogrammed cells are not dependent on the exogenous factors for their self-renewal. Another way to control viral gene expression utilizes genes flanked by *loxP* sites, which could later be excised by transiently expressing Cre recombinase. Alternatively, *PiggyBac* transposons, mobile genetic elements that could be inserted into the genome, could be used instead of the transgenes. This is an attractive method as they can be removed by transient expression of transposases (Yusa *et al.* 2009). Non-integrating vectors have also been used successfully to induce pluripotency. Initial trials involved transduction of mouse cells with

21

adenovirus and non-viral methods including plasmid transfections (Okita *et al.* 2008, Stadtfeld *et al.* 2008). Adenovirus was later proved to be capable of inducing pluripotency in human dermal fibroblasts as well (Zhou *et al.* 2009). Interestingly, Yamanaka's group has recently reported a highly efficient reprogramming of human dermal fibroblasts and dental pulp cells using episomal vectors carrying the four classical transcription factors in addition to *L-MYC* and *P53* shRNA (Okita *et al.* 2011). Finally, extensive research is being carried out to screen for compounds that might permit the process of iPSC induction without the introduction of genetic materials (Lin *et al.* 2009).

Special considerations and technical challenges for iPSC-based neurotoxicological applications

A number of obstacles stand between these promises of iPSC technology and their practical application. This review seeks to find a realistic optimism for what can reasonably be accomplished in the coming years as well as detail some of the key roadblocks that must be addressed before the hope of such applications can be realized.

Generation, maintenance and selection of appropriate iPSCs for toxicity testing

The process of iPSC induction encompasses multiple steps with many possible hurdles. The efficiency of reprogramming varies greatly depending on many overlapping technical and biological factors. Although different labs report the efficiency of reprogramming in different ways, the overall rates are not satisfactory. Indeed, ever since the first human iPSC was made, extensive work has been focused on improving both the quality and efficiency of the reprogramming process (**Figure 3** (**4.1**)). Adding small molecules to manipulate certain signaling pathways has attracted special attention recently because of the reproducibility and consistency of the results. Most commonly, the targets of these attempts are either the epigenetic state of the reprogrammed cells or certain cellular pathways responsible for cell growth and fate determination. Certain epigenetic

characteristics are particularly pervasive in hESCs, and screening for molecules that alter the epigenetic state of the reprogrammed cells has identified some compounds that add to the reprogramming efficiency (Rada-Iglesias *et al.* 2011). For example, treating partially reprogrammed cells with the DNA methyltransferase inhibitor 5-aza-cytidine (AZA) has been found to both improve the reprogramming efficiency and to induce a rapid and stable transition to fully reprogrammed iPSCs (Huangfu *et al.* 2008, Mikkelsen *et al.* 2008). Finally, it has been shown that iPSC generation is markedly enhanced by p53 gene suppression, and implementation of this knowledge dramatically improves reprogramming by episomal vectors (Hong *et al.* 2009, Okita *et al.* 2011). It remains to be determined what impact the choice of reprogramming method may have on neurotoxicological outcome measures of neuronal lineages derived from hiPSCs.
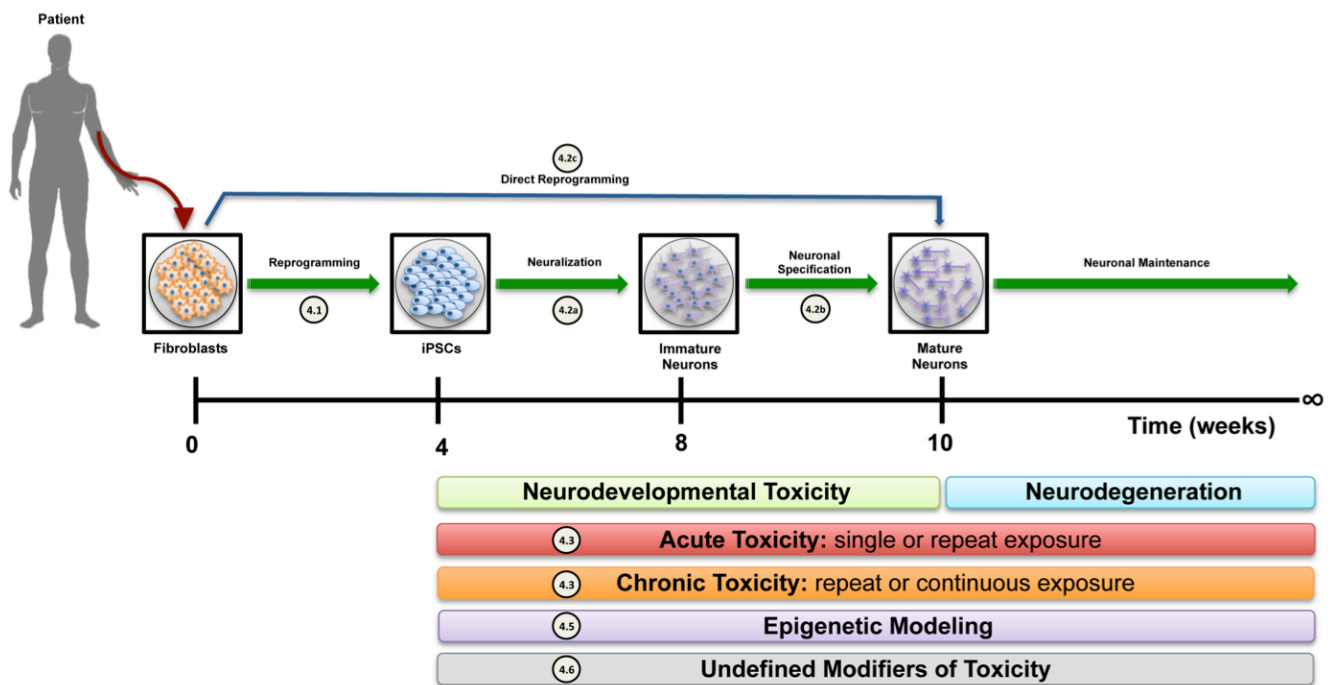
Figure 3 – Generation of human induced pluripotent stem cells for neurotoxicological studies. Schematic representation of the generation and differentiation of hiPSCs into mature neurons. Approximate timeline of this process are indicated underneath each stage of development. The colored bars indicate the types of toxicological assays and the periods in which they can be performed. The circled numerical cross-references adjacent to individual steps or experimental paradigms highlight the sub-chapter in the text discussing specific technical challenges.

Selection of iPSC lines appropriate for neurotoxicological studies relies on their behavior in culture, validation of their pluripotency characteristics (i.e. assessment of their pluripotency), their ability to differentiate with good efficiency to the required cell type, and the fidelity of their genome and epigenome. Here we will consider the first two points, and we will leave the later points to subsequent sections.

Characterization of pluripotency in iPSC lines has rested heavily on the degree by which they show similarities to ESCs in their colony and cellular morphology, molecular and expression characteristics, and their qualitative and quantitative capacity to differentiate into the three embryonic germ layers. Research has delineated defining characteristics of hESCs that may be used as a reference in the process of pluripotency validation (Initiative *et al.* 2007). Some of these classical characteristics, which are widely used to assess the pluripotency of iPSCs, include the expression of certain biomolecular markers such as the tissue-nonspecific alkaline phosphatase, and the expression of surface markers specific to pluripotent cells. Examples of these latter markers include TRA-1-60, SSEA-3 and SSEA-4; and the developmentally regulated genes, like *NANOG* and *OCT4*. These classical markers, however, are not specific enough to be considered markers for stem cells, as other cell types like teratocarcinoma cells also express these same markers (Josephson *et al.* 2007). Thus, the use of these markers alone is insufficient to characterize iPSCs.

The most widely accepted test of pluripotency is the *in vivo* demonstration of a stem cell line's competence to differentiate into the three embryonic germlayers as a teratoma (Müller *et al.* 2010). Briefly, iPSCs are injected subcutaneously or intramuscularly in an immunocompromised mouse and a few months later teratomas are expected to form. These tumors are resected and sectioned for immunohistochemical staining for markers of endoderm, mesoderm, and ectoderm. This test is both expensive and time consuming, and the methods of performing the test and reporting the results are largely inconsistent (Müller *et al.* 2010). Moreover, some researchers have demonstrated the ability of partially reprogrammed cells and iPSC lines with genetic and epigenetic aberrancies to pass the test successfully. This failure to distinguish lines exhibiting normal hESC-like

pluripotency marker expression has led some to call for new standards of pluripotency (Dolgin 2010, Williams *et al.* 2011). Furthermore, the inability of this approach to assess pluripotency in a quantitative and high-throughput manner exacerbates the need for robust methods of selecting lines for further testing. A more simplified approach of *in vitro* differentiation into embryoid bodies and analysis for generation of the three embryonic germ layers has been suggested as an alternate validation approach (Boulting *et al.* 2011, Okita *et al.* 2011). An alternative approach to differentiation has been proposed in which new pluripotent lines can be compared and contrasted to reference expression maps of 12 hiPSC and 20 hESC lines that were generated to enable high-throughput characterization (Bock *et al.* 2011). This novel approach allows the generation of an expression "deviation scorecard" as an indirect quality control measure of pluripotency by finding gene expression patterns that uniquely identify high-quality pluripotent lines. These authors sought to confirm their findings by comparison to a "lineage scorecard" by assessing lineage-specific expression patterns from embryoid bodies derived from their reference set of pluripotent lines. They found that the "lineage scorecard" could accurately distinguish biases in differentiation propensity between pluripotent lines and identify lines that exhibit impaired differentiation towards neuronal lineages. Such validation has obvious applications in selecting lines for neurotoxicity testing by enabling the collection of phenotypically matched hiPSC lines from different subjects with similar neuronal differentiation propensities, as well as matched epigenetic and transcriptional profiles. Finally, hiPSCs that exhibit a high degree of spontaneous differentiation may need to be excluded – a potential explanation for such a phenotype is an inherent instability in maintaining a normal diploid karyotype.

Inconsistency and low-efficiency of neuronal differentiation methods

hiPSCs are in many aspects similar to hESCs and can be differentiated in culture into multiple cell types including neurons (Chamberlain *et al.* 2008, Dimos *et al.* 2008, Ebert *et al.* 2009). The availability of robust differentiation protocols to generate a variety of neuronal types from hiPSCs is a necessary requirement to perform neurotoxicological studies. This is not always the case in practice unfortunately, and accurate

assessment of the toxicity of a certain compound is frequently hampered by the inconsistency and/or the inefficiency of the differentiation protocol. While this is true for certain neuronal types (e.g. mesencephalic dopaminergic neurons), the problem seems sometimes to pertain to the nature of the hiPSC line used in the differentiation process rather than the differentiation protocol itself (Hu *et al.* 2010). One of the important factors that causes low efficiency is the persistent reactivation of the latent viruses used in the reprogramming process (Papapetrou *et al.* 2009). However, subsets of hiPSCs generated by integration-free conditions have been found to also exhibit low neuronal differentiation efficiencies (Hu *et al.* 2010).

The process of differentiating hiPSCs to neurons is carried out through successive stages that start with forming the neuroectoderm, which marks the early commitment of the stem cells to the neuronal lineage (**Figure 3** (**4.2a**)) (Muñoz-Sanjuán *et al.* 2002, Liu *et al.* 2005). In the absence of external signals hESC-derived neuroectoderm inherently differentiates towards dorsal telencephalic progenitors and eventually to cortical glutamatergic neurons (Li *et al.* 2009). In the presence of certain morphogens, however, these neuroectodermal cells are further patterned along the ventro-dorsal and rostro-caudal axes forming region-specific progenitors (**Table 1**) that give rise later to fully mature neurons (Li *et al.* 2009). The time of exposure to these morphogens and their concentration are critical factors that determine the fate of neuroectodermal cells. For example, exposure to FGF8 before *SOX1* upregulation results in the generation of mesencephalic dopaminergic progenitors, while forebrain dopaminergic progenitors are typically formed after exposure of *SOX1* positive cells to FGF8 (Yan *et al.* 2005).

Table 1. Representative protocols for differentiation of hiPSC and hESC to region-specific neuroprogenitors.

Target Cell	Source Cell	Duration of Differentiation	Comments	References
Neuroectoderm (NE) (Pax6+, Sox1+)	iPSC hESC	1-2 weeks	>80% of stem cells become NE cells. iPSC exhibit variable efficiency	Hu *et al.* 2010, *PNAS*. Chambers *et al.* 2009, *Nature Biotechnology*.
Telencephalic progenitors (Pax6+, FoxG1+)	iPSC hESC	3-4 weeks	> 90% of NE cells differentiate to this cell type	Zeng *et al.* 2010, *PLoS One*. Li *et al.* 2009, *Development*.
Cortical progenitors (Pax6+, Emx1+)	iPSC hESC	4 weeks	Important stage in the differentiation to glutamatergic neurons	Li *et al.* 2009, *Development*.
Medial ganglionic eminence (MGE) progenitors (Pax6-, Nkx2.1+)	iPSC hESC	4 weeks	Progenitors of GABAergic interneurons and BFCN	Li *et al.* 2009, *Development*.
Lateral ganglionic eminence (LGE) progenitors (Pax6+, Gsx2+)	iPSC hESC	4 weeks	Progenitors of GABAergic projection neurons	Li et al. 2009, *Development*. Aubry *et al.* 2008, *PNAS*.
Midbrain progenitors (FoxA2+, En1+)	iPSC hESC	26 days	Early FGF8 treatment is essential	Yan *et al.* 2005, *Stem Cells*.
Hindbrain/Spinal cord progenitors (Pax6-, Hoxb4+)	iPSC hESC	17 days	Early treatment with retinoic acid is essential	Zeng *et al.* 2010, *PLoS One*. Li *et al.* 2008, *Stem Cells*.
Multipotent neural crest cells (p75+, Hnk+, Ap2+)	iPSC hESC	11 days	Cells successfully underwent >25 passages with retention of multipotency	Menendez *et al.* 2011, *PNAS*.
Ventral spinal cord progenitors (Pax6-, Olig2+)	iPSC hESC	4 weeks	Retinoic acid for caudalizing, and SHH for ventralizing, are utilized	Zeng *et al.* 2010, *PLoS One*. Li *et al.* 2008, *Stem Cells*.

Further maturation of regional specific neuroprogenitors to fully mature neurons follows protocols based on the same principles of the timely treatment with the right concentration of the appropriate morphogen (**Figure 3** (**4.2b**)). Many neuronal types have been generated from both hESCs and hiPSCs using several protocols (**Table 2**) but the efficiency of making the required cell types is generally low. In addition to that, making terminally differentiated neurons consumes a considerable amount of time, and the cost of the different chemicals used in the process is not always affordable for academic researchers.

Table 2. Representative protocols for differentiation of hiPSCs and hESCs to mature neurons.

Target Cell	Source Cell	Duration of Differentiation	Comments	References
Retinal pigment epithelium (RPE) cells	iPSC hESC	8-12 weeks	70-80% of terminal differentiated neurons are RPE	Kokkinaki *et al.* 2011. *Stem Cells*. Idelson *et al.* 2009, *Cell Stem Cell*.
Cortical glutamatergic neurons **(VGLUT1+, TBR1+)**	iPSC hESC	6 weeks	60-70% of stem cells become VGLUT+ even without added morphogens	Zeng *et al.* 2010, *PLoS One*. Li *et al.* 2009, *Development*.
Striatal projection GABAergic neurons **(DARPP32+)**	hESC	9 to 10 weeks	The yield is low (22% MAP+, of those 36% are GABA+)	Aubry *et al.* 2008, *PNAS*.
Basal forebrain cholinergic neurons (BFCN) **(ChAT+)**	hESC	35-40 days	SHH is essential in the protocol. Efficiency is high (~90% of final neurons)	Bissonnette *et al.* 2011, *Stem Cells*.
Midbrain dopaminergic neurons **(TH+, Girk2+)**	iPSC hESC	~40 days	TH+ cells form 30-60% of the terminal neurons. Generated TH+ neurons are functional	Andrezej Swistowski *et al.* 2010, *Stem Cells*. Myung Soo Cho *et al.* 2008, *PNAS*.
Forebrain dopaminergic neurons **(TH+, GABA+)**	hESC	~40 days	Protocol yields 30% GABA+ &TH+ neurons in the final culture	Yiping Yan *et al.* 2005, *Stem Cells*.
Spinal motor neurons **(HB9+, ChAT+)**	iPSC hESC	5-8 weeks	~30% of final neurons exhibit motor neuron markers	Li *et al.* 2005, *Nature Biotechnology*. Hu *et al.* 2009, *Nature Protocols*. Karumbayaram *et al.* 2009. *Stem Cells*.
GABAergic interneurons			These cells differentiate alongside glutamatergic, projection GABAergic, and basal forebrain cholinergic neurons	Liu and Zhang 2011. *Cell Mol. Life Sci.*
Astrocytes **(S100b+, GFAP+)**	iPSC hESC	180 days	Almost 90% of final cultures cells are astrocytes in these protocols.	Krencik *et. al.* 2011, *Nature Biotechnology*.
Oligodendroglial cells **(Olig2+, Nkx2.2+, S0x10+, PDGFR+)**	iPSC hESC	4 months	Almost 80% of final cultures cells are oligodendrocytes	Hu *et al.* 2009, *Nature Protocols*. Hu *et al.* 2010, *PNAS*.

Recently, fully mature murine neurons have been made by direct conversion of fibroblasts (Vierbuchen *et al.* 2010). Following that, attempts have been made to make human neurons based on the same principle, using lentiviral vector-based gene delivery system to force the expression of a set of transcription factors peculiar to the final cell type. Indeed, fully mature and functional glutamatergic and dopaminergic neurons were made directly from fibroblasts, circumventing the intermediate step of iPSCs induction (**Table 3**, **Figure 1** (**4.2c**)) (Caiazzo *et al.* 2011, Qiang *et al.* 2011). The generated neurons seem to undergo major epigenetic reset expected to occur during such a switch between two terminally differentiated somatic cells. The duration of these protocols is significantly short (18 to 21 days) compared to the iPSC-based protocols, but the efficiency of making the final neuronal type is still low. Clearly though, direct differentiation methods will not be a viable strategy for studies of neurodevelopmental toxicity as the cells bypass the normal neurodevelopmental stages of neuralization, specification and maturation.

Table 3. Generation of glutamatergic and dopaminergic neurons by direct conversion from fibroblasts.

Target Cell	Source Cell	Duration of Differentiation	Comments	References
Human induced neuronal cells (hiN)	Fibroblasts	3 weeks	50-60% of final neuron in culture (~30%) were vGLUT1+. Study limited by the functionally heterogeneous mutations	Qiang et al. 2011, *Cell*.
Mesencephalic dopaminergic neurons	Fetal and adult fibroblasts	18 days	Very low yield (10% of final culture MAP+ and 6% TH+)	Caiazzo *et al.* 2011, *Nature*. Pfisterer *et al.* 2011. *PNAS*.

To improve the efficiency of the current protocols for neural differentiation of iPSCs, certain measures should be considered. Using integration-free iPSC induction methods eliminate the problem of persistent activity of viral genome and its negative effect on the differentiation process. Careful and consistent iPSC culture techniques are necessary to watch for iPSC lines that exhibit aberrant behavior in culture or are found to have abnormal genomes (Neely *et al.* 2011). Using small molecules inhibitors of Activin/Nodal and BMP signaling pathways significantly increases the efficiency of neural differentiation (Chambers *et al.* 2009, Morizane *et al.*

2011). In fact, the variability and inefficiency of iPSCs to differentiate to the early neuroectodermal stage has

been effectively overcome by such a regimen (Kim *et al.* 2010). As mentioned earlier, optimization of the time

of treatment and concentration of the used morphogens is an absolute requirement for an efficient

differentiation protocol. Knowledge of such details is greatly enhanced by a parallel understanding of the

normal development of the nervous system in human embryos.

Measures to reduce the cost and duration of neural differentiation make it possible to perform more

neurotoxicological experiments on neurons that would otherwise be unaffordable. One strategy has been to

come up with inexpensive compounds that could substitute for their more expensive counterparts used usually

in the differentiation process. An example is the replacement of sonic hedgehog, an important neural

morphogen, by the much cheaper puromorphamine, a purine derivative that activate hedgehog pathway (Sinha

et al. 2006). Maintenance and propagation of hiPSC-generated neuroprogenitors that retain the capability to

differentiate to mature neurons is a viable option to shorten the duration of differentiation and to unify the tested

neuronal populations (Li *et al.* 2011). Crypopreservation and later thawing of neurprogenitors could be possible

as well, although cell death is observed based on the technique and the used freezing medium (Milosevic *et al.*

2005).

Exposure paradigms

Perhaps one of the most powerful applications of iPSC technology in the field of neurotoxicology is the ability

to assess the response of neurons and neural progenitors to various toxicants (**Figure 3** (**4.3**)). Not only can

many different potentially noxious agents be screened, but also the temporal properties of their administration

can be used to simulate different patterns of potential human exposure. Many neurotoxicants, methylmercury

being a prominent example, show both acute and latent effects. Additionally, they can exhibit heightened

toxicity for specific neurodevelopmental stages, cell types, or time points under either acute or chronic

exposures (Weiss *et al.* 2002, Farina *et al.* 2011, Ni *et al.* 2011). One advantage of working with iPSCs is that both neural progenitors and terminally differentiated neurons can be assessed. Furthermore, the influence of exposure on developing neurons and the adult phenotype of differentiated neurons can be assessed under a number of exposure paradigms designed to mimic true environmental exposures within a single experimental model. Thus *in vitro* neuronal differentiation of hiPSCs enables assessment of interactions between early exposure and subsequent risk of neurodegenerative phenotypes in response to acute, chronic, latent and multi-hit toxicant exposure paradigms. A number of toxicants including ethanol, methymercury, PCBs, and cocaine have been shown to elicit neurodevelopmental toxicity by disrupting neural stem cell differentiation (Tateno *et al.* 2004, Fritsche *et al.* 2005, Tamm *et al.* 2006, Radio *et al.* 2008). Until the advent of iPSCs, these cell types could only be studied through primary culture or ESC derived neural progenitors, which require great effort to obtain and are not patient-specific. Thus, the use of hiPSCs is particularly attractive given that differential susceptibility of iPSC-derived cells from patients of various genetic backgrounds can be studied. However, it is important to note that the *in vitro* model of iPSC-derived neurons is limited in its capacity to simulate the complex extracellular environment, diversity and organization of various neuronal and glial cell types and the connectivity and activity of the neural circuitry found *in vivo.* For example, generation of mixed neuronal-glial cultures may be required to accurately model neurotoxicity. This approach would require parallel differentiation of stem cells into neuronal and glial lineages followed by co-culturing both cell types at the desired time point (Haidet-Phillips *et al.* 2011). However, the methods to obtain consistent mixed or single-lineage neuronal or neuronal-glial cultures from *in vitro* differentiation protocols of independent hiPSC lines have yet to be achieved.

Chronic toxicity is known to play a substantial role in many neuropathologies. Chronic exposure to the heavy metal manganese likely contributes to PD or PD-like pathology in patients (Aschner *et al.* 2009, Guilarte 2010). Acute exposures to manganese are known to produce a subclinical and clinical movement disorder collectively referred to as Manganism; but despite similarities between Manganism and PD, the relationship between

31

chronic manganese exposure and PD remains unclear (Aschner *et al.* 2009, Lucchini *et al.* 2009, Guilarte 2010). iPSC-derived neurons and neural progenitors may permit the study of chronic heavy metal exposures in developing and mature neurons. Such paradigms are useful to study the effect of exposure to a toxicant over a long period of time, possibly mimicking the effect of the cumulative toxicity of environmental toxicants on the CNS throughout the age of the affected individual. Usually the suspected toxicant is applied at low doses whose effect might not be apparent immediately, like the case in acute exposure paradigms, but might eventually exhaust the cellular repertoire of defense mechanisms and eventually manifest as a decrease in the number of viable neuronal subpopulation and/or altered cellular mechanisms that are crucial for normal function. The duration of exposure varies but is often limited by the time required to differentiate stem cells to the desired neuronal type.

This approach confers several advantages given that a wide array of cell types can be assessed via toxicological assays at several time points. Furthermore, the iPSC approach for chronic exposure toxicity testing is consistent with calls to reduce reliance on vertebrate animal models (Buzanska *et al.* 2009, Harrill *et al.* 2011). However, a major limitation of hiPSC models for studying chronic neurotoxicants is the lack of endogenous detoxification mechanisms (e.g. peripheral detoxification mechanisms of the liver, or neuroprotective mechanisms within the brain by astrocytes and microglia). The lack of such systems in iPSC-based *in vitro* differentiation models are extremely difficult to appropriately account for experimentally, although they play a major role in modulating toxicity *in vivo*. Thus early applications of hiPSC based models may need to focus on toxicants in which the *in vivo* metabolites are known and their neuronal distribution is understood. As mentioned above, the use of neuronal-glial mixed cultures could be achieved – however even here our basic understanding of regional differences in how toxicological mechanisms and detoxification pathways differ between discrete regions of the brain is insufficient to accurately model the *in vivo* condition. Nonetheless, cell autonomous mechanisms of vulnerability to and protection against chronic neurotoxicants is presently accessible to investigation. Thus genetic differences between individuals that mechanistically act at the cellular or molecular level of the target

will provide insight into patient-specific toxicological risk assessment in a manner not presently addressable by any other model system.

Finally, iPSCs have limitations in evaluating repeated toxicant exposures over the extended lifespan of a given neuronal or glial cell. Although investigators have devised a number of assays to assess pathological processes in iPSC-derived neurons, it may be difficult to demonstrate complex phenomena such as hormesis that act over extended periods of time and rely on undefined cellular functions or interactions. Work has been performed assessing electrophysiological profiles of iPSC-derived neurons, but conclusions regarding repeated exposures at a clinically relevant level may be confounded by a number of variables specific to iPSC reprogramming (Brennand *et al.* 2011). Despite these caveats, iPSCs may be able to be used to study phenomena, such as preconditioning, in circumstances in which the protective role of an early limited toxicant exposure is not dependent on another cell type. The exploration of preconditioning and hormesis is particularly valuable in the study of neurodevelopmental toxicity. It has been established that low-levels of oxidative stress can lead to hypomethylation and down-regulation of key stress mediators such as heat shock proteins and DNA methyltransferases (Shutoh *et al.* 2009). Whether such mechanisms occur in iPSC-derived neuronal lineages, and mimic the conditions that give rise to these mechanisms *in vivo,* remains to be determined. Nonetheless, even if the set point for such mechanisms may differ *in vitro* from the *in vivo* condition – human-specific and genetic variation-dependent differences in these mechanisms may still be detectable.

Coherence of genotype and phenotype

One of the major challenges with hiPSC models is establishing a clear relationship between genotype and phenotype in cells derived from a given patient. It has been previously reported that cell lines derived from individual patients can differ based on DNA methylation pattern and variable gene expression (Chin *et al.* 2009, Doi *et al.* 2009, Stadtfeld *et al.* 2010, Boulting *et al.* 2011). This variability is believed to underlie variable

efficiencies of neuronal differentiation between iPSC lines. Another confounding factor that could disrupt a clear relationship between genotype and phenotype is the presence of reprogramming vectors in virally reprogrammed cells. Variability between lines has been difficult to identify early in the differentiation process. Furthermore, no direct relationship has been noted between expression of pluripotency markers and differentiation capacity (Boulting *et al.* 2011). Overcoming this difficulty has been addressed by recent work, which was able to successfully predict differentiation potential through analysis of epigenetic and transcriptional differences between lines (Bock *et al.* 2011, Boulting *et al.* 2011). In another comparison of 22 human iPSC lines, it was revealed that there were an average of five protein-coding point mutations in sampled regions (Gore *et al.* 2011). These mutations consisted of splicing, nonsense, and non-synonymous variants that appeared both before and after fibroblast reprogramming (Gore *et al.* 2011). Similarly, early passage hiPSCs were found to contain a significantly higher frequency and degree of mosaicism for copy number variations compared to late passage hiPSCs or hESCs (Hussein *et al.* 2011). These *de novo* mutations, likely stemming from the reprogramming process itself, may obscure genotype-phenotype associations behind this mutational noise.

Genetic and epigenetic abnormalities in hiPSCs can arise either during the process of induction or during the subsequent culture process (Gore *et al.* 2011, Hussein *et al.* 2011, Lister *et al.* 2011). Genetic abnormalities may be at the chromosomal, sub-chromosomal or single-base levels, and their potential occurrence could have crucial implications for the appropriate use of iPSCs for research purposes. Some studies have suggested a high mutational load present in many hiPSC lines. It has been proposed that whole genome or complete exome sequencing may help identify lines with fewer mutational events and eliminate variability between lines (Gore *et al.* 2011). The loss of genetic fidelity may be reflected in aberrancies of cell behavior in tissue culture, abnormal morphology, growth rate alteration, and frequent differentiation. While most of the genetic variation involves a small subset of cells, there are recurrent mutational events such as trisomy 12 and trisomy 17 that convey a selective advantage whereby mutant cells replace euploid population after a few passages (Meisner *et*

al. 2008). It is thus reasonable to check the karyotype and genetic integrity of cultured hiPSCs for abnormalities at regular intervals; though at a significant added expense for research laboratories.

Appropriate modeling of epigenetic influence and 'residual epigenetic marks'

Epigentic state is known to have a powerful influence on chemical toxicity (LeBaron *et al.* 2010, Fragou *et al.* 2011, Perera *et al.* 2011). Thus an important consideration in the application of iPSC technology in the study of neurotoxicology is the status of epigenetic modifications such as genomic DNA methylation and histone modifications (**Figure 3** (**4.5**)). Given the critical role of epigentic state in development and differentiation, understanding the epigenetic profiles of hiPSCs is an important component to validating patient-specific experimental findings. The induction of somatic cells to iPSCs is known to alter their epigenetic profile (Guenther *et al.* 2010). The iPSC epigenetic profile, while similar to that of ESCs, has notable characteristic features. These epigenetic modifications can have a significant influence on the ability of iPSCs to differentiate into various cellular subtypes (Kim *et al.* 2010). In order to generate a greater understanding of the nature of the unique epigenetic profile of iPSCs, a recent study generated a whole-genome single-base resolution DNA "methylome" via bisulphite sequencing (Lister *et al.* 2011). Investigators found that iPSC lines were methylated at CG dinucleotide pairs at a higher frequency than somatic cells, in a manner similar to that of ESCs (Lister *et al.* 2011). Furthermore, upon comparison of the methylomes of iPSCs with that of ESCs, notable unique methylation loci were identified between cell types. One challenge when analyzing iPSC epigenetics is distinguishing between methylated regions that are vestiges of the somatic cell from which they are derived and those that result directly from reprogramming. It has been established that low-passage number iPSCs contain DNA methylation signatures derived from the tissue of origin (Kim *et al.* 2010). Many of these methylated regions are shared between individual iPSC lines, suggesting certain loci have an increased susceptibility to *de novo* methylation (Lister *et al.* 2011). Potentially, these high susceptibility regions can be monitored for stochastic methylation, a valuable tool when characterizing the efficiency of reprogramming and differentiation

of a given line (Lister *et al.* 2011). Interestingly, a recent study has noted that iPSCs methylation patterns become similar to ESCs with each sequential passage number (Nishino *et al.* 2011). The mechanism of this methylation is thought to be the result of the convergence of stochastic *de novo* hyper-methylation in adjacent genomic regions (Nishino *et al.* 2011). As the mechanisms of *de novo* methylation become revealed, interventions with chromatin-modifying drugs have the potential to address these concerns. Furthermore, given that fibroblasts are a common somatic tissue source, the methylation profile of iPSCs used in neurotoxicological assays may need to be standardized before disease modeling of neurological disease can be directly comparable between studies.

Undefined modifiers of toxicity

Perhaps one of the greatest challenges in applying iPSC technology to the field of neurotoxicology is replicating the toxicological conditions that reflect the insults arising *in vivo* from actual environmental exposures. Influences due to the specific route of exposure, interactions with other toxicants and environmental modifiers, as well as previous exposures, nutritional state, or chronic illness of the individual are currently difficult to account for using *in vitro* models, including differentiated neuronal lineages of hiPSCs. Furthermore, the actions of such undefined modifiers of toxicity may occur across diverse temporal and spatial axes (**Figure 3 (4.6)**). Thus the environmental, anatomical and developmental history of the primary target cell of a toxicant may be influenced by previous exposures, nutritional state, and status of support tissues or neuronal connectivity that is challenging to model *in vitro.* Furthermore, this issue is complicated by potential differences in the epigenetic status of iPSC derived cells that may not reflect the *in vivo* epigenetic state of the intended neuronal populations being modeled from the individual or human population being studied. The multi-factorial and synergistic potential of unknown modifiers to influence both the type and magnitude of toxicological outcomes are likely critical to actual disease etiology. Furthermore, it is often of particular interest to examine the role of neurotoxicants under specific disease states. Similar spatial, temporal, and anatomic constraints

impact neurological disease modeling by hiPSCs as well (Saha *et al.* 2009). Thus undefined modifiers of

neurotoxicity are layered upon the additional complexities of *in vitro* disease modeling. However, it should be

pointed out that similar challenges in interpreting experimental data apply to most model systems.

At the present state, effort should be directed toward standardization of iPSC phenotypes and development of

adequate controls and appropriate validation of experimental results. For example, iPSCs derived from

unaffected siblings are valuable controls as they generally have a similar environmental and genetic background

as the patient. Thus, experimental differences in the sensitivity of phenotypic outcomes to toxicant exposure of

differentiated or differentiating neuronal cells are more likely due to known genetic or epigenetic differences

between the subjects. Furthermore, multiple lines should be generated from each subject to account for the

inherent variability between individual lines.

Aging and senescence is also an important concern when generating iPSCs. It has been established that

fibroblasts derived from older mice have lower efficiency of reprogramming (Li *et al.* 2009). This may be

mediated by expressions of genes related to senescence such as the *Ink4b/Arf* locus, which is upregulated in

biological aging. It has been demonstrated that the generation of iPSC lines from older patients can be improved

by inhibiting senescence with siRNAs, treating somatic cells with antioxidants, or reprogramming in low-

oxygen conditions (Utikal *et al.* 2009, Yoshida *et al.* 2009, Banito *et al.* 2010, Esteban *et al.* 2010). An

important question, particularly in the study of neurodegenerative diseases, is whether aging can be reproduced

in iPSC-derived cells. Reprogramming of fibroblasts into iPSCs is thought to reset markers of cellular age such

as telomere length (Suhr *et al.* 2010). This change in telomere length is transient however, as telomere

shortening was observed in iPSC-derived cells after differentiation (Suhr *et al.* 2010). Similarly, it has been

established that the "energetic capacity" of cells can be reset through reprogramming, by reestablishing

mitochondrial compliment to a neonatal-like state (Suhr *et al.* 2010). As mitochondrial capacity decreases with

aging largely due to oxidative stress, these findings suggest that future studies utilizing iPSCs may focus on

replicating the cellular state of older subjects through prior exposure to reactive oxygen species. Nutritional variables could also be addressed with a similar approach; simultaneous treatment with naturally occurring antioxidants or chronic alcohol exposure could give insight into neuroprotective or neurotoxic roles of various substances. Upon further standardization of patient derived iPSCs, disease-modifying variables such as developmental history, early-life environmental exposures, epigenetic status, nutritional state, and age may be able to be accounted for in toxicological studies.

Challenges of scale

In the area of neurotoxicology, iPSCs can help address questions regarding why individuals with similar genetic backgrounds demonstrate differential susceptibility to toxicants. But before hiPSC-based neurotoxicological approaches can be broadly applied for toxicological risk assessment and in depth patient-based mechanistic and neuroprotective studies the critical hurdles of high cost and poor scalability associated with maintenance and analysis of multiple hiPSC lines simultaneously must be addressed. Significant person-hours are required to reprogram, validate, differentiate, and toxicologically assess multiple cell lines from just a single patient. Consequently, a seemingly straightforward study seeking to explore differences between patients with a given mutation and controls can easily become overwhelming for even a moderately sized research group. Thus, studies using hiPSCs remain quite low-throughput at present time, with recent published data comparing simple measures in no more than 10-20 lines, and even fewer lines for more complex phenotypic analysis. But significant improvements may be within reach by use of robotic automation and more efficient methodology (Dolmetsch *et al.* 2011). Perhaps the two disciplines that would benefit most from high-throughput hiPSC development are drug development and toxicology. For example, drug screening would require sufficient cells and sample size such that thousands of compounds could be screened (Ellis *et al.* 2011).

Modern tissue culture protocols are both time consuming and have tremendous batch-batch variability that may influence downstream assays. One recently proposed approach is the wide-scale utilization of stirred suspension bioreactors, which dramatically reduce cost and increase yield of expansion 58-fold (Shafa *et al.* 2011). iPSCs generated in stirred suspension bioreactors retain all pluripotency markers and are able to differentiate into all germ layers. However the aggregation into multicellular structures that occur under this approach will require adaptation to neuronal differentiation and neural specification methods that use monolayer iPSC cultures as their starting point. This approach has yet to be widely adapted in research laboratories owing to its high costs and specialized equipment, but may represent an important step toward high-throughput assays and commercialization of iPSCs.

Issues regarding scalability are an active area of discussion as it hinders collaboration between research groups. These issues include: reproducibility of protocols, cell line nomenclature, intellectual property issues, and lack of a detailed and centralized database of available hiPSC lines (Luong *et al.* 2011). There is a strong demand within the field to establish an iPSC library in conjunction with a clinical database, tissue bank, and genome wide association studies (GWAS) (Hankowski *et al.* 2011). Such a database would address concerns regarding reproducibility and nomenclature, making data directly comparable across studies.

The rapid development of hiPSC technology has benefited tremendously from the tailwind of hESC research. Aside from the unique reprogramming method, the reagents, differentiation protocols, and media are near identical to that of hESCs. However, the patient-specific nature of hiPSCs has generated a new demand for scaling up these protocols in a high-throughput manner. Thus, current cost-constraints and difficulties in cross-institutional collaboration will likely spur rapid innovation in scalability in the near future. This positive outlook of high-throughput screening utilizing iPSCs should incentivize investigators interested in toxicological assessment of neurological disease to adapt this technology as soon as possible.

The potential hiPSC technology for personalized medicine and risk assessment

As discussed above, hiPSCs have a wide-range of potential clinical applications, particularly in the field of personalized medicine. These applications include generation of cells for transplantation therapy and as a model of human disease (Hankowski *et al.* 2011). The major advantage of iPSCs over other disease models is that it has the potential to model any disease and toxicological phenotype, especially those that do not currently have an animal model. Furthermore, hiPSCs permit the study of diseases that are both genetic and environmental in nature. Thus, for the first time, the study of gene-environment interactions utilizing cellular subtypes derived from patients afflicted with a given illness is possible. Data derived from such studies in the future may provide a critical translational link between model organism-based, computational, and *in vitro* toxicological data to epidemiological and other human population studies. Furthermore, this approach is not solely for learning more about disease pathogenesis, but may be directly utilized in clinical practice. For example, by using patient-specific iPSC-derived neurons to customize neuroprotective strategies and environmental safety information for individuals. These future applications may also include direct transplantation of patient derived cells, toxicity studies, and drug efficacy and safety evaluations.

A lofty but often stated goal for hiPSC technology is its potential to provide personalized neurotoxicological risk assessment. For example, iPSC lines generated from an individual may enable assessment of individualized sensitivities to common environmental pollutants enabling targeted prophylactic measures. Likewise, assessment of heightened sensitivity to particular common toxicological insults (e.g. oxidative stress, mitochondrial dysfunction, protein misfolding, calcium handling deficits) may enable personalized neuroprotective strategies to be derived and prescribed. However, a measure of skepticism is warranted given the novelty of iPSC-associated approaches.

hiPSC technology has the potential to accelerate the pace of drug discovery and improve understanding of disease pathogenesis. Clinical, genetic and exposure history data of patients for which hiPSC are generated is especially relevant and should be collected as thoroughly as possible, abiding by IRB and HIPPA regulations to protect patients' privacy (Hankowski *et al.* 2011). Disease modeling using hiPSCs has already shown promise given recent success modeling RETT syndrome, Alzheimers disease, neuronal lysosomal disorders, Amyotrophic lateral sclerosis, schizophrenia, Parkinson's Disease and others (Marchetto *et al.* 2010, Brennand *et al.* 2011, Lemonnier *et al.* 2011, Marchetto *et al.* 2011, Seibler *et al.* 2011, Yagi *et al.* 2011). In the field of drug discovery, iPSCs have the ability to fill the information not covered by genome-wide association studies and databases. For example, novel compounds can be screened on mature cells derived from iPSCs generated from patients with a given illness. Through this approach, both a toxicity and efficacy profile for a given therapeutic agent can be generated (Hankowski *et al.* 2011).

Similarly, toxicity phenotypes can be studied *in vitro* by exposing iPSC-derived neurons to various toxicants and inflammatory factors (Marchetto *et al.* 2010, Wichterle *et al.* 2010, Inoue *et al.* 2011). Utilization of hiPSC-based toxicity testing for drug development, includes the promise of developing high-throughput assays utilizing iPSC-derived hepatocytes to examine the metabolism of novel compounds (Laustriat *et al.* 2010, Inoue *et al.* 2011). The effects of aging on disease-toxicity relationships may be challenging to model given that iPSC-derived cells present from the early stages of development. Future efforts can be directed towards inducing cellular injury and metabolic changes that simulate the effects of aging in this process. Although iPSCs show promise in the study of neurological disease, one must acknowledge the difficulty of validating iPSC models of psychiatric illness. Since disorders such as schizophrenia, autism, and depression have a poorly understood molecular and cellular basis, investigators will face difficulty defining which iPSC-derived neuronal lines demonstrate the disease-specific phenotype (Dolmetsch *et al.* 2011).

Conclusions

The ability of iPSC lines to be isolated from patients with any neurological disease provides an important tool for characterization of susceptibility to various toxicants. Neurotoxicological studies of iPSC-derived cells are readily adaptable to existing toxicity assays, which allows experiments to be controlled against primary neuronal cultures. Validation of iPSC-based findings will likely be dependent on appropriate validation of the iPSCs themselves. For example, expressions of surface markers of pluripotency markers after reprogramming and lineage specific markers during differentiation by immunocytochemistry or flow cytometry are critical validation steps (Vojnits *et al.* 2010). One of the foremost challenges facing neurotoxicological application is residual epigenetic signatures from reprogramming. Another challenge is the heterogeneous nature of cell types generated during differentiation (Anson *et al.* 2011). Ultimately, these concerns regarding the quality of the iPSC models necessitate that resulting neurotoxicological findings be validated in other model systems. Should a differential susceptibility to a neurotoxicant be identified in iPSC-derived cells, these results will need to be supported by epidemiological, animal, and human studies for the conclusion to be deemed valid.

The translational value of iPSC-based studies may be helped by identification of the key determinants and markers of the experimentally introduced genetic and epigenetic differences that contribute to measurable toxicological and phenotypic variation between iPSC lines and their derivatives. Controlling for these differences in the iPSC lines used for studies should minimize experimental noise and increase the coherence of human genotype – phenotype correlations. At present, since the impact of such experimental variation is currently unmeasured – it remains to be seen the numbers of iPSC lines per subject or the numbers of subjects needed to have sufficient statistical power to draw meaningful conclusions in neurotoxicological studies. However, as more studies are reported in the literature, a meta-analysis could be performed to evaluate these features and inform experimental design. One important caveat of iPSC-based neurotoxicological assays is the inability to completely model the *in vivo* neuronal environment, including the spectrum of neuronal network

connections and glial interactions. Thus at present only toxicological phenotypes that can be modeled in a cell autonomous manner, or perhaps simplistic mutlicellular models, are likely to provide meaningful information. Toxicities that depend on multi-regional interactions between brain regions or the periphery are not likely to be captured by iPSC-based modeling. However, when suitable iPSC-based neurotoxicological assays can be designed such systems may be uniquely powered as a translatable screening tool to inform and guide resources for appropriate human and animal model *in vivo* studies.

CHAPTER IV

OPTIMIZATION OF FLUORESCENCE ASSAY OF CELLULAR MANGANESE STATUS FOR HIGH THROUGHPUT SCREENING[2]

Abstract

The advent of high throughput screening (HTS) technology permits identification of compounds that influence various cellular phenotypes. However, screening for small molecule chemical modifiers of neurotoxicants has been limited by the scalability of existing phenotyping assays. Furthermore, the adaptation of existing cellular assays to HTS format requires substantial modification of experimental parameters and analysis methodology to meet the necessary statistical requirements. Here we describe the successful optimization of the Cellular Fura-2 Manganese Extraction Assay (CFMEA) for HTS. By optimizing cellular density, manganese (Mn) exposure conditions, and extraction parameters, the sensitivity and dynamic range of the fura-2 Mn response was enhanced to permit detection of positive and negative modulators of cellular manganese status. Finally, we quantify and report strategies to control sources of intra- and inter-plate variability by batch level and plate-geometric level analysis. Our goal is to enable HTS with the CFMEA to identify novel modulators of Mn transport.

Introduction

Manganese (Mn) is an environmentally abundant metal that serves as a critical cofactor for numerous enzymes such as glutamine synthetase, SOD2, and arginase. Despite active research into the physiological regulation of cellular and tissue Mn levels, this process is not fully understood. Mn is believed to primarily enter the central nervous system (CNS) across the capillary endothelium at normal physiological concentrations (Aschner *et al.* 2007). In addition, at high blood concentrations, transport across the choroid plexus dominates (Murphy *et al.* 1991, Rabin *et al.* 1993, Aschner *et al.* 2007). Mn transport across the blood-brain barrier involves a diverse set of cellular mechanisms including facilitated diffusion and active transport. Greater understanding of Mn transport has profound clinical relevance, given that Mn has neurotoxic properties that cause debilitating neurological and psychiatric pathologies such as manganism, a condition with features similar to Parkinson's Disease (Aschner *et al.* 2009). Furthermore, the integral use of Mn in manufacturing sectors such as welding, oil refinement, and glass production increase the potential of excess Mn exposure in industrialized nations (Bowman *et al.* 2011). In addition, there have been few advances in therapeutics that protect against Mn influx into neurons or promote efflux of the metal once it enters. Although variably effective, chelation therapy with ethylenediaminetetraacetic acid (EDTA) or 4-aminosalicylic acid and treatment with levodopa are currently the only therapeutic interventions for Mn toxicity (Crossgrove *et al.* 2004). Despite the critical need to study Mn transport, one of the greatest limitations in the study of this process has been the development of novel assays that have the potential to be scaled for high throughput screening (HTS).

Our group has previously developed the Cellular Fura-2 Manganese Extraction Assay (CFMEA) to quantify intracellular Mn concentrations (Kwakye *et al.* 2011, Kwakye *et al.* 2011). CFMEA indirectly measures total cellular Mn content via its quenching of fura-2 fluorescence by Mn^{2+}. The fura-2 isosbestic point for calcium (Ex_{360}/Em_{535}) is used to avoid interference by cellular Ca^{2+} ions. This assay permits the highly accurate assessment of extracted Mn levels over a range of 0.1-10μM.

The advent of HTS, the interrogation of large chemical libraries in the context of a biological target to identify active compounds, has been a critical advance in the process of drug development and identification of pharmacological candidates for translational applications (Johnston *et al.* 2002). Although variability within routine laboratory assays can be accounted for by performing technical and biological replicates, reliable single-sample assays are critical for successful high throughput screens. As a result, assays must be optimized for a highly robust yet consistent response. Cell-based assay optimization is multi-factorial; including cell density, exposure time, compound concentration, assay reagent concentration, and extraction volume. The goal of this optimization process is to achieve a Z-factor greater than 0.5 (a statistical parameter that accounts for the signal dynamic range and data variation of signal measurements) (Zhang *et al.* 1999).

Here our ultimate goal is to apply the CFMEA for HTS to permit the identification of small molecule modifiers of cellular Mn transport and storage. Given its ease of scalability, culture requirements, and previous success measuring Mn homeostasis, we have selected an immortalized murine striatal neuron cell line for these studies. One of the greatest challenges in converting a cellular assay into HTS format is limiting the influence of confounding variables on the output response. Thus, we sought to accomplish three goals: (1) determination of the experimental conditions that elicit approximately 50% quenching of fura-2 signal, (2) characterization of plate-based geometric variability and batch-to-batch variability across varying Mn exposure levels, and (3) statistical evaluation of the suitability of the CFMEA as an HTS assay. By accomplishing these stated objectives, we hope to identify sources of variability inherent in this assay and propose analytical techniques to limit their influence. Furthermore, we hope that the process adapting the CFMEA for HTS will be directly applicable toward developing other cellular plate-based assays.

Results

Determination of optimal cellular density and exposure time

In an initial pilot study using 96-well plates to determine the optimal cell density and exposure time for HTS was performed utilizing the wild-type ST*Hdh*$^{Q7/Q7}$ murine striatal cells. Three physiologically relevant Mn concentrations were tested plus a vehicle control (0μM, 25μM, 50μM, and 100μM) to determine a condition that produced 50% quenching of the vehicle fura-2 signal at a concentration of 0.5μM fura-2. This concentration of fura-2 had been shown in the original assay development of CFMEA to be optimal for quantification of cellular Mn levels (Kwakye *et al.* 2011, Kwakye *et al.* 2011). Concurrently, four different cell counts were tested (5000, 7500, 10000, 20000 cells/well) under each of the exposure conditions **(Figure 4)**. To evaluate the degree of fluorescence quenching all values are normalized to the fluorescence on the vehicle control (%Veh). The data indicate that multiple conditions satisfied our assay goals, such as achieving a 50%Veh signal and non-overlapping of SD between adjacent concentrations (+/- 1SD). However, both conditions were only achieved upon 60-minute exposure of 100μM Mn at either 10,000 or 20,000 cells/well (**Figure 4**). To enhance the scalability of this assay, we utilized the lower cellular density (10,000 cells/well) as it also displayed a smaller degree of experimental error suggesting that higher cell densities may exhibit greater experimental noise. This set-up served as a basis for further optimizations to reduce variability and modulate fura-2 response.
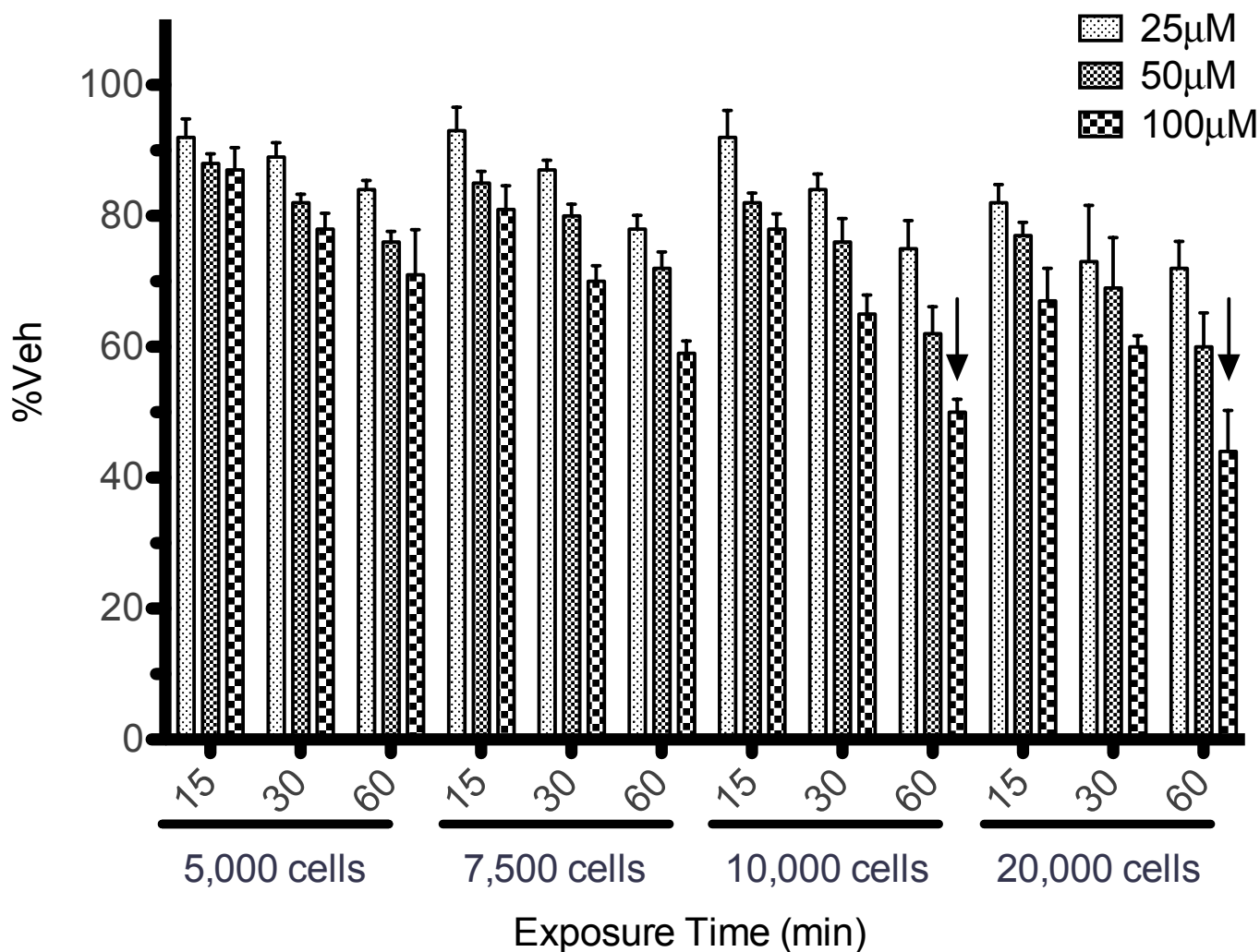
Figure 4 – Determination of optimal cellular density and exposure time of CFMEA. Data are presented as %Veh vs. exposure time (min) and sorted by plated cell density and Mn exposure concentration (μM). n=4 for each condition. Arrows indicate exposure conditions that produced approximately 50% quenching of fura-2 signal.

Evaluation of optimal fura-2 concentration, extraction volume, and analysis method

Utilizing the aforementioned cell density and exposure conditions (60-minute, 100μM Mn exposure and a plating density of 10,000 cells/well in a 96-well plate), a series of experiments were conducted to evaluate whether well-to-well variability (i.e. changes in fura-2 signal between replicates across plate regions) could be minimized while maintaining a robust response in the dynamic range. Under the hypothesis that optimizing the

concentration of fura-2 could enhance the sensitivity of the assay and decrease statistical noise, we sought to explore the impact of concentration changes on variability. Varying the concentration of fura-2 (0.25µM, 0.50µM, 0.75µM) and normalizing the fluorescence quenching by adjusting to %Veh we determined that variance (SD) was minimized with 0.75µM fura-2 (**Figure 5A**). In a similar fashion, we also explored the impact of extraction volume on the sensitivity of CFMEA with the goal of achieving near 50 %Veh while minimizing error. The extraction volume for CFMEA was varied between 75µL, 100µL, and 125µL reported in raw fluorescence values (**Figure 5B**), indicating the highest signal intensity with 125µL. Subsequently, to determine the ideal method to analyze data for HTS using CFMEA, the raw fluorescence values were used to derive %Veh and [Mn] extracted values (**Figure 5C,D**) respectively (Kwakye *et al.* 2011, Kwakye *et al.* 2011). These results indicated that the higher extraction volume (125µL) resulted in slightly greater precision (smaller SD values) across all three quantitative approaches presented here.
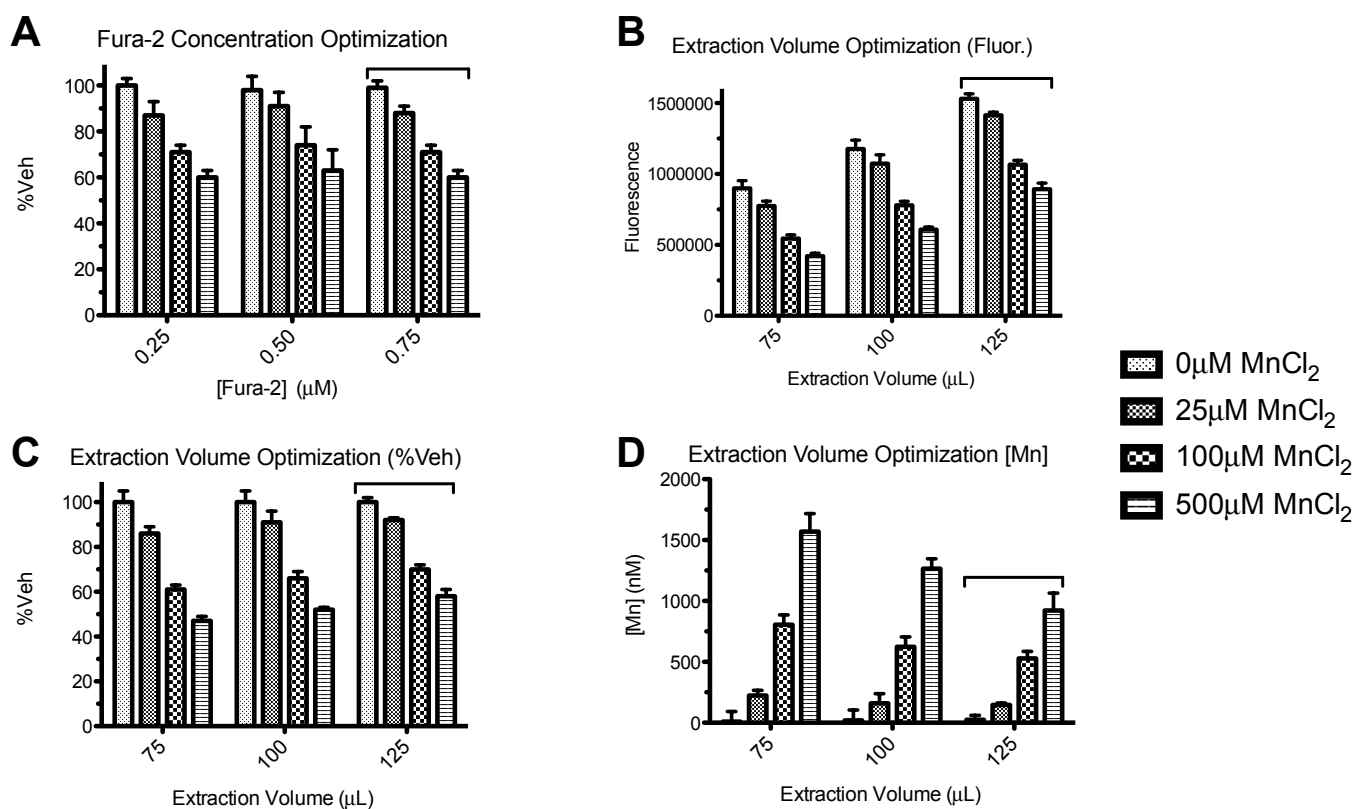
Figure 5 – Optimization of fura-2 concentration and extraction volume. (**A**) Fura-2 concentration optimization. Data are presented as %Veh vs. concentration of fura-2 (μM) across multiple Mn exposure concentrations (μM), n=8 for each condition. (**B-D**) Extraction volume optimization using 0.75μM fura-2. (**B**) Data are presented as raw fluorescence (Fluor.) vs. volume of fura-2 (μL) across multiple Mn exposure concentrations (μM). n=24 for each condition. (**C**) Extraction volume optimization (%Veh). Data are presented as %Veh vs. volume of fura-2 (μL) across multiple Mn exposure concentrations (μM). n=24 for each condition. (**D**) Extraction Volume Optimization (Mn). Data are presented as concentration of Mn extracted (nM) vs. volume of fura-2 (μL) across multiple Mn exposure concentrations (μM). n=24 for each condition. (**A-D**) Bracketed bars indicate selected fura-2 concentration and extraction volume data for subsequent downstream assays.

Based on the newly optimized fura-2 concentration of 0.75μM for HTS, a new *in vitro* (cell-free) standard curve was generated (**Figure 6**) to determine the Mn concentration that yields a 50% signal relative to vehicle to ensure the highest sensitivity for changes in Mn levels. The target sample response of approximately 50% quenching of the fura-2 signal maximizes the detection of both positive and negative modulators of cellular Mn status. This mirrors a common approach utilized in activity based *in vitro* assays that utilize the half-maximal activity concentration, $AC_{50,}$ as an output (Inglese *et al.* 2006). As a result, for a given increase or decrease in Mn extracted by CFMEA, there would be the greatest change in fluorescence.

0.75µM Fura-2 Standard Curve
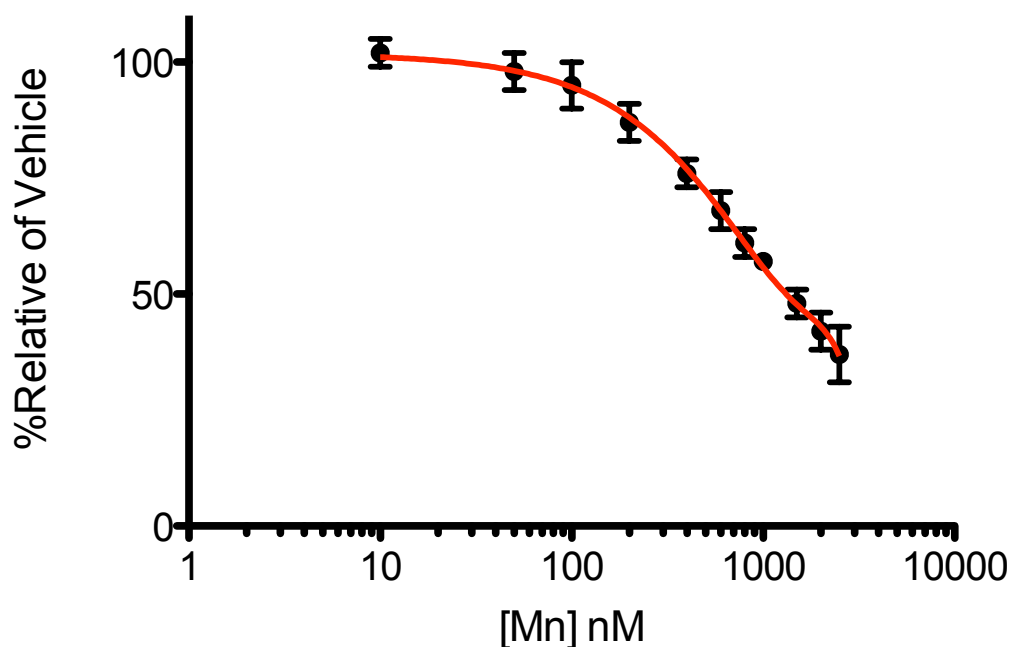
Figure 6 – 0.75µM fura-2 standard curve. Data are presented as %relative to vehicle vs. concentration of Mn (nM). n=4 for each concentration.

Examination of geometric and batch-to-batch variability

Based on the optimal fura-2 concentration of 0.75µM, a series of experiments was conducted to evaluate the inherent geometric variability within a plate (horizontal and vertical) and across experimental batches. A batch is defined as the series of plates in which cells were plated, exposed to Mn, and CFMEA performed concurrently. Cells grown in 96-well plates were treated with vehicle, 25µM, 100µM, and 500µM Mn for one hour and analyzed by both raw fluorescence and %Veh (**Figure 7A**). In order to segregate major sources of geometric variability, cells were plated vertically while Mn exposures and fura-2 extraction buffer were delivered horizontally by multi-channel pipetting (Supplemental Figure 2). In addition, three batches consisting of multiple plates were analyzed independently and are identified here in downstream analyses by batch and plate number (e.g. 1.3 denotes Batch 1, Plate 3). Examination of plate geometric variability by fluorescence

revealed pronounced horizontal-related effects, with corresponding decreases and sharp increases within particular plates. For example, plate 2.4 exhibited a decreased level of fluorescence in horizontal rows G-H, while there was a noticeable increase in fluorescence in row G-H of plate 3.4. Analysis by fluorescence also revealed a striking batch-to-batch variability with Batch 1 exhibiting higher overall levels of fluorescence compared to Batches 2 and 3. Interestingly, this effect was less noticeable as the Mn exposure concentration increased, suggesting that the levels of Mn extracted influence variability of the CFMEA. Based on these observations, we suspect that the primary sources of geometric variability are caused by differences in extraction buffer volume delivery.

The amount of variability observed by analyzing raw fluorescence values guided us to explore whether this phenomenon could be accounted for by normalizing to %Veh (**Figure 7A**). After reanalyzing by this alternative quantitative methodology, there was a substantial decrease in overall variability. Importantly, this method of analysis appeared to eliminate batch-to-batch variability, but individual plates still retained some horizontal variability. This suggests that differences in the baseline fluorescence of the fura-2 solution prepared for each batch was a major source of variability between batches. In order to further evaluate the change in variability by standardizing to %Veh, we calculated a normalized SD (for %Veh values versus fluorescence values), which adjusted the scale of the SD of each horizontal row to the average SD of all horizontal rows of a given exposure. This was necessary since the magnitude of SD values is directly related to the magnitude of the measurements themselves. By normalizing the mean fura-2 signal for a given exposure condition within each plate to the respective mean fura-2 signal of all rows, of that given exposure condition, across the entire experimental set (all plates, all batches) we could compare the degree of variance independent of differences in the magnitude of the measured values themselves. Specifically, the mean fura-2 signal values for each plate (fluorescence or %Veh) for a given exposure (25µM, 100µM or 500µM Mn) was divided by overall mean signal of every row of every experimental plate at that exposure level, generating a normalized mean signal of each row. Calculation of the SD of these normalized row values for each experimental plate (i.e. the normalized SD) effectively

allowed direct comparison of the relative magnitude of experimental variation across all plates irrespective of exposure condition. These average normalized SD values for all rows of a given exposure for each plate were plotted and color coded by batch and compared between analytical methods (fluorescence versus %Veh; **Figure 7B**). The normalized SD plot revealed that batch-to-batch variability was controlled by quantitative measurements accounting for %Veh. Interestingly, when the dataset was analyzed for vertical-based variability across plate region (left, middle, right column groups), there was substantially less variability across the vertical axis of the plate relative to the horizontal-dependent variability (data not shown). In agreement with the horizontal analysis, a similar pattern of batch-to-batch variability as observed in the vertical-based analysis.
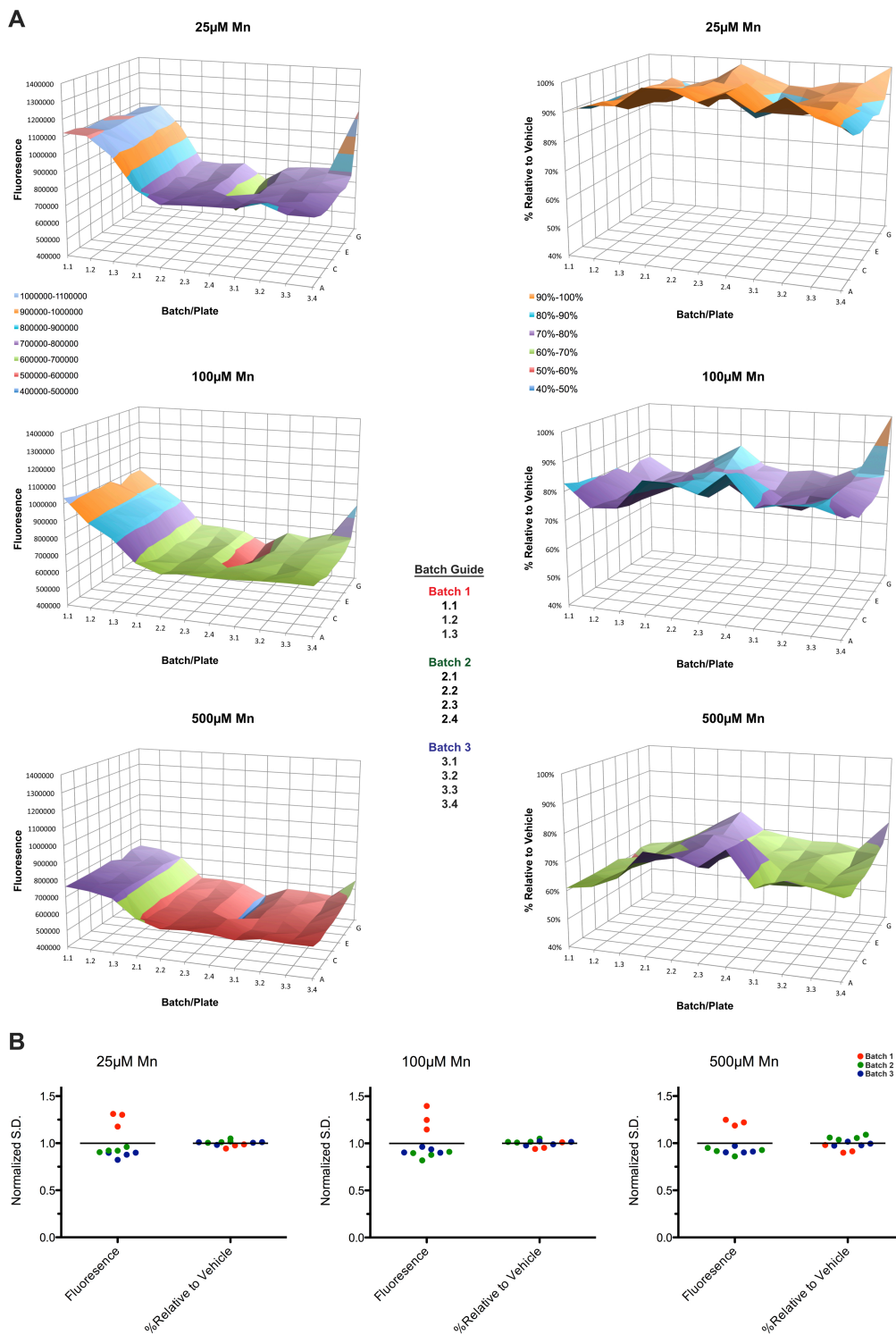
Figure 7 – Sources of variability and analytical technique. (**A**) Examination of plate-based geometric and batch-to-batch variability. Data are presented in three-dimensional surface plots showing raw fluorescence/percent relative to vehicle (Y-axis), by each batch/plate number (X-axis; e.g. 1.2 is plate 2 of batch 1), by the eight horizontal row positions of each plate (Z-axis; rows A-H). Coloration within the surface plot indicates demarcated value ranges along the Y-axis. Separate graphs were generated for each Mn exposure (μM) and analysis method (Fluorescence vs. %Relative to Vehicle). n=8 for each condition. (**B**) Impact of analysis method on normalized SD. Data are presented as normalized SD vs. analysis method (Fluorescence vs. %Relative to Vehicle). Separate plots were generated for each Mn exposure (μM). n=8 for each condition.

54

In the final phase of this study, we sought to calculate the Z-factor of each plate to assess whether CFMEA could be utilized for HTS. The Z-factor was calculated between each of the tested concentrations (vehicle, 25µM, 100µM, and 500µM Mn). The optimal scores were the Z-factors between vehicle and 500µM Mn, as presented (**Table 4**).

Table 4. **Z-factors by batch and plate.**

Batch	Plate	Z-Factor	HTS Quality
1	1	0.73	Excellent
1	2	0.73	Excellent
1	3	0.36	Borderline
2	1	0.27	Borderline
2	2	0.40	Borderline
2	3	0.50	Excellent
2	4	-0.66	Poor
3	1	0.47	Borderline
3	2	0.51	Excellent
3	3	0.38	Borderline
3	4	-0.93	Poor

Z-factors were evaluated for HTS based on the following criteria: $Z > 0.5$ was classified as excellent, $0 < Z < 0.5$ as borderline, and < 0 as poor. Based on these standards, 4 of 11 plates were classified as excellent, 5 of 11 plates as borderline, and 2 of 11 as poor. The high proportion of plates classified as borderline or poor was not unexpected, given that these pilot assays were conducted by manual liquid dispensing. Utilization of an automated pipetting process should substantially reduce variability; thus we sought to explore if controlling for the observed horizontal variation would improve the Z-factors for the plates with poor or borderline Z-factors. As a proof of principle, plate 2.4 which originally had a Z-factor of -0.66, was separated in two areas (rows A-C

and D-H). Using this independent analysis, the Z-factor of each area was improved to 0.42 and 0.45 respectively.

In the final phase of this study, we sought to calculate the Z-factor of each plate to assess whether CFMEA could be utilized for HTS. The Z-factor was calculated between each of the tested concentrations (vehicle, 25μM, 100μM, and 500μM Mn). The optimal scores were the Z-factors between vehicle and 500μM Mn, as presented (**Table 4**). Z-factors were evaluated for HTS based on the following criteria: $Z>0.5$ was classified as excellent, $0<Z<0.5$ as borderline, and <0 as poor. Based on these standards, 4 of 11 plates were classified as excellent, 5 of 11 plates as borderline, and 2 of 11 as poor. The high proportion of plates classified as borderline or poor was not unexpected, given that these pilot assays were conducted by manual liquid dispensing. Utilization of an automated pipetting process should substantially reduce variability; thus we sought to explore if controlling for the observed horizontal variation would improve the Z-factors for the plates with poor or borderline Z-factors. As a proof of principle, plate 2.4 which originally had a Z-factor of -0.66, was separated in two areas (rows A-C and D-H). Using this independent analysis, the Z-factor of each area was improved to 0.42 and 0.45 respectively.

Discussion

Using the described systematic approach we have optimized conditions of the CFMEA for HTS. In this process, we targeted specific technical and theoretical aspects of the assay in an effort to ensure a consistent and robust response to changes in cellular Mn status. Importantly, it must be noted that each of these pilot assays was conducted manually (e.g. manual liquid exchange and plating of cells). Since HTS is conducted using automated robotic delivery and handling systems, we expect the level of overall variability to decrease substantially in subsequent assays and by inference the accuracy in identifying modifiers of cellular Mn status to increase. Specifically, this conservative approach, one with inherently greater error, suggests that Z-factors in

the borderline range will likely improve into the excellent category after automation. In addition, we determined that some systematic errors, such as horizontal-dependent variability, could be accounted for by independently analyzing the plate along clear demarcated borders in signal response.

Further analyses explored the sources of geometric variability, changes in signal across vertical regions and across horizontal rows solely due to location and not experimental manipulation. By originally plating cells vertically and delivering all subsequent washes, exposures, and fura-2 extraction buffer horizontally, we have identified potential sources of this variability. The minimal level of vertical variability suggests that differences in cell density and growth were not a major contributor to intra-plate variability. In contrast, the high level of horizontal variability observed could be attributed to differences in the aforementioned deliveries that were administered in a horizontal-specific manner. Thus, we recommend that future HTS adaptation record and carefully design delivery patterns of solutions, permitting detection of sources contributing to geometric variability.

As previously mentioned, HTS does not have the luxury of sample replicates and is performed over a period of weeks to months. As a result, these systemic forms of variation must be minimized during this process and accounted for during downstream analyses. As a final point, all optimizations for HTS are targeted to achieve the threshold Z-factor of 0.5, maximizing confidence in candidate small molecules identified by HTS with this method by decreasing the rate of false positive and false negatives.

Furthermore, we discovered that the quantitative method of analysis is critical to account for batch-to-batch variability. The observed signal variability in raw fluorescence could be attributed to a multitude of factors. However, we suspect that the primary source of this variability is based on liquid delivery and handling, particularly of the fura-2 extraction buffer. Given that the readout of CFMEA is a fluorescent signal detected by a multimode detector, variation in fura-2 delivery could produce quantitative differences in detected

fluorescence. Although each experimental batch was prepared independently, the utilized fura-2 was from a single manufacturing lot, making differential fura-2 dye activity unlikely. Additionally, there is the possibility that variation in Mn exposure buffer delivery could have contributed to inter-plate differences in fluorescence intensity. However, the consistent pattern of intra-batch variation across the tested Mn concentrations makes variation in Mn exposure buffer delivery an unlikely culprit given that individual concentrations were composed and delivered independently.

We have previously reported that transforming raw fura-2 fluorescence values into a percentage relative to vehicle could successfully account for signal differences both within and between batches (Kwakye *et al.* 2011). Based on this finding, we recommend standardizing all values during HTS to the average signal value across each plate. This quantitative method controls for inherent changes in signal across batches caused by changes in cellular growth or a given fura-2 aliquot. This standardization would not limit the ability to identify changes in fluorescence caused by the activity of small molecules within a small molecule library. Another advantage to this approach is that it eliminates the requirement of generating a standard curve for each batch, since the goal of HTS is to identify hits based on clear cut-offs in signal rather than quantitative differences among samples. Given the robustness of this method of analysis, CFMEA is well suited for applications detecting small differences ($[Mn] \geq 0.1\mu M$) in cellular Mn status, with or without exogenous Mn exposure. The sensitivity of the assay permits detection of moderate changes in Mn status, a property of direct relevance in drug development for compounds of physiological relevance.

Moving forward, we believe that CFMEA has to potential to be a valuable tool in the detection of cellular Mn levels in HTS protocols. We advise investigators seeking to utilize this method to employ a similar approach in validating the parameters (cell density, exposure paradigm, fura-2 concentration) for their cell-type of interest. Subsequently, determination of the Z-factor for the assay will be essential in determining eligibility for HTS robotic automation. Although we have discussed sources of variance in the context of this study, there are other

factors that may impact future applications of CFMEA for HTS, such as fura-2 manufacturing lot and storage conditions. Furthermore, investigators should be aware of the potential influence that experimental differences in fura-2 concentration, fluorometric plate reader sensitivity, and detection of Mn quenched fura-2 may have on variability in the context of CFMEA HTS (Kwakye *et al.* 2011).

Thus, we have described an approach broadly applicable toward adapting toxicological assays for HTS: (1) determination of the optimal cellular density, exposure concentrations, and conditions targeting the most dynamic range of the standard curve, (2) adjustment of reagent concentration, extraction volume, and analysis method to minimize error, and (3) performance of a multiple batch assay to compute geometric variation, batch-to-batch variability, and Z-factors. This multi-step process permits the rapid ascertainment of the suitability of a cellular-plate assay for HTS without significant investment of laboratory resources or utilization of automated robotic equipment. Should a given assay achieve Z-factors within the target range, further validations and pilot screens can be pursued with reasonable degree of certainty that HTS will be possible. As more toxicological assays are adapted for this purpose, we hope that drug development, toxicant characterization, and our understanding of underlying physiological responses will be improved significantly.

Materials and Methods

Cell Culture Supplies and Reagents

Cell lines were grown in Dulbecco's modified Eagle's medium (DMEM) with 10% fetal bovine serum (Atlanta Biologicals, Lawrenceville, GA, and Sigma, St. Louis, MO), l-glutamine, 400 µg/ml G418 and Penicillin-Streptomycin. Manganese (II) chloride heptahydrate ($MnCl_2 \cdot 7H_2O$), was from Alfa Aesar (Ward Hill, MA). Ultra-pure fura-2 salt (cell-impermeable, ENZ-52007) was obtained from ENZO Biochem (New York, NY). The HEPES salt exposure buffer consisted of 25 mM HEPES buffer (pH 7.2), 140 mM NaCl, 5.4 mM KCl, and

5 mM d-glucose (Sigma). 1X ultra-pure phosphate-buffered saline (PBS), pH 7.4, without calcium and magnesium was used for post Mn exposure washes. Triton X-100 and sodium dodecyl sulfate (SDS) were obtained from Sigma.

Cell Culture

Murine striatal cell lines, wild-type STHdh$^{Q7/Q7}$, were grown at 33°C using previously established protocols (Trettel *et al.* 2000, Kwakye *et al.* 2011, Kwakye *et al.* 2011). Of note, the striatum is amongst brain regions that accumulate the highest levels of Mn (Aschner *et al.* 2007, Aschner *et al.* 2009). These cells were plated in a 96-well plate at varying cellular concentrations cells per 0.32 cm^2 36 hours before Mn treatment and allowed to grow in a 33°C incubator. MnCl$_2$ was added to HEPES salt exposure buffer the morning of exposure. Total extracted Mn levels were assessed by CFMEA.

Cellular Fura-2 Manganese Extraction Assay (CFMEA)

CFMEA was conducted by adapting a previously published protocol by our laboratory (Kwakye *et al.* 2011). Wild-type STHdhQ^7/Q^7 were cultured in 96-well tissue plates for 36 hours, media was removed, wells were washed once with 200μL PBS and exposed to 100μL of varying physiologically and/or toxicologically relevant MnCl$_2$ concentrations (0μM, 25μM, 100μM, 500μM) (Aschner *et al.* 2007, Aschner *et al.* 2009, Bowman *et al.* 2011). After exposure, the media was discarded and cells were washed three times with 200μL PBS. Subsequently, the cells were extracted at 33°C for three hours in the indicated volume of (75μL, 100μL, 125μL) 0.1% Triton X-100 in PBS (PTx) with the indicated concentration of fura-2 (0.25μM, 0.5μM, 0.75μM).

Quantification of Extracted Manganese

An *in vitro* non-cellular Mn standard curve was generated at 0.75µM fura-2 utilizing a sixteen point dataset with samples containing 1µL of different 100X stock Mn standards (0–100mM) added to 99µL of 0.5 µM fura-2 in PTx and assayed in a 96-well plate (n=3). The average raw fluorescence signal values (RFU) of the 0µM Mn samples within each independent standard curve were defined as the 100% maximal fluorescence (mean fluorescence$_{vehicle}$ = 100%) for that experiment after background subtraction. Based on this value, a ratio relative to vehicle and expressed as a percentage (%Veh) was calculated for each sample (%Veh = 100 x (fluorescence-$_{sample}$/mean fluorescence$_{vehicle}$)). These plotted values were then used to generate a cubic function using Prism (GraphPad) that related the concentration of Mn in nM (y) to %Veh at each concentration (*y= -11693*(%Veh)^3+30939*(%Veh)^2-28623*(%Veh)+9403.6*), r^2=0.9740. We then utilized this function to solve for the concentration of Mn extracted in experimental samples using Microsoft Excel.

Statistical Analysis

Calculations of subtracted background levels, %Veh, and solving for Mn concentration were performed in Microsoft Excel. Downstream analyses characterizing variability and calculation of standard deviation (SD) and normalized SD to allow comparisons of variance over different numerical scales are discussed in depth in the Discussion. Z-factor was calculated using the function below as originally described by *Zhang et al. (Zhang et al. 1999)*.

$$Z=1-(3*SD_{concentration1}+3*SD_{concentration2})/|\mu_{conentration1} - \mu_{concentration2}|$$

CHAPTER V

CELLULAR MANGANESE CONTENT IS DEVELOPMENTALLY REGULATED IN HUMAN DOPAMINERGIC NEURONS[3]

Abstract

Manganese (Mn) is both an essential biological cofactor and neurotoxicant. Disruption of Mn biology in the basal ganglia has been implicated in the pathogenesis of neurodegenerative disorders, such as parkinsonism and Huntington's disease. Handling of other essential metals (e.g. iron and zinc) occurs via complex intracellular signaling networks that link metal detection and transport systems. However, beyond several non-selective transporters, little is known about the intracellular processes regulating neuronal Mn homeostasis. We hypothesized that small molecules that modulate intracellular Mn could provide insight into cell-level Mn regulatory mechanisms. We performed a high throughput screen of 40,167 small molecules for modifiers of cellular Mn content in a mouse striatal neuron cell line. Following stringent validation assays and chemical informatics, we obtained a chemical 'toolbox' of 41 small molecules with diverse structure-activity relationships that can alter intracellular Mn levels under biologically relevant Mn exposures. We utilized this toolbox to test for differential regulation of Mn handling in human floor-plate lineage dopaminergic neurons, a lineage especially vulnerable to environmental Mn exposure. We report differential Mn accumulation between developmental stages and stage-specific differences in the Mn-altering activity of individual small molecules. This work demonstrates cell-level regulation of Mn content across neuronal differentiation.

Introduction

Most essential metals are highly regulated throughout development, serving as required co-factors while also implicated in cytotoxic processes (Finney *et al.* 2003). Metal homeostasis is maintained through concerted mechanisms involving metal transporters, metallochaperone proteins, metal responsive signaling pathways and transcription factors, and sequestration of metals within sub-cellular organelles (Domaille *et al.* 2008). A complex regulatory biology is known to underlie the transport and handling of most essential metals including iron, copper, and zinc (Zecca *et al.* 2004, Cousins *et al.* 2006, Choi *et al.* 2009). However, little is known about intracellular handling of Mn, despite it being an essential cofactor of cellular processes that rely on Mn-dependent enzymes such as superoxide dismutase (Mn-SOD), arginase, glutamine synthetase, and neurotransmitter synthetic enzymes (Aschner *et al.* 2007). In excess, Mn is neurotoxic, producing a variety of motor and psychiatric disturbances that can be attributed to basal ganglia dysfunction (Bowler *et al.* 2003, Takeda 2003, Stredrick *et al.* 2004, Josephs *et al.* 2005) and an enhanced susceptibility to Mn exposure has been reported during fetal and infant development (Aschner *et al.* 2005, Erikson *et al.* 2007). Mn preferentially accumulates and elicits toxicity within basal ganglia structures such as the caudate, putamen, substantia nigra, and globus pallidus (Bowman *et al.* 2011). Specifically, Mn has been implicated in parkinsonism and Huntington's disease, two neurodegenerative syndromes that show neuronal loss in the basal ganglia (Finkelstein *et al.* 2007, Lucchini *et al.* 2007, Williams *et al.* 2010, Gonzalez-Cuyar *et al.* 2013, Lechpammer *et al.* 2014).

Mn transport into the central nervous system has been well characterized at the level of the blood-brain barrier (BBB), consisting of facilitated and active transport through divalent metal transporter 1 (DMT1), transferrin receptor (TfR), ZIP8 (Rabin *et al.* 1993, Erikson *et al.* 2002, Garrick *et al.* 2003), and other transporters. However, the role of these and other metal transporters in neuronal Mn transport is not well understood (Tuschl *et al.* 2013). Indeed, while a number of transporters (e.g. SLC30A10, ATP13A2, SPCA1 and SPCA2)

63

contribute to Mn detoxification, and other transporters have been identified as contributing to Mn uptake (e.g. DMT1, ZIP8 and ZIP14), none of these are selective to Mn and most have been studied only under extracellular Mn concentrations well above the levels of brain Mn ($60\mu M$–$150\mu M$) associated with neurotoxicity *in vivo* (Tuschl *et al.* 2013, Bowman *et al.* 2014). Mn-specific binding proteins or signaling pathways responsive to physiological Mn concentrations have not been described.

Because optimal intracellular Mn concentrations likely change over developmental time and lineage, we postulated that neurons, and perhaps other cells, have cell-level homeostatic processes that regulate intracellular Mn content to cover cellular physiological demands while preventing cytotoxicity. Furthermore, utilization of distinct cellular Mn handling mechanisms may vary as physiological demand and availability of this co-factor change. Such regulatory processes may consist of similar mechanisms that have been identified for other essential metals (Zecca *et al.* 2004, Cousins *et al.* 2006, Choi *et al.* 2009), including: intracellular Mn sensors, Mn chaperones or storage proteins, and cell signaling systems with transcriptional and post-transcriptional control processes to regulate the balance of Mn across intracellular compartments. Identification of neuronal Mn handling processes has proven rather intractable by genetic and biochemical approaches, perhaps in part because phenotypes associated with insufficient or excess Mn are not clearly defined. We hypothesized that Mn handling mechanisms can be identified, and later studied, by using a novel chemical biology approach that relies on intracellular Mn levels as the outcome measure. To identify small molecules that modify cellular Mn content, we performed a high throughput screen for modifiers of intracellular Mn status under biologically relevant levels of Mn. We then utilized these small molecules to test the hypothesis that cellular mechanisms of Mn handling are developmentally regulated between the highly relevant human floor-plate lineage neuroprogenitors and their derivative mesencephalic dopaminergic neurons (Chun *et al.* 2001, Takeda 2003, Gitler *et al.* 2009).

Results

High throughput screen identifies small molecules for manipulating neuronal Mn status

Our laboratory had previously developed the Cellular Fura-2 Mn Extraction Assay (CFMEA) to enable rapid

fluorescent-based measurements of intracellular Mn content (Kumar *et al.* 2013). Here, we utilized CFMEA for

high throughput screening (HTS). The overall HTS approach consisted of pretreatment with the test small

molecule, followed by co-exposure to 125μM MnCl$_2$, representative of *in vivo* brain Mn levels at which aberrant

function would be observed(Bowman *et al.* 2014). An immortalized murine striatal neuron lineage

(STHdh$^{Q7/Q7}$) was used the HTS, as the striatum, like other structures of the basal ganglia, has a relatively high

basal Mn level and an especially high capacity for Mn accumulation (Kwakye *et al.* 2011, Kumar *et al.* 2013).

After the Mn and small molecule incubation period, extracellular Mn was washed away and CFMEA performed
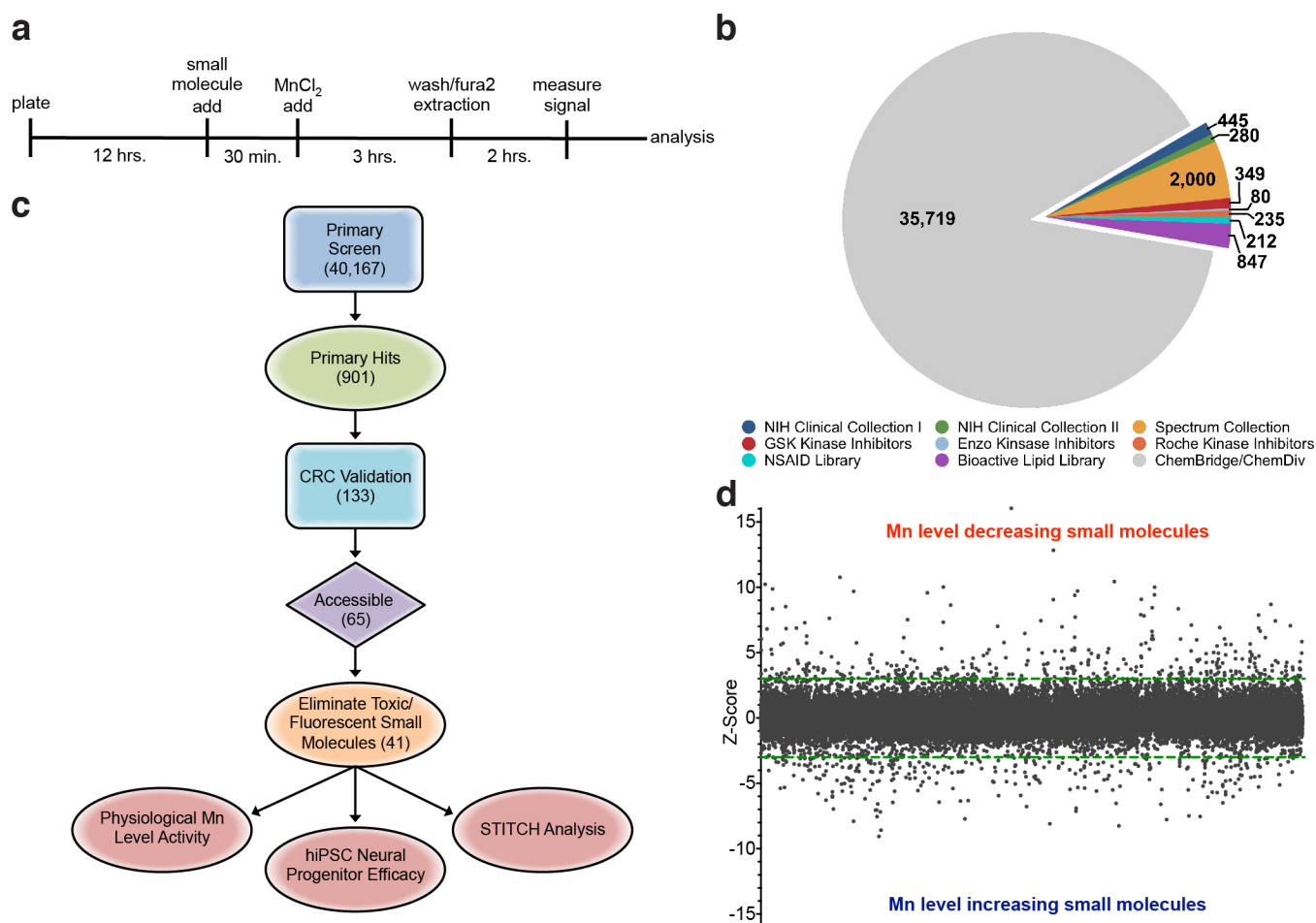
(**Figure 8A**).

Figure 8 – HTS identifies modulators of neuronal Mn status. (**a**) HTS screening protocol. Timeline of screening paradigm indicating cell plating, 10µM small molecule addition, Mn addition, washing, fura-2 extraction, signal measurement, and analysis. (**b**) Composition of 40,167 screened small molecules. Individual small molecule libraries are labeled and total compounds in that collection are indicated. (**c**) HTS paradigm. Each stage of the screen and number of compounds refined at that stage. (**d**) Scatterplot of primary screen. Z-score of each small molecule is indicated (n=1, per compound). A hit was defined as a small molecule with a z-score or b-score (not shown) cutoff of ± 3.0 or larger, as indicated by dotted line (**green**).

During optimization of the assay for 384-well format, we determined the major sources of intra-plate variability to be volumetric delivery of fura-2 extraction buffer. We developed a strategy to control for variability in delivered fura-2 by supplementing the fura-2 extraction buffer with a dextran-coupled fluorophore (Alexa-568) that does not interfere with fluorometric readings of fura-2. This enabled us to correct for variations in robotic volumetric delivery (achieving Z'>0.5) (**Figure 9**). These and other optimizations enabled detection of changes in fura-2 signal as low as 10%, corresponding to a z-score of ± 3.0.
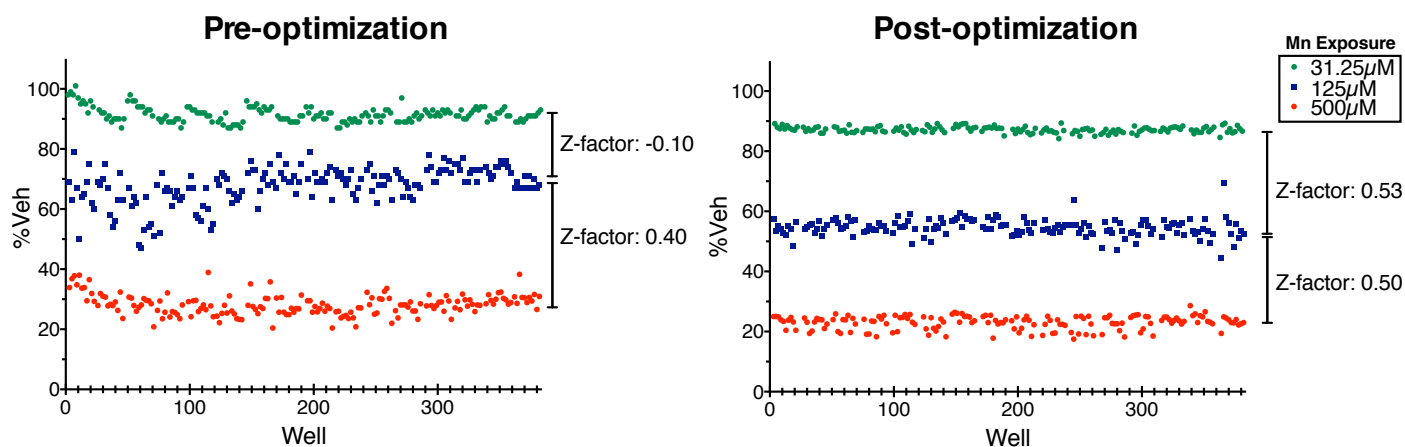
Figure 9 – Checkerboard assay HTS-CFMEA pre- and post-assay optimization using Alexa-568 to control for variability in volumetric delivery. Percent fluorescence is plotted relative to vehicle exposure (%Veh) by plate position (384-well format). Concentration of Mn exposure indicated in legend: 31.25µM (green), 125µM (blue), 500µM (red). Z-factor calculated by $Z = 1 - (3 \cdot SD_{concentration1} + 3 \cdot SD_{concentration2}) / |\mu_{conentration1} - \mu_{concentration2}|$. Z'≥0.5, bidirectionally was observed after optimization of assay conditions by controlling for volumetric delivery variance.

To comprehensively identify small molecules that modulate neuronal Mn levels, we screened a total of 40,167 small molecules spanning multiple chemical libraries (**Figure 8B**). Of these, 901 (2.2% hit rate) small molecules increased or decreased Mn levels (z-score or b-score > ±3.0) (**Figure 8C,D**). These hits were first validated by replication in duplicate followed by generation of 1nM-10µM concentration response curves (CRCs). A total of 133 small molecules (0.33%) passed these criteria, displaying a variety of potencies and patterns of activity (**Figure 10**).
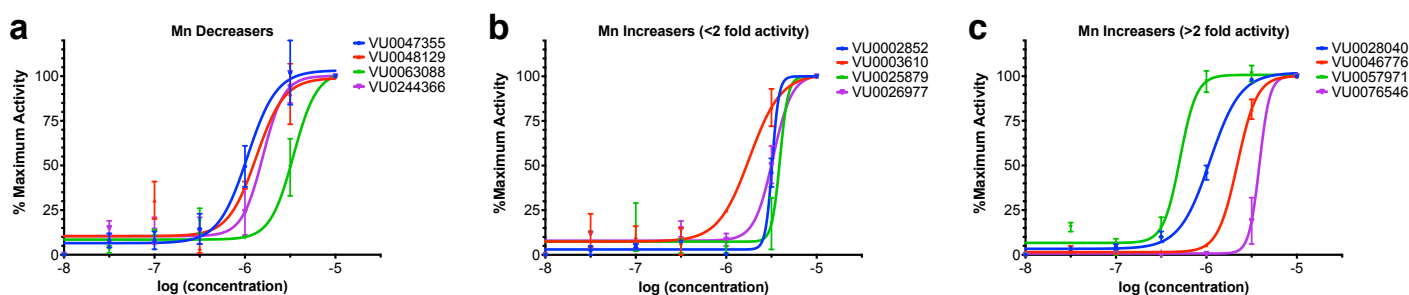
Figure 10 – Concentration response curves (CRCs) of primary screen hits. (**A**) Representative Mn decreasing small molecules CRCs plotted as percentage of maximum activity vs. log(concentration) of the indicated small molecule. (**B**) Representative Mn increasing small molecules CRCs with a less than two-fold effect size. (**C**) Representative Mn increasing small molecules CRCs with a greater than two-fold effect size. For all quantifications, data are mean ± SEM (n=2 per concentration). Convergence of curves was determined based on iteratively reweighted least squares analysis.

We then culled the toolbox of small molecules not readily obtainable from commercial or academic sources, leaving 65 for subsequent study. We further refined the toolbox by excluding fluorescent small molecules that could give false positive increases in fura-2 signal (**Figure 11**) and molecules that altered the number of cells under the conditions of the HTS screen due to cytotoxicity or other mechanisms (**Figure 12**).
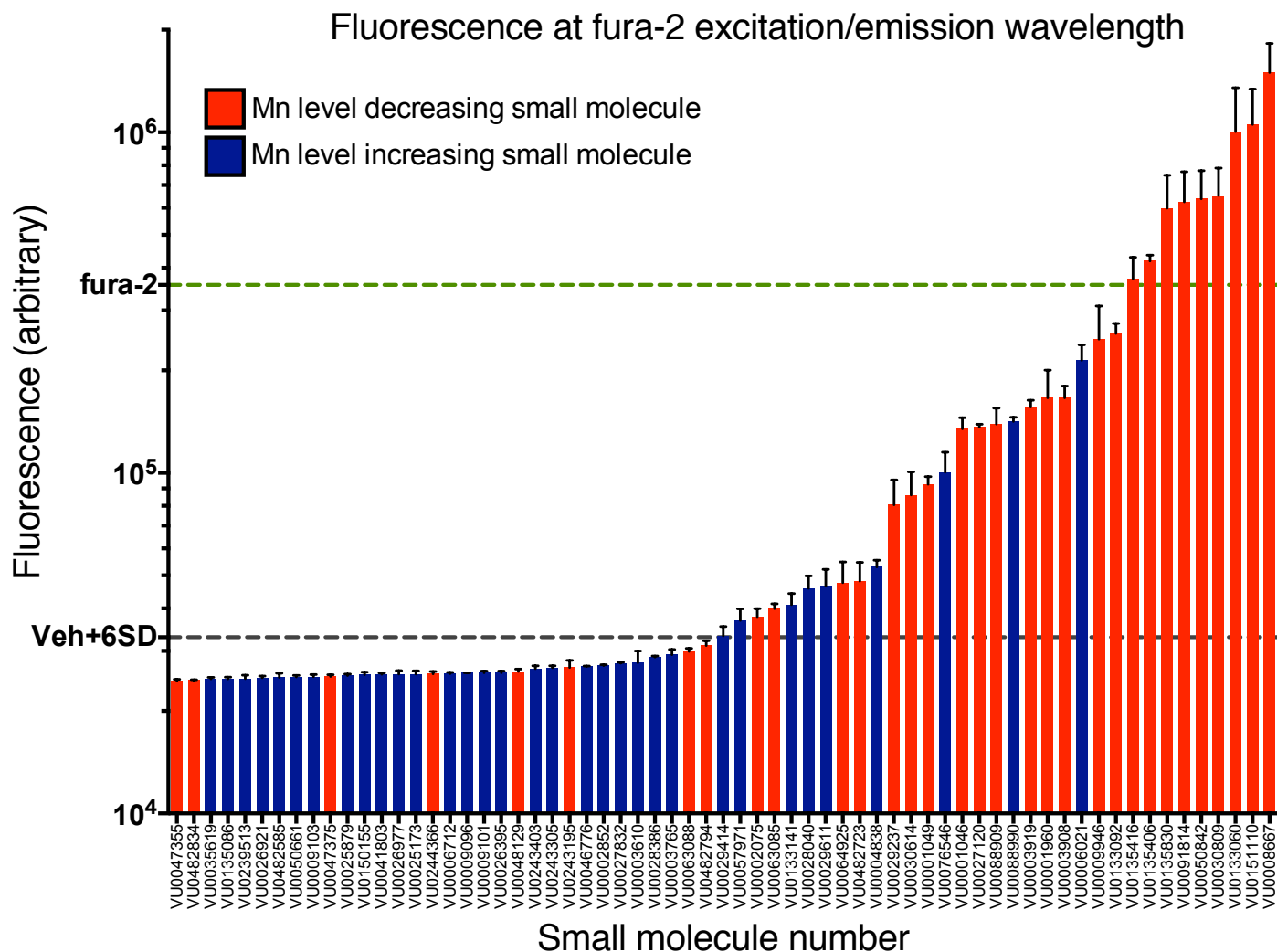
Figure 11 – Native fluorescence of validate small molecules at fura-2 excitation/emission wavelength used in CFMEA. Data plotted as raw fluorescence for each small molecule ordered by mean raw fluorescence (n=3). Small molecule activity is indicated; Mn level increasing small molecules (in **blue**), and Mn level decreasing small molecules (in **red**). Horizontal lines indicate the detection limit of fura-2 fluorescence (**green**), and fluorophore cutoff (**grey**). Threshold for fluorescent properties was based on culling Mn level decreasing small molecules (which are detected by an increase in fluorescence signal relative to the no small molecule plus Mn control, thus fluorescence could lead to a false-positive detection) with a mean raw fluorescence greater than the vehicle (DMSO) + 6SD. This statistical cutoff corresponds to Z'=0 suggested for a yes/no determination assay.
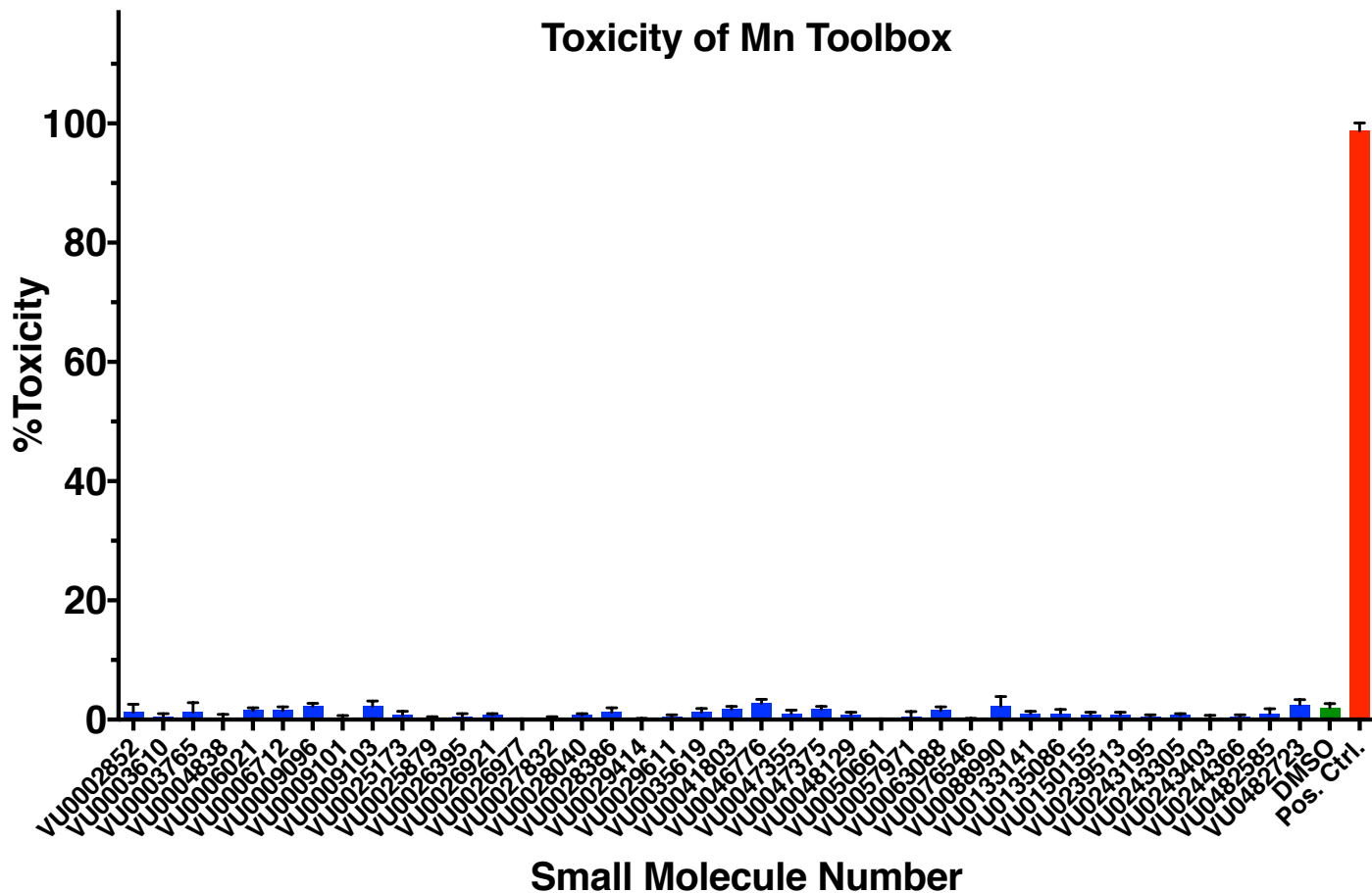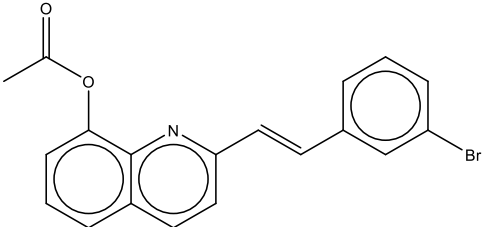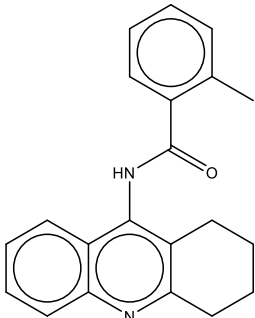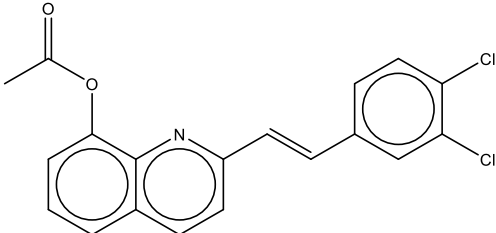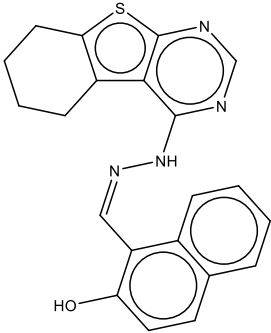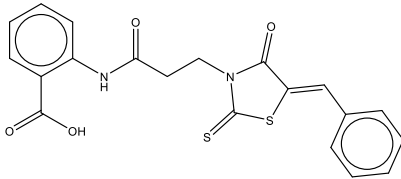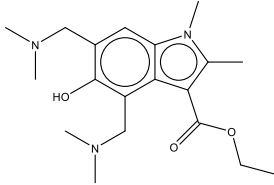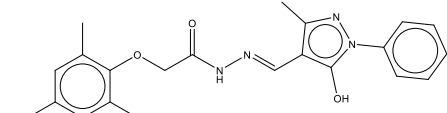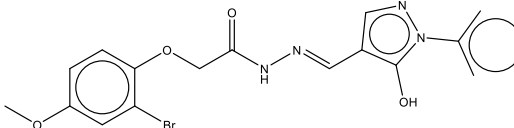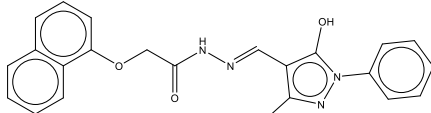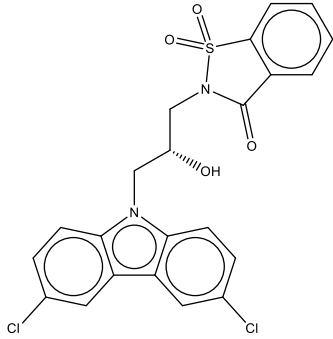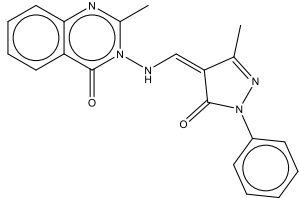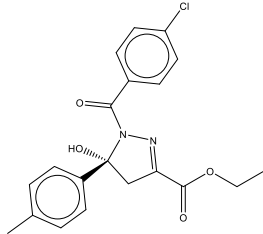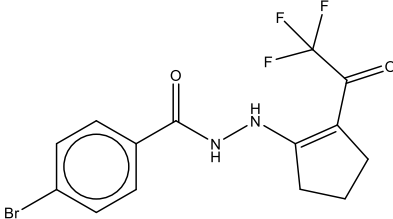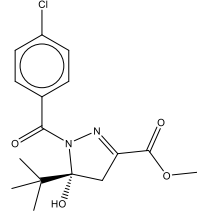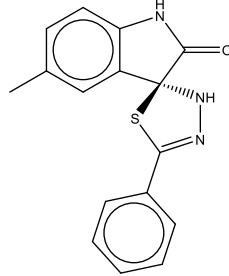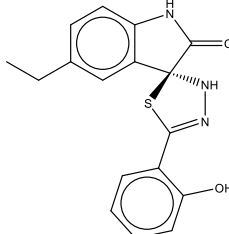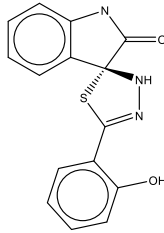
Figure 12 – Toxicity of small molecules in the Mn toolbox. Toxicity of small molecules within Mn toolbox (**blue**) reported as percentage +/- of the positive control fluorescence in the vehicle treated cells (**red**) (n=4). None of the small molecules tested exhibited a statistically significant change in total viable cells, measured by one-way ANOVA relative to the DMSO vehicle control (**green**) ($p<0.05$). Two molecules, VU0482834 and VU0482794 were not available at time of toxicity testing.
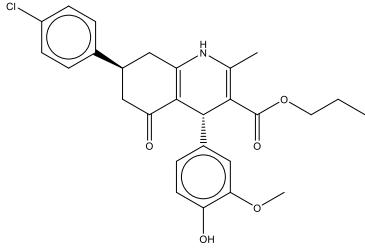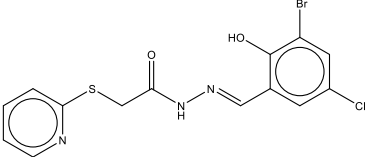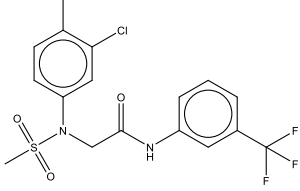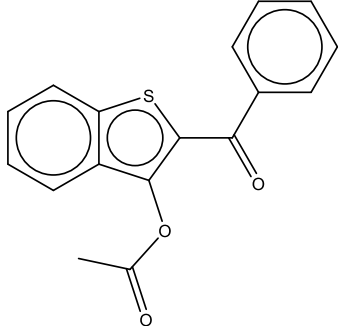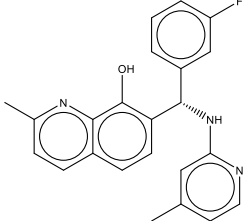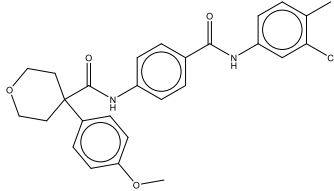
These validation and quality control measures resulted in a final Mn toolbox of 41 small molecules. The

functional properties of this toolbox consisted of significantly more Mn level increasing small molecules than

Mn level decreasing small molecules (**Table 5**) (Chi-square, $p<0.05$).
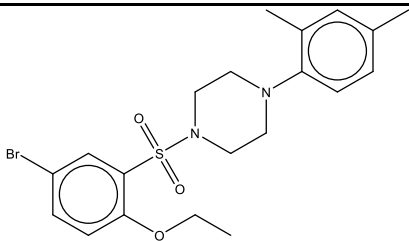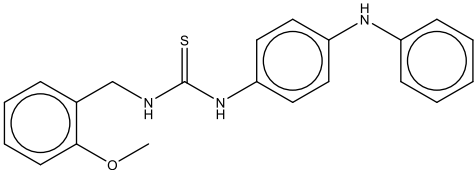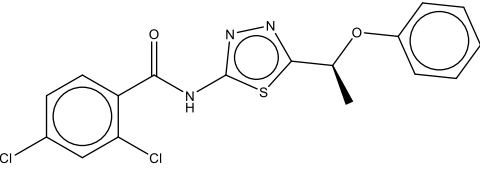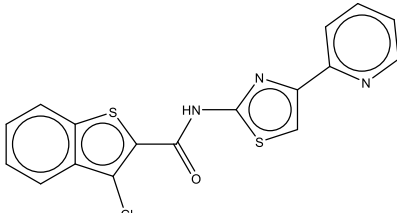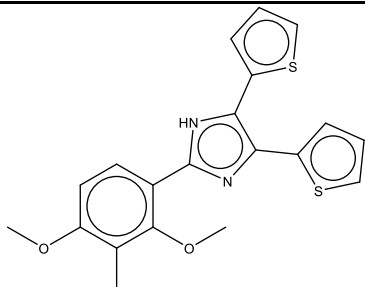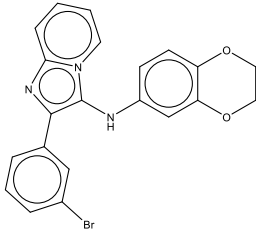
Table 5. Chemical structures of all 41 validated small molecules in the Mn toolbox. Data displayed include small molecule identity, chemical structures with IUPAC name, source small molecule library, direction of activity, and EC_{50} concentration.

Small Molecule	Structure	Library	Mn Activity	$\log EC_{50}$
VU0002852	 (*E*)-2-(3-bromostyryl)quinolin-8-yl acetate	ChemBridge /Div	Increase	-5.457
VU0003610	 2-methyl-*N*-(1,2,3,4-tetrahydroacridin-9-yl)benzamide	ChemBridge /Div	Increase	-5.752
VU0003765	 (*E*)-2-(3,4-dichlorostyryl)quinolin-8-yl acetate	ChemBridge /Div	Increase	-5.360
VU0004838	 (*Z*)-1-((2-(5,6,7,8-tetrahydrobenzo[4,5]thieno[2,3-*d*]pyrimidin-4-yl)hydrazono)methyl)naphthalen-2-ol	ChemBridge /Div	Increase	-5.687
VU0006021	 (*Z*)-2-(3-(5-benzylidene-4-oxo-2-thioxothiazolidin-3-yl)propanamido)benzoic acid	ChemBridge /Div	Increase	-5.454

70
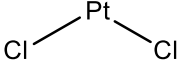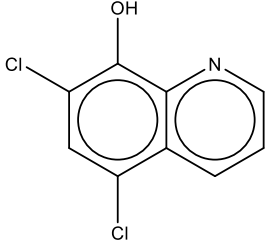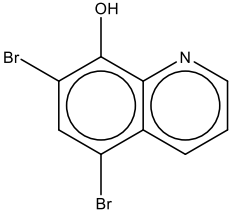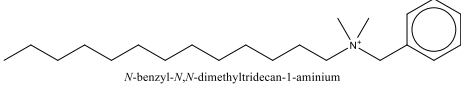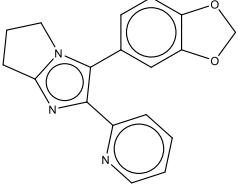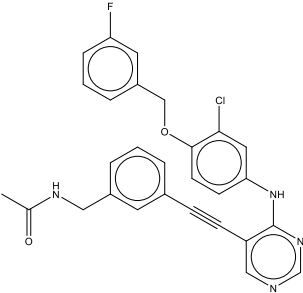
VU0006712	ethyl 4,6-bis((dimethylamino)methyl)-5-hydroxy-1,2-dimethyl-1*H*-indole-3-carboxylate	**ChemBridge/Div**	**Increase**	**-6.385**
VU0009096	(*E*)-2-(4-bromo-2,6-dimethylphenoxy)-*N'*-((5-hydroxy-3-methyl-1-phenyl-1*H*-pyrazol-4-yl)methylene)acetohydrazide	**ChemBridge/Div**	**Increase**	**-6.377**
VU0009101	(*E*)-2-(2-bromo-4-methoxyphenoxy)-*N'*-((5-hydroxy-3-methyl-1-phenyl-1*H*-pyrazol-yl)methylene)acetohydrazide	**ChemBridge/Div**	**Increase**	**-6.412**
VU0009103	(*E*)-*N'*-((5-hydroxy-3-methyl-1-phenyl-1*H*-pyrazol-4-yl)methylene)-2-(naphthalen-1-yloxy)acetohy	**ChemBridge/Div**	**Increase**	**-6.294**
VU0025173	(*R*)-2-(3-(3,6-dichloro-9*H*-carbazol-9-yl)-2-hydroxypropyl)benzo[*d*]isothiazo	**ChemBridge/Div**	**Increase**	**-6.834**
VU0025879	(*Z*)-2-methyl-3-(((3-methyl-5-oxo-1-phenyl-1,5-dihydro-4*H*-pyrazol-4-ylidene)methyl)amino)quin 4(3*H*)-one	**ChemBridge/Div**	**Increase**	**-5.416**

VU0026395		ChemBridge /Div	Increase	-5.723
	ethyl (*R*)-1-(4-chlorobenzoyl)-5-hydroxy-5-(*p*-tolyl)-4,5-dihydro-1*H*-pyrazole-3-carboxylate			
VU0026921		ChemBridge /Div	Increase	-5.638
	4-bromo-*N'*-(2-(2,2,2-trifluoroacetyl)cyclopent-1-en-1-yl)benzohydra			
VU0026977		ChemBridge /Div	Increase	-5.451
	methyl (*R*)-5-(*tert*-butyl)-1-(4-chlorobenzoyl)-5-hydroxy-4,5-dihydro-1*H*-pyrazole-3-carboxylate			
VU0027832		ChemBridge /Div	Increase	-5.834
	(*S*)-5-methyl-5'-phenyl-3'*H*-spiro[indoline-3,2'-[1,3,4]thiadiazol]-2-one			
VU0028040		ChemBridge /Div	Increase	-5.920
	(*S*)-5-ethyl-5'-(2-hydroxyphenyl)-3'*H*-spiro[indoline-3,2'-[1,3,4]thiadiazol]-2-one			
VU0028386		ChemBridge /Div	Increase	-7.043
	(*R*)-5'-(2-hydroxyphenyl)-1-methyl-3'*H*-spiro[indoline-3,2'-[1,3,4]thiadiazol]-2-one			

VU0029414	propyl (4*R*,7*S*)-7-(4-chlorophenyl)-4-(4-hydroxy-3-methoxyphenyl)-2-methyl-5-oxo-1,4,5,6,7,8-hexahydroquinoline-3-carboxylate	**ChemBridge/Div**	**Increase**	**-5.927**
VU0029611	(*E*)-*N*'-(3-bromo-5-chloro-2-hydroxybenzylidene)-2-(pyridin-2-ylthio)acetohydrazide	**ChemBridge/Div**	**Increase**	**-5.078**
VU0035619	2-(*N*-(3-chloro-4-methylphenyl)methylsulfonamido)-*N*-(3-(trifluoromethyl)phenyl)acetamide	**ChemBridge/Div**	**Increase**	**-6.338**
VU0041803	2-benzoylbenzo[*b*]thiophen-3-yl acetate	**ChemBridge/Div**	**Increase**	**-5.706**
VU0046776	(*S*)-7-((3-fluorophenyl)((4-methylpyridin-2-yl)amino)methyl)-2-methylquinolin-8-ol	**ChemBridge/Div**	**Increase**	**-5.629**
VU0047355	*N*-(4-((3-chloro-4-methylphenyl)carbamoyl)phenyl)-4-(4-methoxyphenyl)tetrahydro-2*H*-pyran-4-carboxamide	**ChemBridge/Div**	**Decrease**	**-5.968**

VU0047375	1-((5-bromo-2-ethoxyphenyl)sulfonyl)-4-(2,4-dimethylphenyl)piperazine	ChemBridge/Div	Decrease	-5.917
VU0048129	1-(2-methoxybenzyl)-3-(4-(phenylamino)phenyl)thiourea	ChemBridge/Div	Decrease	-5.899
VU0050661	(*S*)-2,4-dichloro-*N*-(5-(1-phenoxyethyl)-1,3,4-thiadiazol-2-yl)benzamide	ChemBridge/Div	Increase	-6.677
VU0057971	3-chloro-*N*-(4-(pyridin-2-yl)thiazol-2-yl)benzo[*b*]thiophene-2-carboxamide	ChemBridge/Div	Increase	-6.286
VU0063088	2-(2,4-dimethoxy-3-methylphenyl)-4,5-di(thiophen-2-yl)-1*H*-imidazole	ChemBridge/Div	Decrease	-5.501
VU0076546	2-(3-bromophenyl)-*N*-(2,3-dihydrobenzo[*b*][1,4]dioxin-6-yl)imidazo[1,2-*a*]pyridin-3-amine	ChemBridge/Div	Increase	-5.370

74

VU0088990		**ChemBridge /Div**	**Decrease**	**-7.271**
(*R*)-*sec*-butyl (4*R*,7*S*)-7-(4-chlorophenyl)-4-(2-methoxyphenyl)-2-methyl-5-oxo-1,4,5,6,7 hexahydroquinoline-3-carboxylate				
VU0133141		**ChemBridge /Div**	**Increase**	**-5.744**
(*S*)-5'-(2-hydroxyphenyl)-3'*H*-spiro[indoline-3,2'-[1,3,4]thiadiazol]-2-one				
VU0135086		**ChemBridge /Div**	**Increase**	**-5.332**
(*S*)-(2-hydroxy-3,5-diisopropylphenyl)(5-hydroxy-3-methyl-5-(trifluoromethyl)-4,5-dihydro-1*H*-pyrazol-1-yl)methanone				
VU0150155		**ChemBridge /Div**	**Increase**	**-7.274**
3-butyramido-4-((4-chlorophenyl)sulfonyl)-*N*-cycloheptylbenzamide				
VU0239513		**Spectrum Collection**	**Increase**	**-5.324**
5,7-diiodoquinolin-8-ol				

VU0243195	platinum(II) chloride	**Spectrum Collection**	**Decrease**	**-5.610**
VU0243305	5,7-dichloroquinolin-8-ol	**Spectrum Collection**	**Increase**	**-5.713**
VU0243403	5,7-dibromoquinolin-8-ol	**Spectrum Collection**	**Increase**	**-5.747**
VU0244366	*N*-benzyl-*N*,*N*-dimethyltridecan-1-aminium	**Spectrum Collection**	**Decrease**	**-5.808**
VU0482585	3-(benzo[*d*][1,3]dioxol-5-yl)-2-(pyridin-2-yl)-6,7-dihydro-5*H*-pyrrolo[1,2-*a*]imidazole	**GSK Published Kinase Inhibitor Set**	**Increase**	**-4.082**
VU0482794	*N*-(3-((4-((3-chloro-4-((3-fluorobenzyl)oxy)phenyl)amino)pyrimidin-5-yl)ethynyl)benzyl)acetamide	**GSK Published Kinase Inhibitor Set**	**Decrease**	**-4.546**
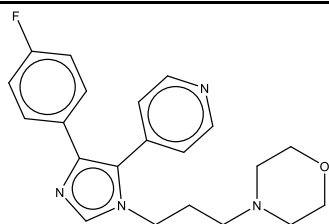
VU0482834	4-(3-(4-(4-fluorophenyl)-5-(pyridin-4-yl)-1*H*-imidazol-1-yl)propyl)morpholine	**GSK Published Kinase Inhibitor Set**	**Decrease**	**-8.634**

Given the tendency of small molecules from pharmacological screens to inhibit (antagonistic) rather than enhance (agonistic) the function of their biological target (Austen *et al.* 2005), this skewing toward Mn level increasing small molecules suggests Mn efflux mechanisms are more susceptible to pharmacological disruption than mechanisms of Mn influx.

High structural diversity of validated small molecules

We generated a heat map of pairwise Tanimoto coefficients (**Figure 13**), a measure of chemical structure similarity, using an upper triangle distance matrix considering largest common substructure between two molecules. As the majority of our identified small molecules have no known biological targets, we sought to reveal potential relationships between their chemical structure by performing hierarchical agglomerative clustering using complete linkage to generate functional dendrograms.
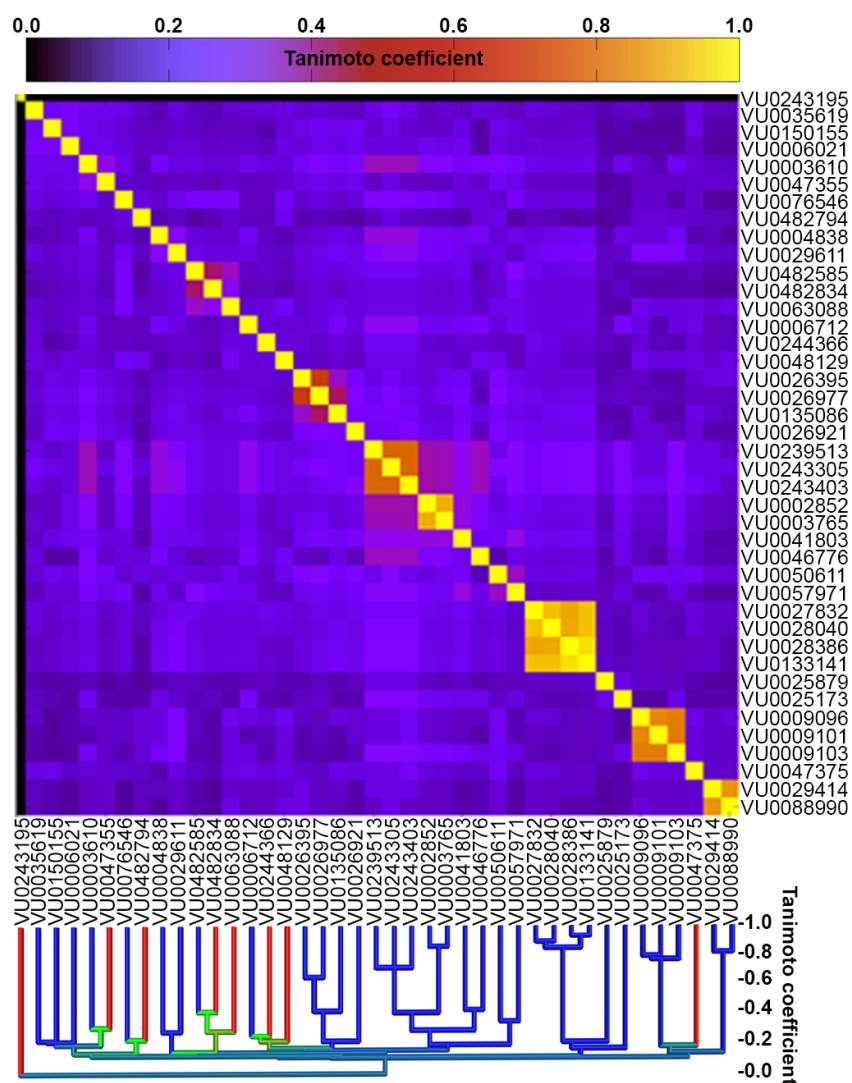
Figure 13 – Structure activity dendrogram and Tanimoto plot of Mn toolbox. Functional dendrogram with clustering based on chemical similarity as determined by Tanimoto score (1=identical, 0=unique). Small molecule activity pattern per node is indicated by color: Mn level decreasing small molecules (**red**), Mn level increasing small molecules (**blue**), and mixed activity (**green**). Compound Tanimoto scores for each small molecule were plotted across all compounds in the Mn toolbox represented by heat map.

This analysis revealed a high degree of structural diversity, with an average pairwise Tanimoto coefficient of 0.19, where a 1.0 translates to identical compounds and a 0.0 to compounds that have no common substructure. While three clusters of 2-4 similar molecules (Tanimoto coefficients >0.8) exist, most had little structural similarity with other active molecules (Tanimoto coefficient <0.5) (Maggiora *et al.* 2014). This finding suggests that the screen did not identify the complete range of structure-activity relationships, likely reflecting both the diversity of biological targets that influence cellular Mn status, as well as the potential of diverse

structures to influence common targets. The identified small molecule clusters all had Mn level increasing activity (Cluster 1 (VU0002852 and VU0003765), Cluster 2 (VU0088990, VU0029414), Cluster 3 (VU0027832, VU0028040, VU0028386, VU0133141)).

Activity of small molecules at normal brain Mn levels

In the screen, small molecules were identified using a concentration of Mn associated with mammalian neurotoxicity *in vivo* (125µM). Subsequently, we sought to assess the Mn modifying activity of these small molecules under normal brain Mn levels. Although *in vivo* concentrations of Mn may not directly translate to *in vitro* exposures, it has been shown that normal levels of human brain Mn range from 20µM to 53µM (Bowman *et al.* 2014). Thus, we tested for activity at 31.25µM Mn, a four-fold dilution from the concentration used in the primary screen, that is also just above the minimum limit of Mn detection by CFMEA. The vast majority of small molecules (39/41, 95%) exhibited Mn-modifying activity at this Mn concentration (**Figure 14**).
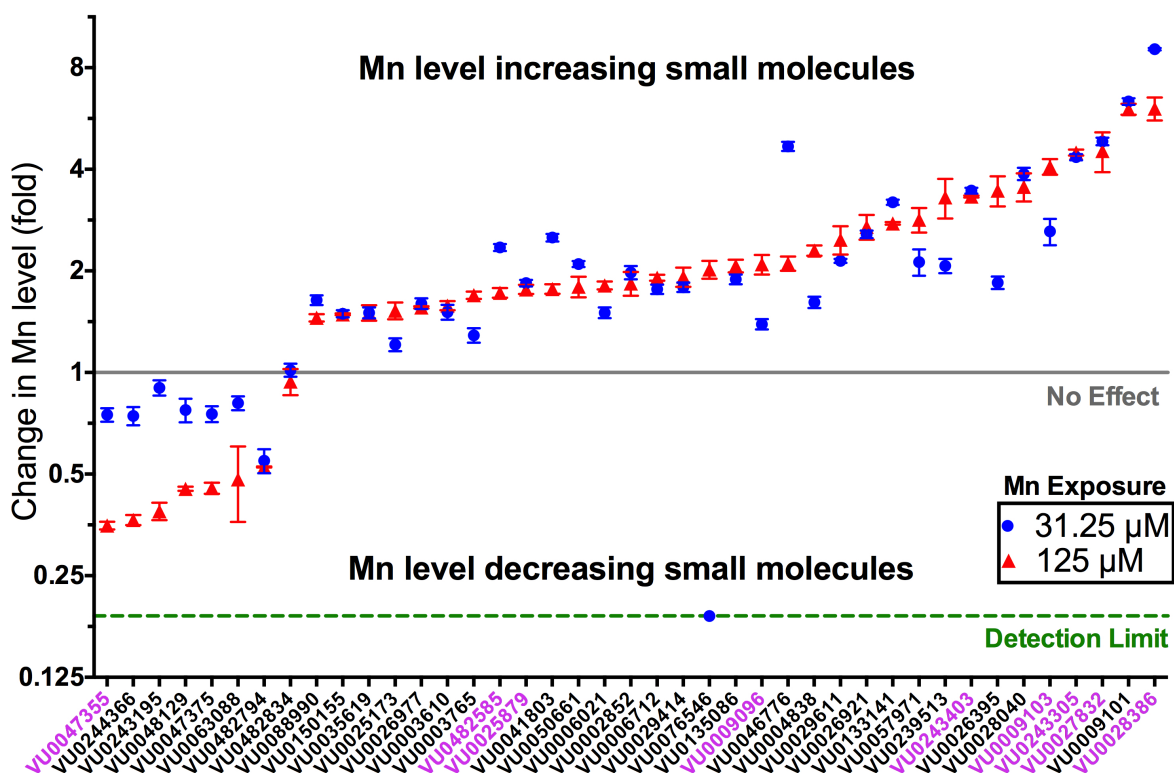
Figure 14 – Activity of validated small molecules at physiological and toxicological Mn exposures. Fold change in Mn levels at both 31.25μM (**blue**) and 125μM (**red**) MnCl$_2$ is plotted versus small molecule identity. Small molecules tested in hiPSC-derived mesencephalic floor plate neuroprogenitors and post-mitotic neurons are marked in (**purple**). 'NS' indicates small molecules that do not show significant activity for 31.25μM concentration. Horizontal lines indicate the detection limit of CFMEA (**green**), and no effect on Mn levels (**grey**). Data plotted as mean ± SEM (n=16 for 31.25μM, n=2 for 125μM). Statistical significance (all not marked by NS) was determined by comparing small molecule versus vehicle by one-way ANOVA, p<0.05.

There was considerable variation in effect size between our high and low Mn exposure conditions, with some small molecules having greater activity (fold change of Mn) at 125μM Mn and others having greater activity at 31.25μM Mn. Two molecules failed to have significant activity at 31.25μM (VU0243195 and VU0482834). One molecule, VU0076546, had a unique pattern of activity, increasing intracellular neuronal Mn levels at the high Mn concentration, but strongly decreasing intracellular Mn levels at the lower Mn concentration.

Chemical informatics reveals common pathways among predicted targets

We performed a chemical informatics analysis of the 41 small molecule toolbox to identify potential biological targets. In order to reveal functional relationships between small molecules, we aggregated information regarding known targets of each molecule and its similar chemical homologs (Tanimoto coefficient >0.7). The structures of the entire Mn toolbox were inputted into STITCH 4.0 analysis generating two major signaling node clusters, with only 5 of the 41 chemicals having structural homologs with known or suspected biological activity. VU0482585, VU0239513, VU0482834, and VU0243195 exhibited multi-nodal interactions with a network comprised of mitogen-activated protein kinase 14 (MAPK14), transforming growth factor beta receptor I (TGFBR1), glutathione S-transferase P (GSTP1), superoxide dismutase 1 (SOD1), copper-transporting ATPase 1 (ATP7A), ATP-binding cassette sub-family C member 2 (ABCC2), and ATP-binding cassette sub-family G member 2 (ABCG2) (**Figure 15A**). These predicted interactions were further supported by the fact that VU0482585 and VU0482834 were from the GSK Published Kinase Inhibitor Set (Drewry *et al.* 2014), suggesting a mechanism related to kinase inhibition or disruption of ATP-dependent transporters. In addition, homologs of VU0003610 have known binding to butyrylcholinesterase (BCHE) and acetylcholinesterase (ACHE) (**Figure 15B**).
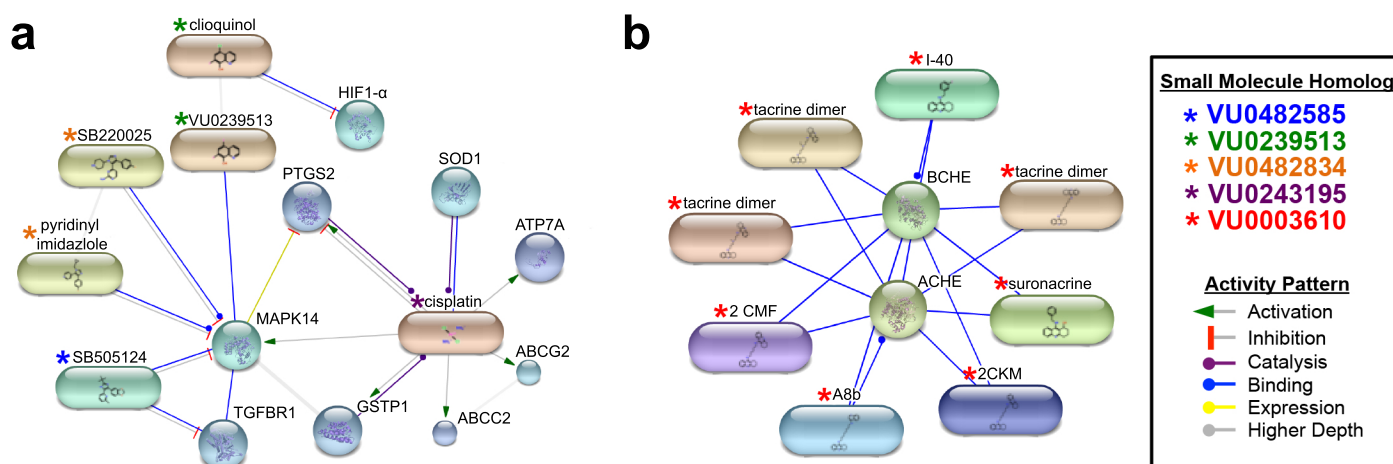
Figure 15 – Chemical informatics analysis of Mn toolbox. (A,B) STITCH analysis of Mn toolbox small molecules. Each node represents a small molecule or target protein. Color coded asterisk indicates corresponding small molecule or small molecule homolog (Tanimoto score > 0.7) validated in the HTS, identified in the legend. Color of connections between nodes indicates known function and description of the type of evidence available: activation (**green**), inhibition (**red**), binding (**blue**), catalysis (**purple**), and expression (**yellow**).

While these findings provide some insight into potential biological targets, the majority of our identified small molecules, and their close chemical homologs, do not have other published biological activities. This suggests that the neuronal Mn status modifying activity of our validated small molecules is relatively specific since such structures have not been identified in other published screens performed on the same publically available chemical libraries.

Differential regulation of Mn handling in developing mesencephalic dopaminergic neurons

We hypothesized that small molecules in our Mn-modifying chemical toolbox would exhibit differential activity across neurodevelopmental time as the biological requirements for Mn change. We tested this hypothesis in developing human mesencephalic (floor plate lineage) dopaminergic neurons, given this lineage's particular susceptibility to Mn toxicity and involvement in neurodegenerative syndromes such as parkinsonism (Chun *et al.* 2001, Takeda 2003, Gitler *et al.* 2009). Human induced pluripotent stem cells (hiPSCs) generated from a control subject were differentiated into FOXA2+, LMX1A+ floor-plate lineage neuroprogenitors (12

days differentiation) and further to Tyrosine hydroxylase (TH)+, β3-Tubulin+, LMX1A+ post-mitotic early

dopaminergic neurons (26 days differentiation) (**Figure 16A**). Mn handling was quantified by CFMEA

following 125μM MnCl$_2$ exposure (Okita *et al.* 2008, Kriks *et al.* 2011). Early dopaminergic neurons (day 26)

accumulated significantly ($p<0.05$) more intracellular Mn than the more immature floor plate neuroprogenitors

(day 12) (**Figure 16B**).
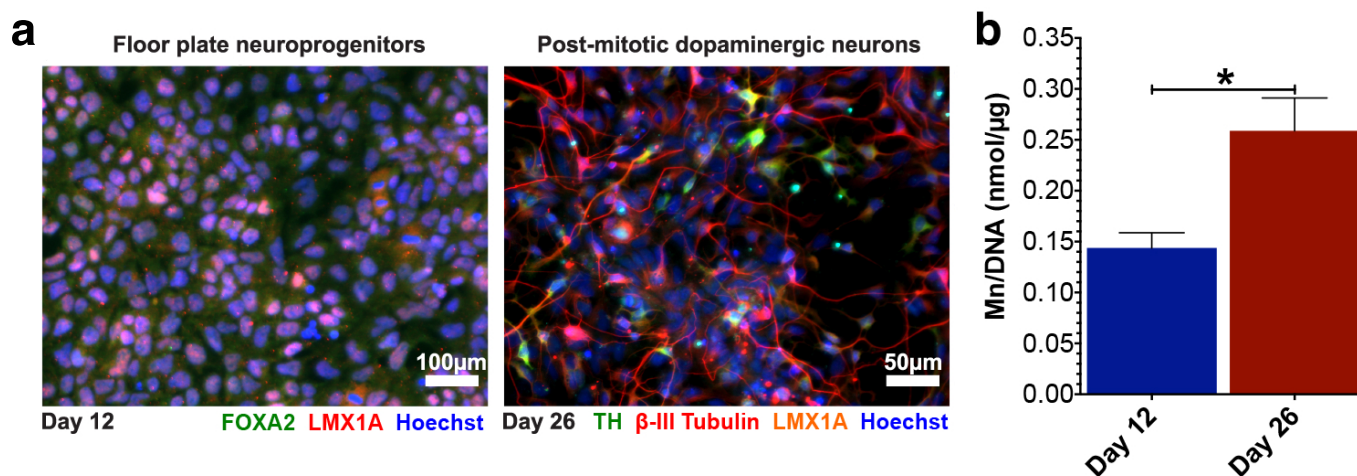
Figure 16 – Mn accumulation changes across developmental time in mesencephalic floor-plate neuroprogenitors and/or post-mitotic dopaminergic neurons. (**a**) Immunocytochemistry of day 12 floor plate neuroprogenitors and day 26 post-mitotic dopaminergic neurons. Appropriate developmental stage markers indicated by legend. (**b**) Mn accumulation in day 12 and day 26 neuroprogenitors after Mn exposure (125μM). Data is expressed as Mn/DNA (nmol/μg) versus developmental time point. Data are mean ± SEM (n=3). Statistical significance by one-way ANOVA (*$p<0.05$).

Nine small molecules of varying structures and effect sizes were selected to evaluate their activity in this human

system and test for potential developmental stage specificity. All tested small molecules (9 of 9) showed

activity in hiPSC-derived mesencephalic dopaminergic neuroprogenitors (one-way ANOVA, $p<0.001$). Three

of the small molecules (3 of 9, 33%) showed similar magnitude of activity at both neurodevelopmental time

points (**Figure 17A-C**). Four of the small molecules (4 of 9, 44%) exhibited greater activity in floor plate

neuroprogenitors than post-mitotic dopaminergic neurons (**Figure 17D-G**). Finally, two small molecules

showed developmental-stage specific activity (2 of 9, 22%) (**Figure 17H,I**). VU0047355, a negative modulator

of Mn concentration, and VU0482585, a positive modulator of Mn concentration, exhibited a significant impact

on intracellular Mn levels exclusively in the more mature dopaminergic neurons, the developmental time point with the highest Mn accumulation between the two stages of differentiation (**Figure 17H,I**). These results demonstrate that the validated small molecules act on developmentally regulated targets involved in control of intracellular neuronal Mn handling.
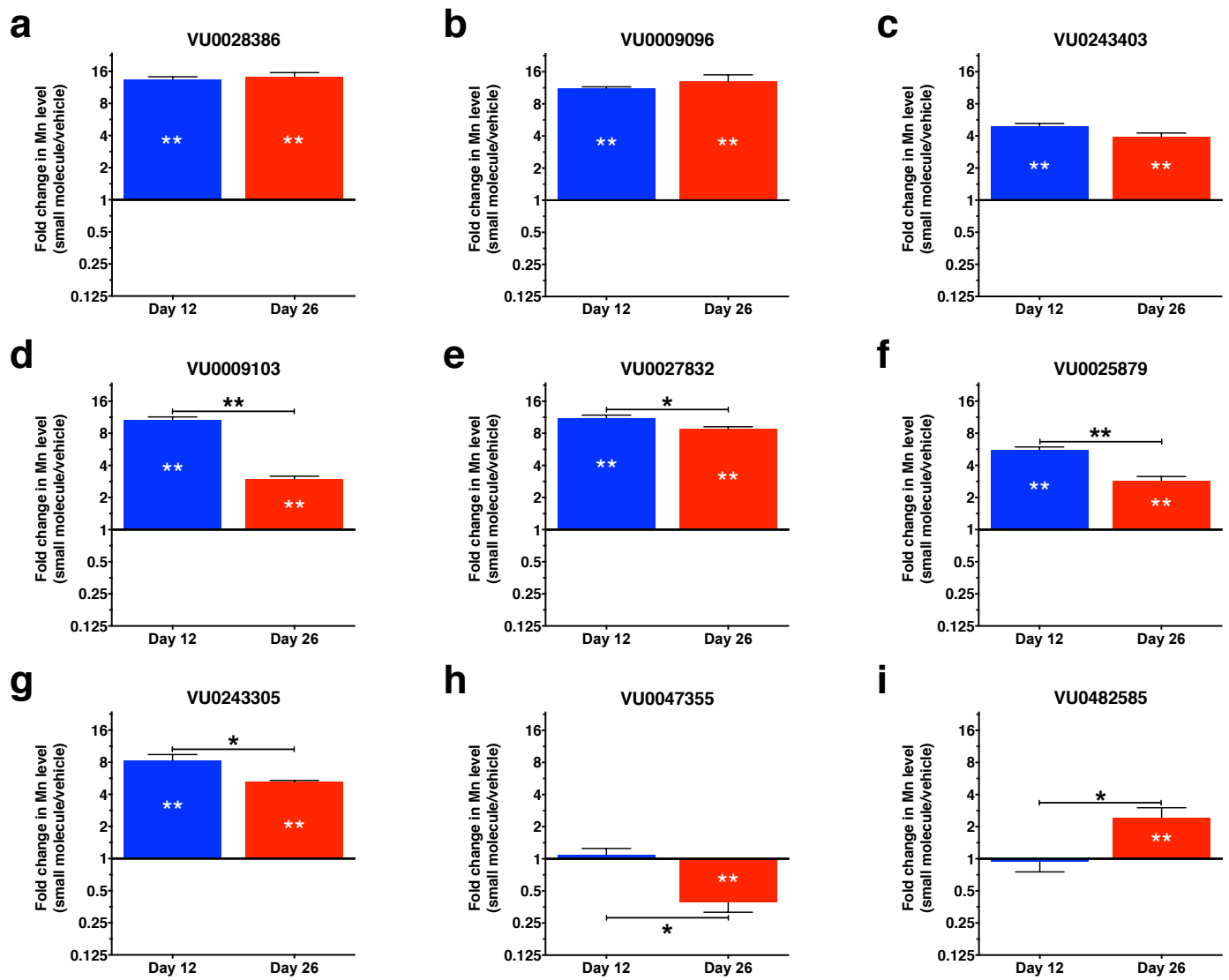
Figure 17 – Mn toolbox is effective in hiPSC-derived mesencephalic floor-plate neuroprogenitors and/or post-mitotic dopaminergic neurons. (A-I) Activity of selected small molecules at indicated neurodevelopmental stage. Data is expressed as fold change in Mn level of small molecule versus vehicle at indicated developmental time point. Data are mean ± SEM (n=3). Statistical significance by one-way ANOVA (small molecule versus vehicle) is indicated by white asterisks within the colored bars of the graph, and significance by unpaired t-test (day 12 versus day 26) is indicated by asterisks above the brackets between the compared bars; (*p<0.05, **p<0.001).

Discussion

HTS technology permits the rapid testing of thousands of small molecules for their impact on a particular biological system (Inglese *et al.* 2007, Macarron *et al.* 2011). Our application of HTS is distinct from the more typical HTS approaches targeting specific proteins or enzymatic processes. Our approach would thus be expected to lead to a larger number of potential biological targets, increasing the probability of finding true hits over traditional screens with only one or a few targets. The CFMEA high throughput screen identified a chemically diverse toolbox of 41 small molecules that increase or decrease intracellular Mn levels. Despite testing 40,167 small molecules, only a few chemical structural similarity clusters were identified, suggesting we likely did not identify the complete range of structure-activity relationships that influence cellular Mn status. The vast majority (39/41) of small molecules in the Mn toolbox retained activity at low Mn concentrations, representative of normal brain Mn levels (Bowman *et al.* 2014). This conservation of activity at healthy Mn levels suggests that the majority of our small molecules target homeostatic processes mediating normal neuronal Mn content, rather than those functioning only under toxicological concentrations.

We have examined potential structure-function relationships by employing a chemical informatics approach to characterize the validated small molecules. Information was found regarding functional targets for five of the 41 small molecules, implicating a major signaling pathway with known links to Mn biology. For example, MAPK14 (p38-α) has been shown to activate in cells responding to cytotoxic levels of Mn, 250μM Mn or higher (Hirata *et al.* 2004, Bae *et al.* 2006). Excessive Mn can increase oxidative stress, COX-2 expression, and glutathione depletion (Zhang *et al.* 2007). VU0482585, identified by STITCH analysis (**Figure 15A**) as a potential inhibitor of the MAPK14, has confirmed Mn level increasing activity in post-mitotic human dopaminergic neurons (**Figure 15B**). Together, these data suggest a potential link between the MAPK14 signaling pathway and control of neuronal Mn content under conditions of excess Mn. The identification of ABCC2 and ABCG2 as putative targets is also noteworthy given their role in unidirectional efflux of toxic

substances and known expression in stem cell like populations (Patrawala *et al.* 2005, Nies *et al.* 2007). Aside from these putative signaling protein targets, our chemical structure associations implicated interactions with enzymes involved in neurotransmission, ACHE and BCHE, consistent with cholinergic disruption occurring with Mn exposure (Finkelstein *et al.* 2007, Santos *et al.* 2012). These and other functional leads suggest our chemical toolbox has high utility for future studies aimed at identifying mechanisms underlying Mn neurobiology.

We tested the hypothesis that mechanisms regulating intracellular Mn content are developmentally regulated in differentiating dopaminergic neurons, given their known susceptibility to Mn toxicity in the context of parkinsonism (Olanow 2004, Kumar *et al.* 2012). This work provides compelling evidence for the developmental regulation of cellular Mn content, as six of the nine small molecules tested showed significant differences in activity between post-mitotic dopamine neurons and floor plate lineage neuroprogenitors (**Fig. 17D-I**). Furthermore, our data demonstrate the existence of cellular-based Mn handling processes, as pharmacological modes of action acting directly on the Mn ion (e.g. as an ionophore or metal chelator) would not be expected to display developmental stage specific activity. High evolutionary conservation of Mn handling targets is also strongly suggested by the fact that 9 of 9 tested small molecules identified via a mouse neuronal model showed activity in a human neuronal model system. The fact that the small molecules identified with stage-specific activity included both Mn level increasing and Mn level decreasing small molecules suggests that processes capable of responding to both insufficient and excess Mn are utilized to achieve optimal cellular Mn content.

In summary, we utilized a chemical biology approach to develop a highly diverse small molecule toolbox of neuronal Mn content modifiers. This Mn toolbox is comprised of small molecules capable of modulating intracellular Mn levels under both physiological and toxicological conditions. Biochemical informatics analysis has implicated modulation of cellular signaling pathways with intriguing links to Mn biology and human

disease. The identified small molecules exhibit activity in a clinically relevant human dopaminergic neuronal lineage. Furthermore, we report strong evidence for the regulation of intracellular Mn levels over human neurodevelopment. The collection of small molecules described here is the most complete, publically available, resource for interrogation of Mn handling processes and provides a template for development of therapeutic agents for neurological disorders associated with disruption of Mn homeostasis.

Materials and Methods

High throughput screening

CFMEA was optimized for HTS to detect both Mn level increasing and decreasing small molecules of neuronal Mn status in mammalian cells. Checkerboard assays, using either 500μM or 31.25μM $MnCl_2$ as a positive control relative to the 125μM $MnCl_2$ used as the baseline Mn exposure condition, confirmed Z'>0.5 in both directions (Zhang *et al.* 1999) and enabling a robust screen in 384-well format (**Figure 9**). Quality controls were included on each plate for normalization on a plate-by-plate basis. Wild-type StHdh$^{Q7/Q7}$ immortalized murine striatal cells were plated at a density of 3,000 cells per 384-well 16 hours prior to assay start time. Media was removed and the cells washed by ELX405 Microplate Washer (Bio-Tek) with 1X Hank's-Balanced Salt Solution (HBSS) with calcium and magnesium (Corning) prior to application of 20μL of 1.5X (15μM) small molecule in HBSS. Plates were incubated for 30 minutes at 37°C, and 10μL of 3X (375μM) $MnCl_2$ in HBSS was applied leading to a final concentration of 125μM $MnCl_2$ and a nominal concentration of 10μM for the small molecule to be tested. Liquid deliveries were made using a Velocity 11 Bravo liquid handler (Agilent). Plates were incubated for 3 hours at 37°C. Incubation was terminated by a five cycle wash and plate blotting to remove any residual volume. CFMEA was performed by adding 30μL fura-2 extraction buffer (0.1% Triton-X100, 0.5μM fura-2 ultra pure (Enzo Life Sciences), 100μM Dextran Alexa-Fluor 568 (Life Technologies) was loaded by Multidrop Combi Reagent Dispenser (Thermo Scientific). Plates were then incubated for two hours at

37°C and read using FITC filters, 350/25nm (excitation) and 525/25nm (emission) for fura-2, and 545/25nm (excitation) and 620/30nm (emission) for Alexa 568, by EnVision Multilabel Reader (Perkin Elmer). Data was analyzed with Pipeline Pilot (Acellrys) and Microsoft Excel. Hits were identified in the single point primary screen by z-score and b-score approaches (Brideau *et al.* 2003), then confirmed by duplicate experimental replicates. CRCs were generated by iteratively reweighted least squares, allowing determination of convergence and EC_{50} (Street *et al.* 1988, Rousseeuw *et al.* 2002). Native fluorescence of small molecules was assessed by measurement of 0.5µM of the test small molecule (or 0.5µM fura-2 as a positive control) at the same excitation and emission wavelengths used for CFMEA. Fluorescence of each small molecule was compared to +6 S.D. above the DMSO negative control. Cytotoxicity was evaluated by CellTox Green cytotoxicity assay (Promega) under identical conditions as the HTS paradigm. After this period, the CellTox Green dye was added and signal was measured using, monochromatic wavelengths 500nm (excitation) and 523nm (emission) using EnSpire Multimode Plate Reader (Perkin Elmer). Toxicity determination included lysed cells as a positive control. Small molecule libraries included collections from NIH Clinical Collection I/II, Microsource Spectrum Collection, kinase inhibitors from GlaxoSmithKline, Enzo Life Sciences, and Roche, Vanderbilt non-steroidal anti-inflammatory library (NSAIDs), Vanderbilt bioactive lipid library, ChemBridge, and ChemDiv.

Chemical similarity analysis

Similarity analysis using the BCL::CHEMINFO Suite was performed on the 41 validated small molecules (Butkiewicz *et al.* 2013). Three dimensional representations of the molecules were generated using Corina (Sadowski *et al.* 1993). An upper triangle distance matrix considering largest common substructure between two molecules, (A∩B)/(A∪B), was generated using a common subgraph isomorphism algorithm. The vertices and edges were colored by atom type and bond type, respectively. BCL::CLUSTER was used to perform

hierarchical agglomerative clustering using complete linkage to generate color-coded dendrograms to visualize structural similarity and activity simultaneously (Alexander *et al.* 2011).

hiPSC neuroprogenitors

A hiPSC line generated from a control subject (CC3), using established methods in our laboratory following the work of Dr. Shinya Yamanaka (Okita *et al.* 2008, Neely *et al.* 2012), was utilized for all human studies. Pluripotency was validated by Pluritest (Muller *et al.* 2011), euploid karyotype was confirmed (Genetic Associates, Nashville TN), and the absence of the reprogramming plasmid integration was confirmed by PCR.

Mn quantification in human floor-plate lineage dopaminergic neurons

Dopaminergic differentiation of hiPSCs was performed exactly as described (Kriks *et al.* 2011), except LDN193189 (Stemgent) was used at 400 nM. To assess Mn levels on day 12 of differentiation (floor-plate lineage neuroprogenitors) and day 26 of differentiation (post-mitotic dopaminergic neurons) of differentiation, cells were dissociated with Accutase (Stem Cell Technologies) on day 10 or 24 and replated at a density of 50,000 cells/well onto Matrigel-coated 96-well plates containing: 100% N2 medium with ROCK-inhibitor (10 µM, StemCell Technologies) for day 10 cells and Neurobasal medium (Invitrogen) supplemented with B27/glutamax, CHIR (3µM, Stemgent), brain-derived neurotrophic factor (BDNF) (R&D, 20ng/mL), glial cell line-derived neurotrophic factor (GDNF) (R&D, 20ng/mL), ascorbic acid (Sigma, 200mM), TGFβ3 (R&D, 1ng/mL), DAPT (Tocris, 10µM), and dibutyryl cAMP (Sigma, 0.5mM) containing ROCK-inhibitor (10 µM) for day 24 cells. On day 11 and 25 of differentiation, cells were fed with the aforementioned media without ROCK-inhibitor. Net Mn uptake via the same paradigm utilized in the murine striatal cells (30 minutes pre-incubation with vehicle or small molecule at 15µM, followed by 3 hours 125µM $MnCl_2$ in HBSS with continued presence of vehicle or small molecule at 10µM) was assessed the following day by CFMEA.

Immunofluorescence

Immunocytochemistry of human neural lineages was performed as described(Neely *et al.* 2012), with the following antibodies: FOXA2 (1:100, BD Biosciences), LMX1A (1:1000, Millipore), β-III tubulin (TU-20) (1:500, Thermo Scientific), and TH (Pel-Freez, 1:500).

STITCH analysis

Protein chemical interactions were predicted with STITCH 4.0 (Kuhn *et al.* 2014). SMILE strings were exported from all validated small molecules with known functional targets. Analysis included structures with Tanimoto scores greater than 0.7. Action view diagrams were generated to illustrate known protein-chemical relationships of all connected nodes.

UNTARGETED METABOLOMICS IN HUNTINGTON'S DISEASE STRIATAL CELL MODEL SHOWS DISEASE-DEPENDENT AND DISEASE-MANGANESE INTERACTIONS IN METABOLIC PATHWAYS [4]

Abstract

Manganese (Mn) is an essential micronutrient for development and function of the nervous system. Deficiencies in Mn transport have been implicated in the pathogenesis of Huntington's disease (HD), an autosomal dominant neurodegenerative disorder characterized by loss of striatal medium spiny neurons. Brain Mn levels are highest in striatum and other basal ganglia structures, and are also the most sensitive brain regions to Mn neurotoxicity. Murine models of HD exhibit decreased striatal Mn accumulation and HD striatal neuron models are resistant to Mn cytotoxicity. To better understand the physiological basis of this disease-toxicant interaction we sought to define cellular metabolic phenotypes influenced by Mn exposure and/or the pathogenic HD genotype. Here we use an unbiased metabolomics approach by performing ultra-performance liquid chromatography-ion mobility-mass spectrometry (UPLC-IM-MS) on control and HD immortalized murine striatal neurons to identify metabolic disruptions under three Mn exposure conditions, low (vehicle), moderate (non-cytotoxic), and high (cytotoxic). Our analysis revealed lower metabolite levels of pantothenic acid, and glutathione (GSH) in HD striatal cells. HD striatal cells also exhibited lower abundance and impaired induction of isobutyryl carnitine in response to increasing Mn exposure. In addition, we observed induction of metabolites in the pentose shunt pathway in HD striatal cells after exposure to the highest concentration of Mn. These findings provide

---

metabolic evidence of an interaction between the HD genotype and environmentally relevant Mn exposures in a striatal neural lineage. The metabolic phenotypes detected support existing hypotheses that changes in energetic processes underlie the pathobiology of both HD and Mn neurotoxicity.

Introduction

HD is a highly debilitating, autosomal-dominant neurodegenerative disorder characterized by motor dysfunction, behavioral abnormalities, and cognitive decline (Walker 2007). In HD, an expanded CAG repeat generates a pathogenic polyglutamine tract near the *N*-terminus of Huntingtin (HTT). Expansion of this polyglutamine tract is hypothesized to confer a toxic gain of function to HTT (Giorgini 2013). Furthermore, though HTT is universally expressed, HD is characterized by selective neuropathological changes including atrophy of the caudate and putamen with prominent vulnerability of the striatal medium spiny neurons (MSNs) (Vonsattel *et al.* 1998).

Although mechanisms of neurodegeneration in HD are still under investigation, several classes of neuronal stress have been implicated in its pathogenesis, including oxidative stress, mitochondrial dysfunction, glutamine sensitivity, and metabolic dysregulation (Lin *et al.* 2006). Congruently, many environmental toxicants are also known to elicit similar types of neuronal stress, such as the pro-oxidant metal manganese (Mn), which causes striatal neurotoxicity in excess (Brouillet *et al.* 1993, Liu *et al.* 2006). MSNs in the striatum exhibit disruptions in neurochemistry and morphology in the context of Mn exposure (Madison *et al.* 2012). HD genotype prevents characteristic increases in MSN total dendritic length and branching found from week 13-16 in murine development and decreases in total spine density at week 16 (Madison *et al.* 2012). These pathophysiological changes in MSNs coincide with the onset of hyperkinetic behavioral abnormalities observed in murine models of HD (Slow *et al.* 2003). While the mechanism underlying disruptions in synaptic morphology resulting in behavioral phenotypes is poorly understood, it has been proposed that downstream alterations in neuron

connectivity and excitability, impact signal propagation for higher functions (Jaslove 1992, Mainen *et al.* 1996, Woolley *et al.* 1997, Tsay *et al.* 2004, Schmidt-Hieber *et al.* 2007). Interestingly, murine models of HD also exhibit disruptions in dopaminergic signaling (Cha *et al.* 1998, Bibb *et al.* 2000, Ortiz *et al.* 2011) and levels of striatal dopamine (Tang *et al.* 2007). Neurotoxic exposures to Mn have been shown to produce a similar depletion in striatal dopamine levels as is seen in HD (Madison *et al.* 2012). Notably, Mn exposure has been associated with changes in energy metabolism (Levin *et al.* 2005, Guilarte 2010). Furthermore, both *in vitro* and *in vivo* murine models expressing mutant HTT exhibit reduced total Mn accumulation (Williams *et al.* 2010). Despite the specificity of this HD-Mn interaction effect, the mechanisms by which pathogenic alleles of HTT disrupt Mn transport are unknown, though it appears to be independent of the HD iron transport phenotype. We hypothesize that the influence of mutant HTT on Mn cellular transport processes are a consequence of compensatory metabolic responses to HD pathophysiological processes.

Here we interrogate intracellular metabolite profiles from a control and HD striatal cell model, mutant STHdh[Q111/Q111] and wild type STHdh[Q7/Q7]), demonstrated to exhibit a strong HD-Mn interaction phenotype under three extracellular Mn exposure conditions (**Figure 18**) (Williams *et al.* 2010, Williams *et al.* 2010). Given that normal levels of brain Mn in mammals range from 20-53µM, we sought to assess the ability of Mn to influence the metabolic profile at low (0µM), moderate non-toxic (31µM), and high toxicological exposure concentrations (125µM) (Bowman *et al.* 2014). An unbiased assessment of intracellular metabolic perturbations was performed through a comprehensive small molecule profiling approach using ultra-performance liquid chromatography-ion mobility-mass spectrometry (UPLC-IM-MS) (Derewacz *et al.* 2013). This approach enabled study of HD-Mn interactions at a cellular level without *a priori* knowledge of HD or Mn induced protein changes. Sampling the metabolite inventories of cells provides information representative of the striatal cell phenotype, and is reflective of the current biology of the system. The metabolomic profiling method has the potential to reveal mechanistic and therapeutic targets that may not be captured by genetic and transcriptional approaches. Here we describe the first application of unbiased metabolomics to study gene-

environment interactions in a neurodegenerative disorder. Our study provides an integrated overview of the effects of genotype, Mn exposure, and HD-Mn interactions on metabolic pathways via quantifying their respective metabolites independent of any prior association with HD pathogenesis or Mn biology. Specifically, we investigated the metabolomic profiles of mutant (STHdh$^{Q111/Q111}$) and wild type (STHdh$^{Q7/Q7}$) immortalized striatal neuroprogenitors in response to increasing concentrations of extracellular Mn (Trettel *et al.* 2000). Both basal metabolic differences in HD versus wild type striatal cells were observed, as well as the Mn-dependent and HD by Mn interaction dependent responses in metabolite composition were identified.
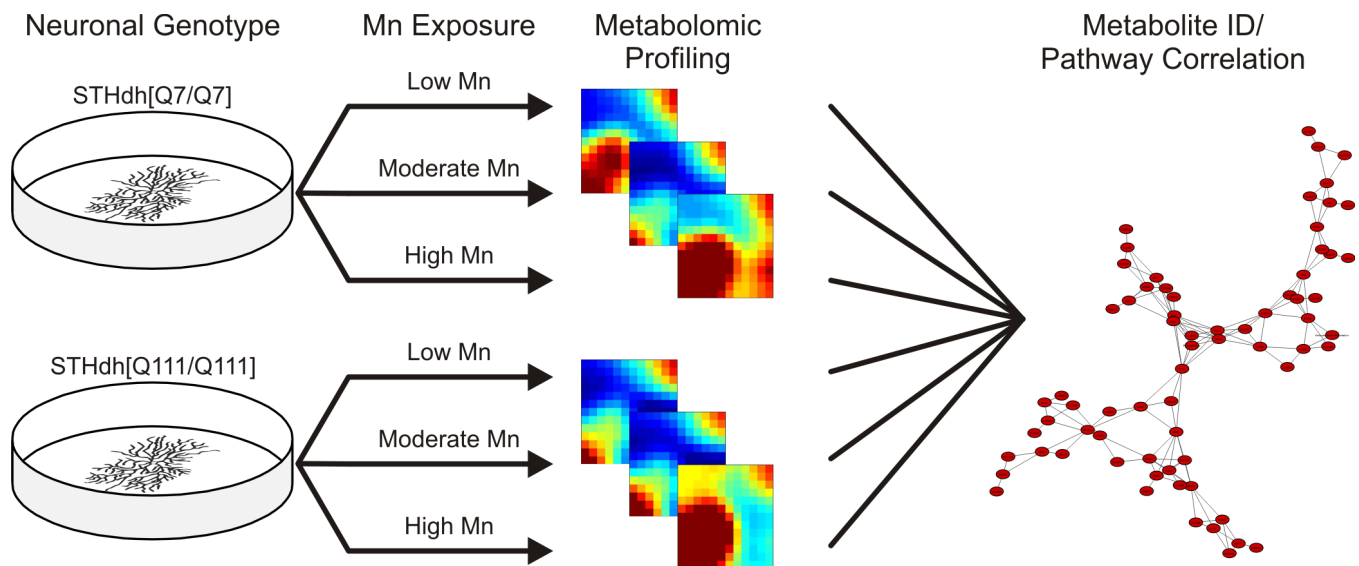
Figure 18 – Study of HD-Mn interaction using untargeted metabolomics. Overall paradigm for experimental approach. Murine control (STHdh$^{Q7/Q7}$) and HD (STHdh$^{Q111/Q111}$) striatal cell model were treated by different Mn exposure conditions. Cells were harvested for metabolomics profiling and identification followed by pathway correlation.

Results

Both HD genotype and manganese concentration affect metabolomic profiles of neurons

In all, 475 features were detected with unique retention time and *m/z* values. We performed ANOVA across all samples, grouping technical replicates, and removing all values with a p-value greater than 0.10. This resulted in 362 filtered features used for all subsequent analyses. Our data suggest deviations in the metabolomic profiles of both control and HD striatal cell lines are driven primarily by the concentration of manganese to which they are exposed. We sought to assess the ability of Mn to influence the metabolic profile both at a physiological Mn concentration (31.25μM) and at an *in vivo* relevant toxicological concentration (125μM) (Bowman *et al.* 2014). Principle component analysis (PCA) shows separation of global metabolomic profiles in principal component one (PC1) based upon treatment conditions (**Figure 19**). Each marker represents the average metabolomic profile of one biological sample analyzed in triplicate and ANOVA filtered. Biological replicates cluster in PCA space, indicating biological consistency of these measurements. However, PC2 separates metabolomic profiles predominantly based upon cell genotype, suggesting differences in basal metabolism between the metabolomic profiles of STHdh[Q7/Q7] and STHdh[Q111/Q111] cells. Self-organized heat maps (**Figure 19**) that cluster metabolites by covariance were then used to visualize global patterns of metabolite changes between control and HD striatal cells with varying Mn exposures (Eichler *et al.* 2003, Goodwin *et al.* 2014). In this method, metabolites self-assemble into groups in a user-defined grid based upon similarities in abundance profiles using an unsupervised computational process. For example, metabolites that are increased in abundance consistently across biological replicates as a generic response to Mn concentration will be grouped in a region of the SOM space, while metabolites that are produced as a genotype-specific response to Mn concentration will group in a separate, distinct region of SOM space. Experimental groups are then represented as heat maps based upon the abundances of organized metabolites. The number of metabolites seeded in each grid location of the SOM in Figure 19B is indicated in the metabolite density map, with blue

representing one metabolite and red corresponding to 44 metabolites. The largest abundance occupying the central region of the SOM space corresponded to a large peptide with a molecular weight of 8561.6 Da, putatively identified as ubiquitin based upon accurate mass (**Table 6**). Through SOM analysis, we observed a decreased production of glutathione (GSH) and pantothenic acid in the STHdh[Q111/Q111] cell line. A general linear model was applied to evaluate significant differences in the abundance of metabolites by genotype, Mn exposure, or genotype by Mn exposure interaction. A significant relationship between genotype and both GSH and pantothenic acid abundance was observed ($p<0.001$). Both genotype ($p<0.05$) and Mn exposure ($p<0.005$) had a significant effect on the levels of isobutyrl carnitine. There was also a statistically significant interaction between genotype and Mn-exposure on isobutyryl carnitine abundance ($p<0.05$). Finally, ribulose-5-phosphate, showed a significant change in abundance by Mn exposure ($p <0.001$), genotype ($p<0.001$), and a genotype by Mn exposure interaction effect ($p<0.01$).

Table 6. Measured accurate masses for metabolite identifications.

Metabolite	Measured Mass	Mass Accuracy (ppm)
Isobutyryl carnitine	232.153	6.0
Ribulose 5-phosphate	231.0254	4.3
Glutathione	308.0926	4.9
Pantothenic acid	220.1192	5.9
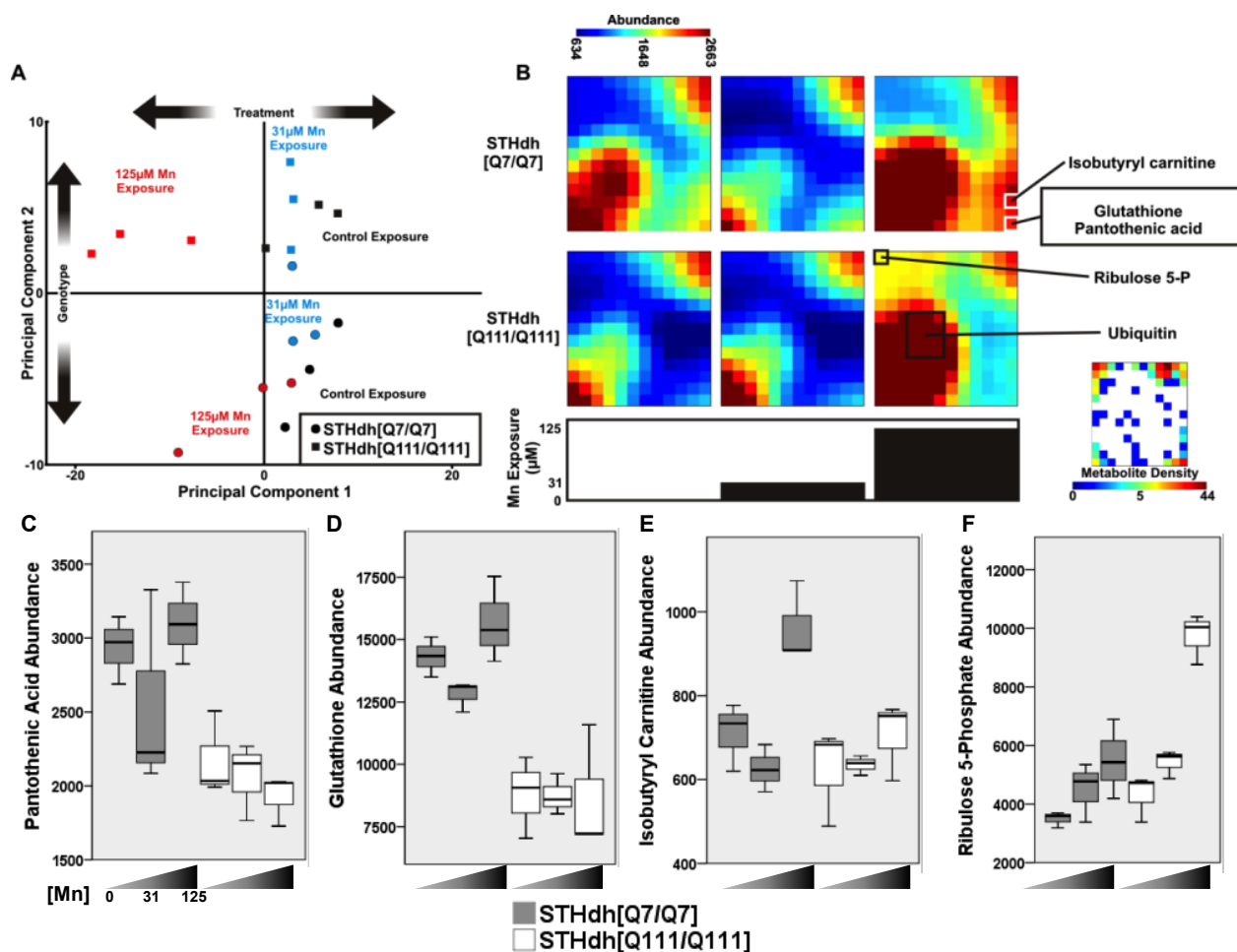
Figure 19 – Untargeted metabolomics reveals metabolites impacted by Mn and/or HD genotype. (**A**) Principal component analysis of metabolomic profiles for STHdh[Q7/Q7] and STHdh[Q111/Q111] cells exposed to varying physiologically-relevant Mn concentrations. (**B**) Self-organized metabolic heat maps with select metabolites annotated. (**C-G**) Box plot production profiles for significant metabolites. (STHdh[Q7/Q7] represented by gray bar, STHdh[Q111/Q111] represented by white, manganese concentration on abscissa, standard error about the mean is shown).

Discussion

The application of untargeted metabolomic profiling to characterize Mn-dependent cellular responses in an HD striatal cell model has revealed several alterations in metabolism based on genotype and Mn-exposure conditions and HD x Mn interaction effects. These findings have the potential to directly link established differences in cellular Mn handling in HD with neuronal responses to Mn burden.

HD striatal cells exhibit lower levels of pantothenic acid and GSH

The identification of lower levels of pantothenic acid (vitamin B5) and GSH in HD striatal cells fits into the complex biology mediating neuronal mitochondrial processes and metal handling. Notably, disruptions in pantothenic acid levels have been described in a related neurodegenerative disorder, brain iron accumulation (NBIA), also known as Hallervorden-Spatz disease (Swaiman 1991, Kotzbauer *et al.* 2005). Mutations in pantothenate kinase 2 (*PANK2*), encoding a neuronal mitochondrial protein responsible for catalyzing the phosphorylation of pantothenic acid to phosphopantothenate, have been identified in one-third of patients with this disorder (Begley *et al.* 2001, Hayflick *et al.* 2003). This process is critical to the synthesis of coenzyme (CoA), a universal acyl carrier involved in the citric acid cycle and cellular energetics. In addition, pantothenic acid is a necessary co-enzyme for the synthesis of GSH, and has been shown to protect cells from peroxidative damage by increasing free GSH levels (Slyshenkov *et al.* 2004). Given our observation of decreased pantothenic acid levels relative to control, downstream impaired cellular energetics and exhausted response to oxidative stress could play a role in neurodegeneration observed in HD. Mn neurotoxicity can result from enhanced production of free radicals that are scavenged by GSH and other antioxidants (Vescovi *et al.* 1989). However, the decreased abundance of GSH and pantothenic acid we observed appear to be independent of cellular Mn burden given the lack of Mn-dependent changes. Importantly, it remains possible that the HD genotype dependent changes in GSH and pantothenic acid may be acting upstream of the changes in Mn cellular biology.

Alterations in levels of ribulose-5 phosphate implicate modulation of the pentose shunt pathway in HD

The pentose shunt pathway functions to regenerate the reducing agent NADPH, which is necessary for the many biosynthetic processes in the brain, such as synthesis of free fatty acids from acetyl-CoA (Magistretti *et al.* 2013). The dehydrogenation of glucose 6-phosphate to ribulose 5-phosphate is the rate-limiting step of the

99

pentose shunt pathway. The pentose shunt pathway is induced by p53, a protein known to mediate cellular dysfunction and behavioral abnormalities in HD (Bae *et al.* 2005). Our data suggest increasing cellular Mn burden results in a corresponding induction of ribulose 5-phosphate, an effect that was exaggerated in HD striatal cells relative to control. This finding corroborates previous studies that demonstrate HD striatal cell impairments in mitochondrial dynamics and energetics (Jin *et al.* 2011, Jin *et al.* 2012). The genotype-dependent difference was apparent only at the cytotoxic 125µM Mn exposure, while changes in cellular Mn burden going from vehicle to 31µM does not significantly increase ribulose 5-phosphate levels. This is consistent with an involvement of ribulose 5-phosphate metabolism in the Mn cytotoxic cellular response. Indeed, NADPH generated in production of ribulose 5-phosphate mediates the generation of GSH by reducing glutathione disulfide (GSSG). Increased ribulose 5-phosphate levels suggest that HD striatal cells are hypersensitive to Mn related oxidative stress, despite their reduced net Mn accumulation. Furthermore, when taken into the context of decreased levels of glutathione and pantothenic acid in HD striatal cells, increased levels of ribulose 5-phosphate may be a cellular response to increase the reduced amount of GSH available for handling oxidative stress.

HD striatal cells exhibit lower abundance and an impaired Mn-dependent increase of isobutyryl carnitine

Isobutyryl carnitine is a product of the acyl-CoA dehydrogenases, mitochondrial enzymes that are involved in the process of metabolism of fatty acids or branched-chain amino acids. In addition to these functions, carnitines have well described roles in the brain including: lipid synthesis, membrane composition, expression modulation, mitochondrial energetics, activation of antioxidant mechanisms, and strengthening cholinergic neurotransmission (Jones *et al.* 2010). Although, increases in isobutyryl carnitine levels have been observed in inborn errors of metabolism such as short chain acyl dehydrogenase deficiency, reduced levels of this metabolite have not been reported in the context of any neurodegenerative disease (Dwight *et al.* 2003). Our data reveal genotype, Mn exposure and genotype by Mn interaction effects for levels of isobutyryl carnitine. We

observed that Mn exposure induces elevated levels of isobutyryl carnitine in control striatal cells but not the HD mutant cells. As HD striatal cells accumulate significantly less cellular Mn levels versus control cells (Williams *et al.* 2010, Williams *et al.* 2010), the genotype specific effect is likely due to a failure to reach a sufficient threshold level of intracellular Mn. The observation that levels of isobutyryl carnitine increased in control striatal cells only at the highest Mn exposure is consistent with this interpretation. Mn toxicity occurs in part via impairment of mitochondrial function (Claudia *et al.* 2004, Dobson *et al.* 2004). The increase in this metabolite under conditions of heavy Mn burden may reflect increased reliance on isobutyrl carninite-mediated process to generate acetyl-CoA for ATP synthesis.

Modeling the HD-Mn striatal cell metabolomics

The striatum is a unique region of the brain, linked to both neurodegeneration in HD and Mn neurotoxicity. The application of untargeted metabolomics to elucidate the mechanisms through which control and HD murine striatal cells respond to low, moderate non-toxic, and high toxicological Mn levels revealed selective alterations in cellular stress responses. Given that the HD genotype disrupts a variety of cellular processes including transcriptional regulation, HD striatal cells may have adapted their metabolism to survive under this genotypic stressor. Their response to the pathogenic processes of mutant HTT may activate compensatory processes that influence Mn toxicity and oxidative stress metabolites (**Figure 20**). In modeling the observed phenotypes, we postulate that the HD genotype produces a state of chronic oxidative stress, depleting cellular GSH reserves. In response, HD striatal cells have a deficit in pantothenic acid, hampering efforts to replenish the limited GSH reserves. A compensatory process may be induced by HD striatal cells, increased reliance on the pentose shunt pathway to regenerate GSH, when cellular Mn burden reaches cytotoxic levels. The exaggerated response to Mn is especially noteworthy given the decreased ability of HD striatal cells to accumulate Mn (Williams *et al.* 2010, Williams *et al.* 2010). The decreased Mn uptake by HD striatal cells may also explain the selective increase of isobutyrl carnitine levels in control cells at toxic Mn levels.
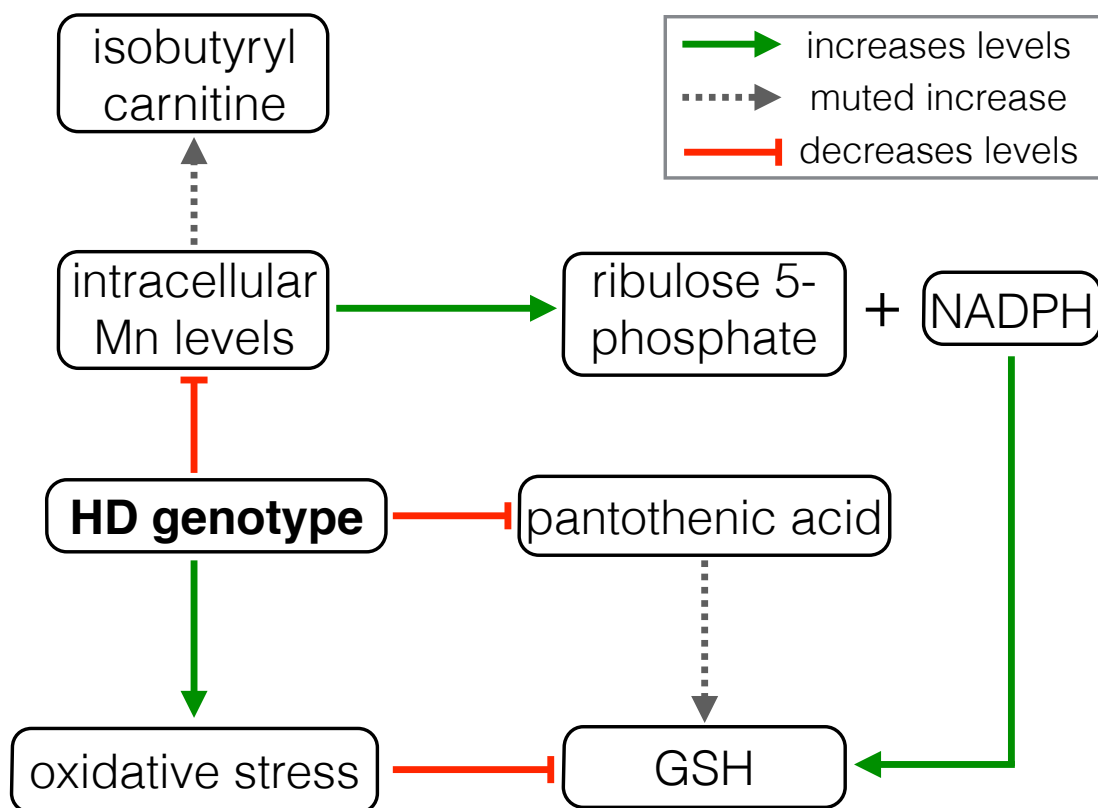
Figure 20 – Metabolic disruption in Huntington's disease. Summary diagram describing the proposed model of HD-Mn interaction based on untargeted metabolomics. Increased metabolite levels indicated by arrows (**green**), decreased metabolite levels by lines (**red**), and muted increases in metabolites by dashed arrows (**gray**).

Conclusions

In summary, we report the application of untargeted metabolomics to provide insight into the processes

mediating the complex interactions of genotype and levels of the essential metal, Mn, in the context of HD. This

unbiased approach revealed disruption in the levels of several diverse physiological and energetic processes by

Mn and/or HD genotype. Furthermore, the examination of response to low, moderate, and high Mn levels using

untargeted metabolomics provided a unique perspective on the response of HD striatal cells on a global cellular

scale. While we identified metabolites with known links to HD pathogenesis such as GSH (Browne *et al.* 2006),

the classification of changes in pantothenic acid and the pentose shunt pathway implicate disruption in basal

energetic metabolism in HD. In addition, our studies identify alterations in the isobutryryl carnitine, a product of fatty acid metabolism. Further examination of the identified cellular processes may provide future mechanistic understanding into the loss of striatal neurons in HD and may serve as a framework for future therapeutic interventions for this highly debilitating disorder. Our approach can be applied to a variety of other poorly understood disease contexts where a particular environmental exposure is linked to disease progression or severity.

Materials and Methods

Cell Culture and Sample Preparation

Biological triplicates were prepared for all experiments performed. The clonal striatal cell lines—both mutant STHdh[Q111/Q111] and wild-type STHdh[Q7/Q7] were grown at 33°C (Trettel *et al.* 2000). Culture and exposures were performed as previously described.(Williams *et al.* 2010, Kumar *et al.* 2013) Subsequently, STHdh[Q111/Q111] and wild-type STHdh[Q7/Q7] cells were plated at equal density the 16 hours before treatment. Cells were exposed for 3 hours in HBSS (Corning-CellGro) with or without 31μM or 125μM MnCl$_2$ added. Cells were harvested post-exposure by HPLC-grade methanol (Sigma) extraction and snap frozen in liquid nitrogen. Prior to the assay day, samples were thawed and vigorously mixed by a laboratory vortexer and centrifuged at 4°C and 14,000×*g* for 10 min to precipitate proteins and particulates. The supernatants were transferred to a fresh tube and vacuum centrifuged until dry. The residuals were stored at -80°C until UPLC-IM-MS^E sample preparation.

The dried metabolite extracts were resuspended in 200μL water with 0.1% formic acid. UPLC-IM-MS^E data acquisition was performed with a 30-minute gradient. Mobile phase A consisted of H_2O with 0.1% formic acid and mobile phase B consisted of ACN with 0.1% formic acid. A 1x100 mm 1.7μm particle BEH-T3 C_{18} column (Waters Co) was used for chromatographic separations with a flow rate of 75 μL/min, a column temperature of 40 °C. An autosampler was used for sample injection and held at 4°C, with a loop size of 5μL. The initial solvent composition was 100% A, which was held for 1 min and ramped to 0% A over the next 11 minutes, held at 0% A for 2 minutes and returned to 100% A over a 0.1 minute period. The gradient was held at 100% A for the next 10.9 minutes for equilibration. Ten column-load injections were performed with 5μL injections of the quality control. Quality control injections were then performed after every 10th sample injection to ensure instrument stability.

IM-MS^E spectra were acquired at a rate of 2 Hz from 50-2000 Da in positive mode for the duration of the injection on a Synapt G2 HDMS platform (Waters, Milford, MA). The instrument was calibrated to less than 1 ppm mass accuracy using sodium formate clusters prior to analysis. A two-point internal standard of leucine enkephalin was infused in parallel at a flow rate of 7μL/min and acquired every 10 seconds. The source capillary was held at 110°C and 3.0 kV, with a desolvation gas flow of 400 L/hr and a temperature of 150°C. The sampling cone was held at a setting of 35.0, with the extraction cone at a setting of 5.0. In the MS^E configuration, low and high energy spectra are acquired for each scan. High energy data performed a collision energy profile from 10-30 eV in the trapping region, providing post-mobility fragmentation. Ion mobility separations were performed with a wave velocity of 550m/s, a wave height of 40.0 V, and a nitrogen gas flow of 90 mL/min, with the helium cell flow rate at 180mL/min. A leucine encephalin internal calibrant correction was performed in real time.

Data processing and statistical analysis

Data were converted to mzXML format using the msconvert tool from the ProteoWizard package as previously described (Kessner *et al.* 2008). Peak picking and alignment were performed using XCMS in R (Smith *et al.* 2006). The resulting data matrix contained 475 detected features. Features were pre-filtered for reproducibility using an ANOVA threshold of $p \leq 0.10$, comparing across all experimental conditions and biological replicates. Prior to self-organizing map (SOM) analyses, MVSA, and further statistical analyses, analytical triplicates were averaged. For GEDI analysis, a grid of 25 x 26 was generated, with 100 first phase training iterations and 160 second phase. An initial training radius of 10.0 was defined with a learning factor of 0.5, a neighborhood block size of 20, and a conscience of 5.0. For the second phase, a neighborhood radius of 1.0, learning factor of 0.05, neighborhood block size of 2, and conscience of 2.0 was defined. A random seed of 10 with a Pearson's correlation distance metric and random selection initialization was used. Further statistical analyses were performed in SPSS version 22 (SPSS, Inc. Chicago, IL).

Metabolite identification

Metabolite identifications were performed using accurate mass measurements and fragmentation spectra extracted from IM-MS[E] data (**Table 6**, **Figures 21-25**). Utilizing drift time correlations, product ions were correlated appropriately to precursors for extraction of high energy spectra. Annotated spectra are presented in Figures 21-25. Identification confidence levels are in accordance with the Metabolomics Standards Initiative proposed minimum reporting standards (Sumner *et al.* 2007).
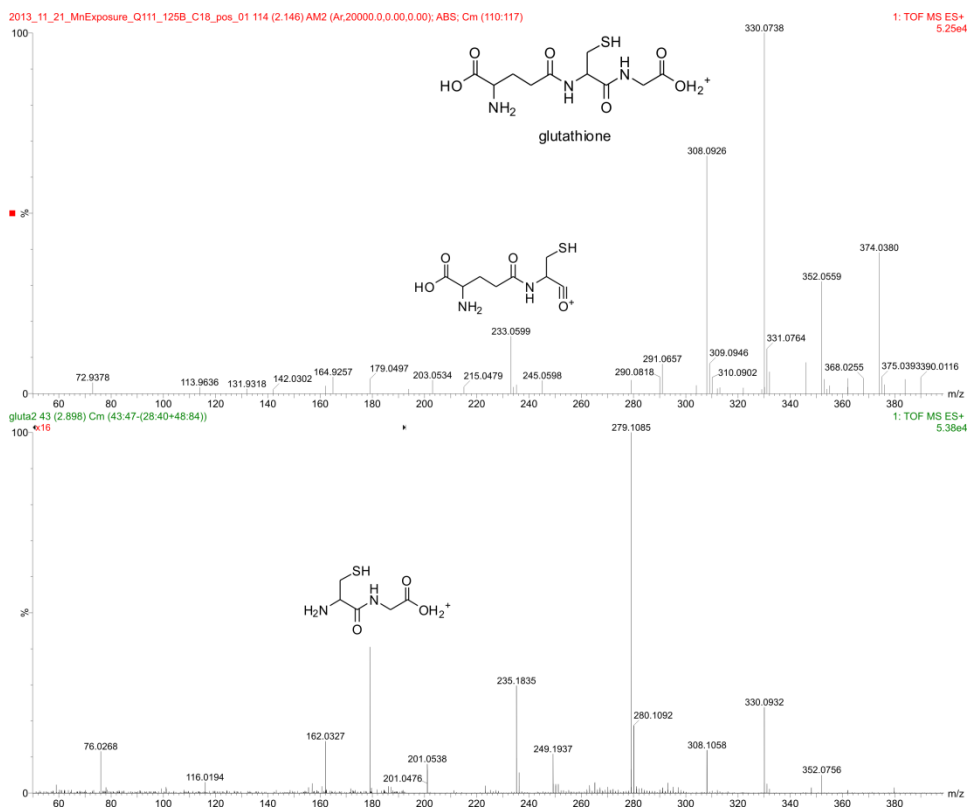
Figure 21 – Intact (above) and mobility-selected fragmentation spectra for glutathione.
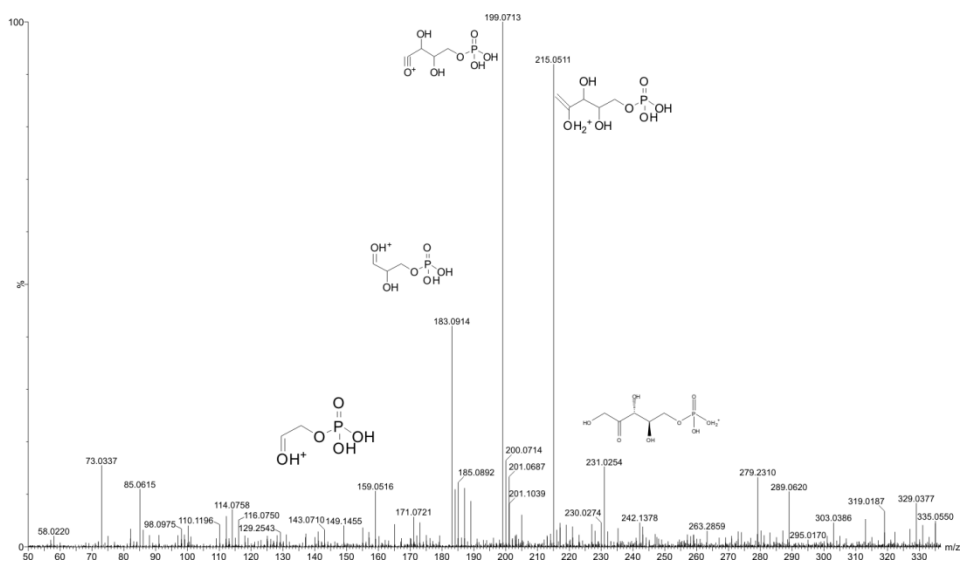
Figure 22 – Fragmentation spectra for ribulose 5-phosphate.

106
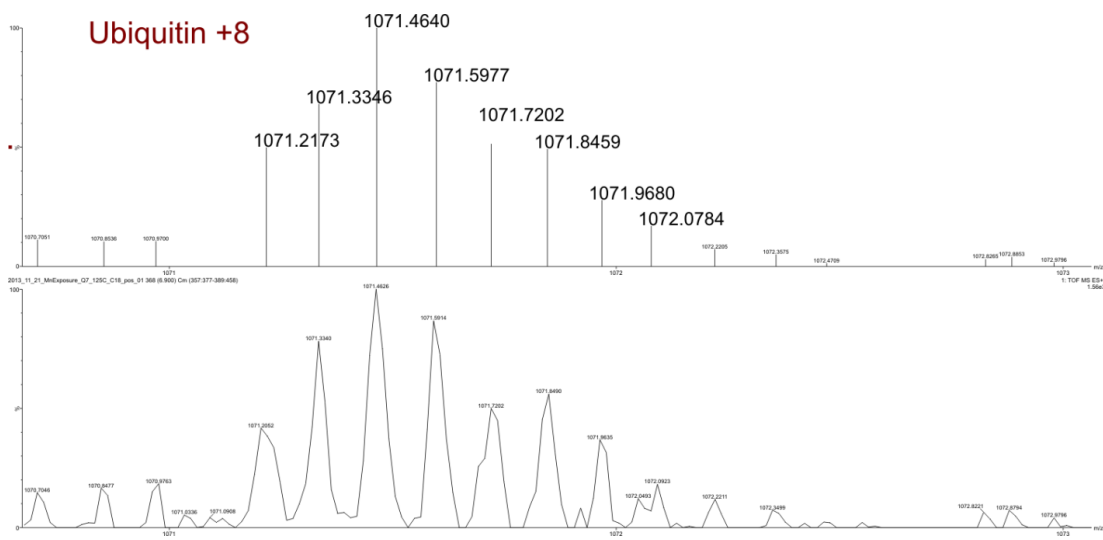
Figure 23 – Isotopic envelope suggesting ubiquitin identification.
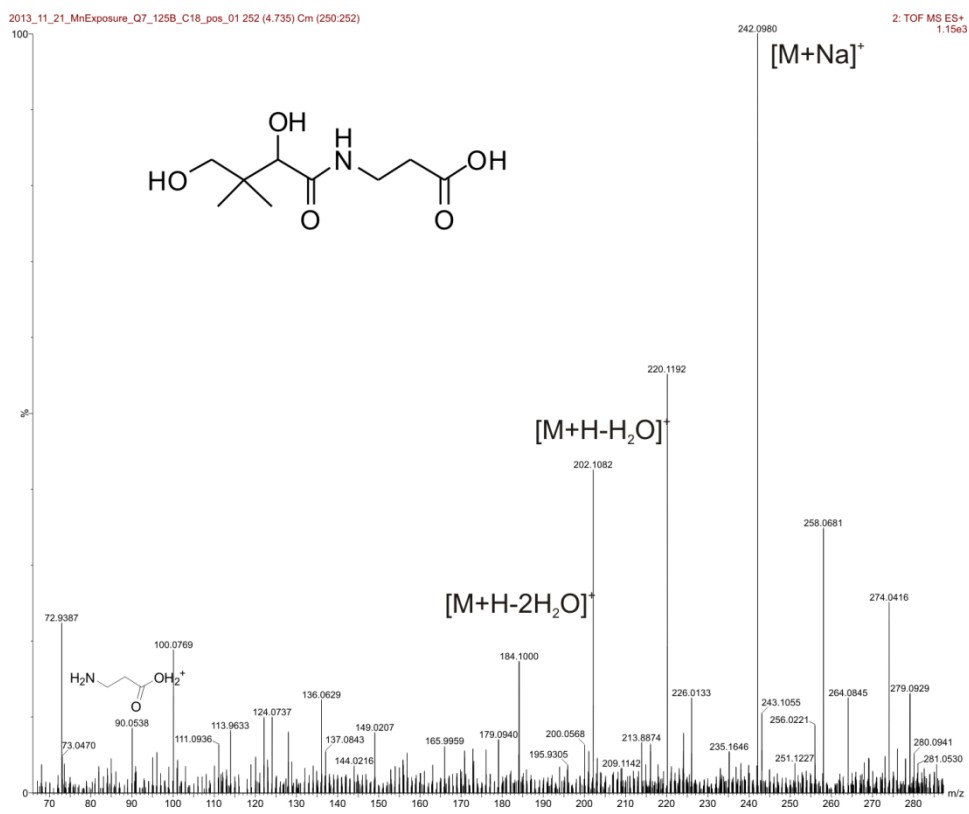
Figure 24 – Pantothenic acid fragmentation spectrum.
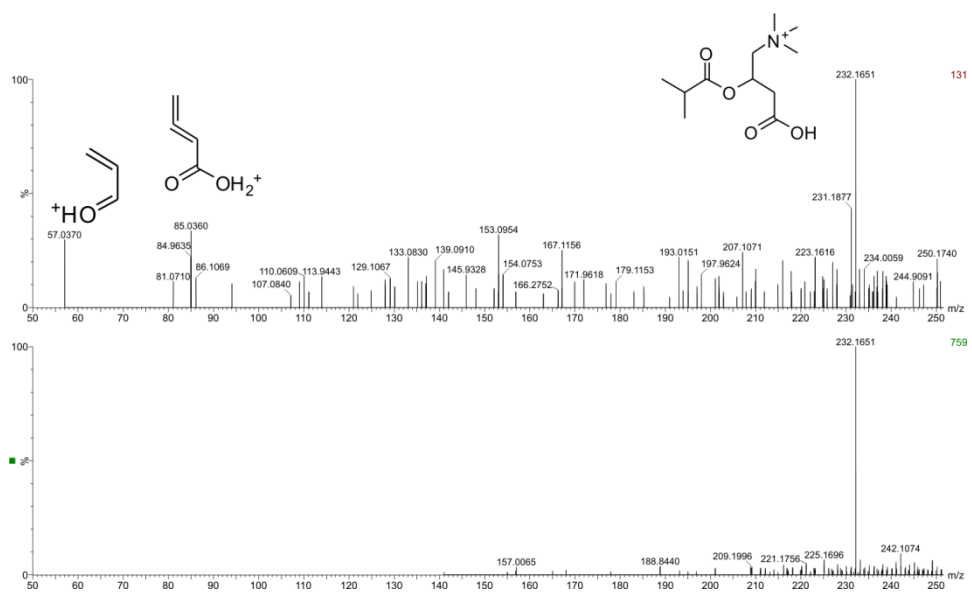
Figure 25 – Mobility-selected high (above) and low (below) energy spectra for isobutyryl carnitine.

CHAPTER VII

REGULATION OF NEURONAL MN IN PHYSIOLOGY AND DISEASE: CONCLUSIONS AND FUTURE DIRECTIONS

Regulation of Mn content in dopaminergic neurons: evidence of homeostatic developmental regulation

The role of essential metals in development and function of the nervous system have been particularly well described for major metals such as iron and zinc. However, the regulation of Mn at the level of neurons is a poorly understood process. Given known developmental exposures and the identified role of Mn as a risk factor for parkinsonism and Huntington's disease, we sought to understand how Mn is regulated in the nervous system. The limited availability of pharmacological agents capable of manipulating neuronal Mn content has impeded the study of this process. To overcome this obstacle, we developed an innovative chemical biology approach consisting of a high throughput screen based on the cellular fura-2 Mn extraction assay (CFMEA), an assay that can detect modulators of cellular Mn status. Using this approach, we developed a highly diverse small molecule toolbox that could increase and decrease Mn levels under toxicologically relevant Mn exposures. Furthermore, the vast majority (39/41) small molecules exhibited activity at physiological Mn levels. We performed a chemical informatics analysis to identify potential signaling pathways and proteins targeted by the small molecule toolbox. This analysis identified major signaling pathways such as MAPK14, TGFBR1, SOD1, and HIF1-α as well as enzymes involved in neurotransmission such as ACHE and BCHE. Identification of novel pathways and enzymes associated with Mn exposure provides direction for future study into the processes underlying Mn biology.

Given that the toolbox was developed in an immortalized murine striatal cell system, we sought to evaluate the efficacy of selected small molecules in a human induced pluripotent stem cell (hiPSC) system. Interrogating Mn

biology in a hiSPC based system provided multiple advantages, including: (1) translating our findings from murine to human system, (2) evaluating changes in Mn content across neurodevelopmental time, and (3) revealing differences in activity of particular small molecules based on developmental stage. Our studies revealed that neuronal Mn content changes across developmental time. Furthermore, the variety of small molecule activity patterns may indicate that the highly complex processes regulating neuronal Mn change across developmental time. This work provides the first evidence of cell-level regulation of neuronal Mn content across neural differentiation.

In addition to our high throughput screening approach, we sought to investigate how neurons respond to altered states of Mn exposure in the context of a genotypic stressor. Using the immortalized murine system, we were able to compare striatal neurons expressing mutant and wild-type Huntingtin in the context of physiological and toxicological Mn states. Using an untargeted metabolomics approach, we revealed metabolic evidence of a genotype-environment interaction between Mn and HD genotype. The physiological processes affected by Mn and/or HD genotype regulate cellular energetics, neuronal function, and response to oxidative stress.

Efficacy of the small molecule toolbox: insights into neuronal Mn regulation

The activity of the small molecule toolbox in murine and human systems provides an insight into the processes regulating neuronal Mn. Firstly, this study establishes that mechanisms of neuronal Mn regulation are pharmacologically targetable. The vast majority of these small molecules are capable of modulating Mn at both physiological and toxicological exposure conditions, suggestive that the targeted regulatory mechanisms that function in normal neuronal physiology modulate Mn under high exposure conditions. The exposure paradigm utilized in our studies is an important consideration when interpreting their findings. The Mn toolbox small molecules were identified in an acute exposure paradigm while epidemiological evidence suggests chronic exposures contribute to neurodegenerative diseases. However, there are a number of acute exposure settings,

such intravenous delivery of diagnostic imaging contrast agents, that have clinical relevance. It is plausible that the mechanisms targeted by the HTS-identified small molecules in an acute exposure function similarly in the context of a chronic exposure. In addition, the majority of small molecules were relatively low potency, requiring concentrations of $0.1 - 10\mu M$ to achieve a detectable effect. This low potency complicates interpretation of the functional targets revealed by STITCH since the observed effect on Mn content could be caused by off-target interactions. The high concentration required could also reflect a lack of affinity of small molecules for their active site, suggestive that a increasing concentration would enhance active site occupancy allowing for a rapid shift in Mn content under an acute Mn exposure. It is plausible that low small molecule concentrations could show efficacy in a chronic exposure paradigm. An additional factor that may contribute to the low potency of the toolbox small molecules is the relative ability of the compounds to cross cell membranes, a property critical for accessing intracellular targets. Regardless of the nature of the observed low potency, there is tremendous potential for lead optimization and medicinal chemistry to improve the affinity and stability of the small molecule Mn toolbox.

Another interesting aspect of the small molecule Mn toolbox is its composition. Despite performing a screen across a highly diverse chemical library, there were substantially more Mn level increasing than decreasing small molecules. The Mn level increasers could be composed of small molecules that enhance Mn uptake or conversely inhibit Mn efflux. Operating under the assumption that the HTS was equally powered to detect Mn level increasing and decreasing small molecules, this finding would suggest that the identified small molecules disrupt the activity of efflux mechanisms. Alternatively, there may exist a limited set of functional targets for which these small molecules act as activators. Notably, 7/8 Mn level decreasers had lower effect size, as defined as the fold change in Mn level, at physiological Mn exposures than at toxicological exposures. In contrast, there was profound variation in the effect size for Mn level increasing small molecules between physiological and toxicological exposures. This variation may reflect diversity of the functional targets for Mn level increasing small molecules whereas the Mn level decreasing may act on the same or functionally similar targets. The

finding that members of chemical families, such as Cluster 3, exhibit similar effect size at physiological and toxicological exposures further supports this observation.

Lastly, we gained insight into the temporal changes in Mn regulation across human dopaminergic neuron developmental time using hiPSC technology. As mesencephalic neural progenitors differentiate to post-mitotic dopaminergic neurons, there is a significant increase in Mn content under toxicological exposure conditions. In addition, all of the tested small molecules identified in the murine-based high throughput screen were effective in the human dopaminergic neuron system. This suggests that the Mn regulatory mechanisms targeted by the small molecules are highly conserved between mice and humans. Furthermore, two of the small molecules exhibited developmental specificity, suggestive that their functional targets change across neural differentiation and that the small molecules act through cell-specific mechanisms. This demonstration of cell-specific Mn homeostatic mechanisms that are modulated across development supports our hypothesis that Mn is regulated at the neuronal level.

Future directions: identification of mechanistic targets of neuronal Mn regulation and *in vivo* studies

Taken together, our innovative chemical biology approach provides evidence of a highly sophisticated, regulatory environment mediating neuronal Mn content. This regulatory system is likely necessary given the role of Mn in critical cellular processes, such as mediating oxidative stress, which neurons are acutely sensitive. Perturbation of Mn biology, particularly in development, has the ability to limit or hasten the onset of neurodegenerative diseases such as parkinsonism and Huntington's disease. In cases where there is a known genetic predisposition or high occupational exposure, there is immense potential in neuroprotective therapeutics to limit Mn-induced pathology. The putative targets identified by the high throughput screen and untargeted metabolomics studies may represent therapeutic targets for manipulation of neuronal Mn handling.

To capitalize on the therapeutic potential of Mn manipulation, future studies are directed along two major aims: (1) further characterization of novel Mn regulatory pathways and (2) translation of the small molecule toolbox for *in vivo* applications. The putative identification of Mn regulatory pathways by our studies provides a known set of proteins that can be targeted. In order to evaluate each regulatory element individually, we will employ a combination of pharmacological and molecular biology techniques. For those small molecules with a known mechanism of action, such as kinase inhibitors, we will conduct activity profiling to determine whether on-target or off-target effects cause the observed effect on Mn content. For those with well-defined targetable site, we will then perform competition experiments with the Mn toolbox small molecule alongside other known inhibitors and activators for the same target. These studies will be able to determine whether a particular small molecule target can be manipulated bidirectionally, both to increase and decrease neuronal Mn content, and evaluate dose responsive activity. This pharmacological approach can be conducted in a high throughput capacity, allowing rapid refinement of the list of functional targets. We have performed preliminary competition studies examining the three small molecules from the GSK Published Kinase Inhibitor Set, which have characterized pharmacological profiles (**Figure 26**). VU0482723 and VU0482794 were designed to target epidermal growth factor receptor/human epidermal growth factor receptor 2 (EGFR/HER2) while VU0482585 was designed to target TGFβ type I receptor kinase (ALK5). The lack of clear additive effects between these small molecules and known target-specific drugs in the competition studies suggests that changes in neuronal Mn status likely resulted from off-target effects at another kinase.
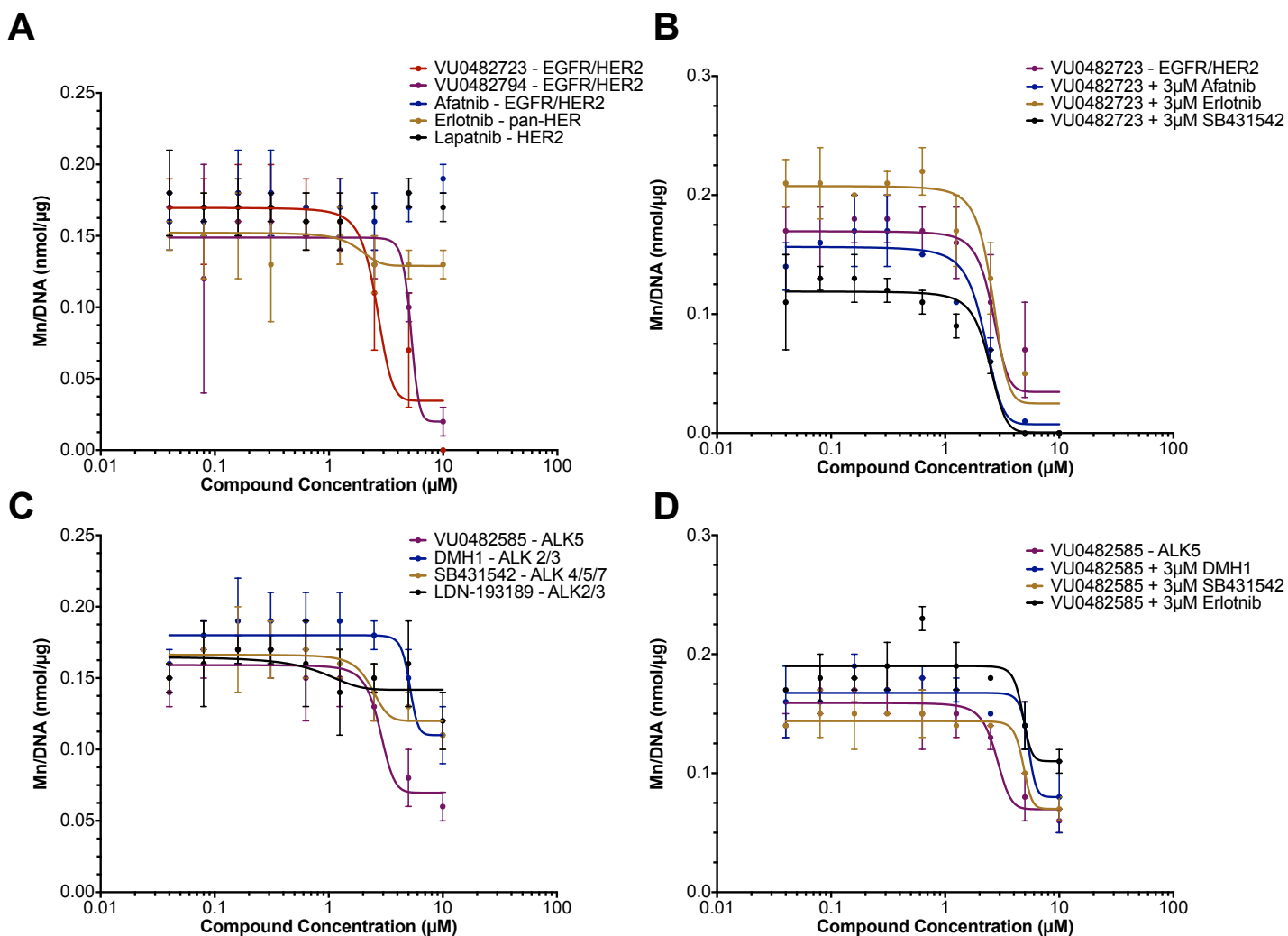
Figure 26 – Competition experiments for GSK Published Kinase Inhibitor Set small molecules. (**A**) Individual activity of EGFR/HER2 primary target small molecules. (**B**) Competition experiment of VU0482723. (**C**) Individual activity of ALK primary target small molecules. (**D**) Competition experiment of VU0482585. Identity of small molecule/drug followed by primary target is indicated by (Small Molecule – Target). Log(inhibitor) vs. response best fit curves were generated and plotted for each small molecule. n=4 for each data point.

Since pharmacological interrogation is limited by the availability of high affinity compounds with established specificity, mechanistic targets can also be explored with molecular biology techniques. For example, using siRNA or CRISPR/Cas system, these Mn regulatory functional targets can be knocked down or out, allowing determination of the specificity of the functional effect. This simple approach has the ability to identify critical genes regulating neuronal Mn.

While refinement of functional targets will permit assessment of the cellular mechanisms regulating neuronal Mn, we have profound interest in whether HTS-identified small molecules will have efficacy *in vivo*. Prior to *in vivo* work in an animal model, extensive pharmacokinetic studies (brain-to-plasma, clearance, metabolism/stability) would first be required. These experiments would determine the route of administration (oral, subcutaneous, or intrathecal) and the clearance of the small molecule in other tissue types. These studies would be followed by any necessary medicinal chemistry and lead optimization of our toolbox small molecules. In addition, adaptation of our *in vitro* Mn exposure paradigms to *in vivo* systems and identifying robust social or motor behavioral outcomes would be required. These prerequisite studies would permit the examination of small molecule efficacy in the developing and adult mouse brain.

A multidisciplinary approach to reveal new therapeutic targets for disease

Aside from the direct conclusions of our work, perhaps one of the most important implications of the overall project was its unique approach. By leveraging the advantages of HTS technology, human induced pluripotent stem cells, and untargeted metabolomics, we were able to explore poorly understood processes underlying regulation of an essential metal from multiple perspectives. Basic science and clinical medicine have made fundamental breakthroughs for pathologies where a single target can halt or reverse disease progression (i.e. VEGF in age related macular degeneration, HER2 in breast cancer) however this is not the case for the vast majority of illnesses. In HD for example, the expanded CAG repeat responsible for the disorder has been known for over 20 years, yet a firm understanding of HD pathogenesis remains elusive. Our group's discovery of resistance of Mn accumulation and toxicity in HD presented the opportunity to interrogate a single phenotype using a multidisciplinary approach. In a similar fashion, Mn was an established epidemiological risk factor for parkinsonism including manganism and PD. Our optimization of CFMEA quantify cellular Mn content permitted screening a large chemical library for modulators of neuronal Mn status while naïve to the mechanism of action of individual small molecules. Similarly, untargeted metabolomics allowed assessment of the global

metabolite changes in response to genotype and Mn burden. Although they each technique provided a different perspective, both approaches provided complementary insight into neuronal Mn regulation. Subsequently, hiPSC technology allowed the application of the small molecule toolbox to assess Mn regulation in the context of human neurodevelopment. The combination of HTS and untargeted metabolomics using hiSPC technology is broadly applicable to any pathology with known links to an environmental or iatrogenic agent. The recent advent of these technologies made a nearly impossible task, screening thousands of chemicals and metabolite identification, an achievable goal. Furthermore, this approach has the potential to accelerate discovery of mechanisms underlying cellular physiology and disease pathogenesis.

REFERENCES

Alexander, N., Woetzel, N. and Meiler, J. (2011). Bcl:: Cluster: A method for clustering biological molecules coupled with visualization in the Pymol Molecular Graphics System. *IEEE,* 13-18.

Ali, S. F., Binienda, Z. K. and Imam, S. Z. (2011). Molecular aspects of dopaminergic neurodegeneration: gene-environment interaction in parkin dysfunction. *Int J Environ Res Public Health,* **8**(12): 4702-4713.

Anson, B. D., Kolaja, K. L. and Kamp, T. J. (2011). Opportunities for use of human iPS cells in predictive toxicology. *Clin Pharmacol Ther,* **89**(5): 754-758.

Arrasate, M., Mitra, S., Schweitzer, E. S., Segal, M. R. and Finkbeiner, S. (2004). Inclusion body formation reduces levels of mutant huntingtin and the risk of neuronal death. *Nature,* **431**(7010): 805-810.

Aschner, J. L. and Aschner, M. (2005). Nutritional aspects of manganese homeostasis. *Mol Aspects Med,* **26**(4-5): 353-362.

Aschner, M. and Dorman, D. C. (2006). Manganese: pharmacokinetics and molecular mechanisms of brain uptake. *Toxicol Rev,* **25**(3): 147-154.

Aschner, M., Erikson, K. M., Herrero Hernandez, E. and Tjalkens, R. (2009). Manganese and its role in Parkinson's disease: from transport to neuropathology. *Neuromolecular Med,* **11**(4): 252-266.

Aschner, M., Guilarte, T. R., Schneider, J. S. and Zheng, W. (2007). Manganese: recent advances in understanding its transport and neurotoxicity. *Toxicol Appl Pharmacol,* **221**(2): 131-147.

Aschner, M., Shanker, G., Erikson, K., Yang, J. and Mutkus, L. A. (2002). The uptake of manganese in brain endothelial cultures. *Neurotoxicology,* **23**(2): 165-168.

Aubry, L., Bugi, A., Lefort, N., Rousseau, F., Peschanski, M. and Perrier, A. L. (2008). Striatal progenitors derived from human ES cells mature into DARPP32 neurons in vitro and in quinolinic acid-lesioned rats. *Proc Natl Acad Sci U S A,* **105**(43): 16707-16712.

Austen, M. and Dohrmann, C. (2005). Phenotype-first screening for the identification of novel drug targets. *Drug Discov Today,* **10**(4): 275-282.

Bae, B. I., Xu, H., Igarashi, S., Fujimuro, M., Agrawal, N., Taya, Y., Hayward, S. D., Moran, T. H., Montell, C., Ross, C. A., Snyder, S. H. and Sawa, A. (2005). p53 mediates cellular dysfunction and behavioral abnormalities in Huntington's disease. *Neuron,* **47**(1): 29-41.

Bae, J.-H., Jang, B.-C., Suh, S.-I., Ha, E., Baik, H., Kim, S.-S., Lee, M.-y. and Shin, D.-H. (2006). Manganese induces inducible nitric oxide synthase (iNOS) expression via activation of both MAP kinase and PI3K/Akt pathways in BV2 microglial cells. *Neuroscience letters,* **398**(1-2): 151-154.

Banito, A. and Gil, J. (2010). Induced pluripotent stem cells and senescence: learning the biology to improve the technology. *EMBO Reports,* **11**(5): 353-359.

Bates, G., Harper, P. S. and Jones, L. (2002). Huntington's disease. Oxford ; New York, Oxford University Press.

Begley, T. P., Kinsland, C. and Strauss, E. (2001). The biosynthesis of coenzyme A in bacteria. *Vitam Horm,* **61**(157-171.

Benito-Leon, J., Bermejo-Pareja, F., Morales, J. M., Vega, S. and Molina, J. A. (2003). Prevalence of essential tremor in three elderly populations of central Spain. *Mov Disord,* **18**(4): 389-394.

Bibb, J. A., Yan, Z., Svenningsson, P., Snyder, G. L., Pieribone, V. A., Horiuchi, A., Nairn, A. C., Messer, A. and Greengard, P. (2000). Severe deficiencies in dopamine signaling in presymptomatic Huntington's disease mice. *Proc Natl Acad Sci U S A,* **97**(12): 6809-6814.

Bissonnette, C. J., Lyass, L., Bhattacharyya, B. J., Belmadani, A., Miller, R. J. and Kessler, J. A. (2011). The controlled generation of functional basal forebrain cholinergic neurons from human embryonic stem cells. *Stem Cells,* **29**(5): 802-811.

Bleicher, K. H., Bohm, H. J., Muller, K. and Alanine, A. I. (2003). Hit and lead generation: beyond high-throughput screening. *Nat Rev Drug Discov,* **2**(5): 369-378.

Bock, C., Kiskinis, E., Verstappen, G., Gu, H., Boulting, G., Smith, Z. D., Ziller, M., Croft, G. F., Amoroso, M. W., Oakley, D. H., Gnirke, A., Eggan, K. and Meissner, A. (2011). Reference Maps of human ES and iPS cell variation enable high-throughput characterization of pluripotent cell lines. *Cell,* **144**(3): 439-452.

Bouchard, M. F., Sauve, S., Barbeau, B., Legrand, M., Brodeur, M. E., Bouffard, T., Limoges, E., Bellinger, D. C. and Mergler, D. (2011). Intellectual impairment in school-age children exposed to manganese from drinking water. *Environ Health Perspect,* **119**(1): 138-143.

Boulting, G. L., Kiskinis, E., Croft, G. F., Amoroso, M. W., Oakley, D. H., Wainger, B. J., Williams, D. J., Kahler, D. J., Yamaki, M., Davidow, L., Rodolfa, C. T., Dimos, J. T., Mikkilineni, S., MacDermott, A. B., Woolf, C. J., Henderson, C. E., Wichterle, H. and Eggan, K. (2011). A functionally characterized test set of human induced pluripotent stem cells. *Nat Biotechnol,* **29**(3): 279-286.

Bowler, R. M., Gysens, S., Diamond, E., Booty, A., Hartney, C. and Roels, H. A. (2003). Neuropsychological sequelae of exposure to welding fumes in a group of occupationally exposed men. *Int J Hyg Environ Health,* **206**(6): 517-529.

Bowman, A. B. and Aschner, M. (2014). Considerations on manganese (Mn) treatments for in vitro studies. *Neurotoxicology,* **41**: 141-142.

Bowman, A. B., Kwakye, G. F., Hernandez, E. H. and Aschner, M. (2011). Role of manganese in neurodegenerative diseases. *J Trace Elem Med Biol,* **25**(4): 191-203.

Brambrink, T., Foreman, R., Welstead, G. G., Lengner, C. J., Wernig, M., Suh, H. and Jaenisch, R. (2008). Sequential expression of pluripotency markers during direct reprogramming of mouse somatic cells. *Cell Stem Cell,* **2**(2): 151-159.

Breier, J. M., Gassmann, K., Kayser, R., Stegeman, H., De Groot, D., Fritsche, E. and Shafer, T. J. (2010). Neural progenitor cells as models for high-throughput screens of developmental neurotoxicity: state of the science. *Neurotoxicol Teratol,* **32**(1): 4-15.

Breier, J. M., Radio, N. M., Mundy, W. R. and Shafer, T. J. (2008). Development of a high-throughput screening assay for chemical effects on proliferation and viability of immortalized human neural progenitor cells. *Toxicol Sci,* **105**(1): 119-133.

Brennand, K. J., Simone, A., Jou, J., Gelboin-Burkhart, C., Tran, N., Sangar, S., Li, Y., Mu, Y., Chen, G., Yu, D., McCarthy, S., Sebat, J. and Gage, F. H. (2011). Modelling schizophrenia using human induced pluripotent stem cells. *Nature,* **473**(7346): 221-225.

Brideau, C., Gunter, B., Pikounis, B. and Liaw, A. (2003). Improved statistical methods for hit selection in high-throughput screening. *J Biomol Screen,* **8**(6): 634-647.

Brinkman, R. R., Mezei, M. M., Theilmann, J., Almqvist, E. and Hayden, M. R. (1997). The likelihood of being affected with Huntington disease by a particular age, for a specific CAG size. *Am J Hum Genet,* **60**(5): 1202-1210.

Brouillet, E. P., Shinobu, L., McGarvey, U., Hochberg, F. and Beal, M. F. (1993). Manganese injection into the rat striatum produces excitotoxic lesions by impairing energy metabolism. *Exp Neurol,* **120**(1): 89-94.

Browne, S. E. and Beal, M. F. (2006). Oxidative damage in Huntington's disease pathogenesis. *Antioxidants & Redox Signaling,* **8**(11-12): 2061-2073.

Butkiewicz, M., Lowe, E. W., Jr., Mueller, R., Mendenhall, J. L., Teixeira, P. L., Weaver, C. D. and Meiler, J. (2013). Benchmarking ligand-based virtual High-Throughput Screening with the PubChem database. *Molecules,* **18**(1): 735-756.

Butterworth, J. (1986). Changes in nine enzyme markers for neurons, glia, and endothelial cells in agonal state and Huntington's disease caudate nucleus. *J Neurochem,* **47**(2): 583-587.

Buzanska, L., Sypecka, J., Nerini-Molteni, S., Compagnoni, A., Hogberg, H. T., del Torchio, R., Domanska-Janik, K., Zimmer, J. and Coecke, S. (2009). A human stem cell-based model for identifying adverse effects of organic and inorganic chemicals on the developing nervous system. *Stem Cells,* **27**(10): 2591-2601.

Caiazzo, M., Dell'Anno, M. T., Dvoretskova, E., Lazarevic, D., Taverna, S., Leo, D., Sotnikova, T. D., Menegon, A., Roncaglia, P., Colciago, G., Russo, G., Carninci, P., Pezzoli, G., Gainetdinov, R. R., Gustincich, S., Dityatev, A. and Broccoli, V. (2011). Direct generation of functional dopaminergic neurons from mouse and human fibroblasts. *Nature,*

Calne, D. B., Chu, N. S., Huang, C. C., Lu, C. S. and Olanow, W. (1994). Manganism and idiopathic parkinsonism: similarities and differences. *Neurology,* **44**(9): 1583-1586.

Cersosimo, M. G. and Koller, W. C. (2006). The diagnosis of manganese-induced parkinsonism. *Neurotoxicology,* **27**(3): 340-346.

Cha, J. H., Kosinski, C. M., Kerner, J. A., Alsdorf, S. A., Mangiarini, L., Davies, S. W., Penney, J. B., Bates, G. P. and Young, A. B. (1998). Altered brain neurotransmitter receptors in transgenic mice expressing a portion of an abnormal human huntington disease gene. *Proc Natl Acad Sci U S A,* **95**(11): 6480-6485.

Chamberlain, S. J., Li, X.-J. and Lalande, M. (2008). Induced pluripotent stem (iPS) cells as in vitro models of human neurogenetic disorders. *Neurogenetics,* **9**(4): 227-235.

Chambers, S. M., Fasano, C. A., Papapetrou, E. P., Tomishima, M., Sadelain, M. and Studer, L. (2009). Highly efficient neural conversion of human ES and iPS cells by dual inhibition of SMAD signaling. *Nat Biotechnol,* **27**(3): 275-280.

Chin, M. H., Mason, M. J., Xie, W., Volinia, S., Singer, M., Peterson, C., Ambartsumyan, G., Aimiuwu, O., Richter, L., Zhang, J., Khvorostov, I., Ott, V., Grunstein, M., Lavon, N., Benvenisty, N., Croce, C. M., Clark, A. T., Baxter, T., Pyle, A. D., Teitell, M. A., Pelegrini, M., Plath, K. and Lowry, W. E. (2009). Induced pluripotent stem cells and embryonic stem cells are distinguished by gene expression signatures. *Cell Stem Cell,* **5**(1): 111-123.

Cho, M. S., Lee, Y. E., Kim, J. Y., Chung, S., Cho, Y. H., Kim, D. S., Kang, S. M., Lee, H., Kim, M. H., Kim, J. H., Leem, J. W., Oh, S. K., Choi, Y. M., Hwang, D. Y., Chang, J. W. and Kim, D. W. (2008). Highly efficient and large-scale generation of functional dopamine neurons from human embryonic stem cells. *Proc Natl Acad Sci U S A,* **105**(9): 3392-3397.

Choi, B. S. and Zheng, W. (2009). Copper transport to the brain by the blood-brain barrier and blood-CSF barrier. *Brain Res,* **1248**: 14-21.

Chun, H. S., Lee, H. and Son, J. H. (2001). Manganese induces endoplasmic reticulum (ER) stress and activates multiple caspases in nigral dopaminergic neuronal cells, SN4741. *Neurosci Lett,* **316**(1): 5-8.

Claudia, Z., Dieter, L. and Alan, S. H. (2004). Brain energy metabolism in a sub-acute rat model of manganese neurotoxicity: an ex vivo nuclear magnetic resonance study using [1-13C]glucose. *Neurotoxicology,* **25**(4): 573-87.

Claveria, L. E., Duarte, J., Sevillano, M. D., Perez-Sempere, A., Cabezas, C., Rodriguez, F. and de Pedro-Cuesta, J. (2002). Prevalence of Parkinson's disease in Cantalejo, Spain: a door-to-door survey. *Mov Disord,* **17**(2): 242-249.

Coon, S., Stark, A., Peterson, E., Gloi, A., Kortsha, G., Pounds, J., Chettle, D. and Gorell, J. (2006). Whole-body lifetime occupational lead exposure and risk of Parkinson's disease. *Environ Health Perspect,* **114**(12): 1872-1876.

Cousins, R. J., Liuzzi, J. P. and Lichten, L. A. (2006). Mammalian zinc transport, trafficking, and signals. *J Biol Chem,* **281**(34): 24085-24089.

Cowan, C. and Raymond, L. (2006). Selective neuronal degeneration in Huntington's disease. *Curr Top Dev Biol,* **75**: 25-71.

Crossgrove, J. and Zheng, W. (2004). Manganese toxicity upon overexposure. *NMR Biomed,* **17**(8): 544-553.

Crossgrove, J. S., Allen, D. D., Bukaveckas, B. L., Rhineheimer, S. S. and Yokel, R. A. (2003). Manganese distribution across the blood-brain barrier. I. Evidence for carrier-mediated influx of managanese citrate as well as manganese and manganese transferrin. *Neurotoxicology,* **24**(1): 3-13.

Davies, S. W., Turmaine, M., Cozens, B. A., DiFiglia, M., Sharp, A. H., Ross, C. A., Scherzinger, E., Wanker, E. E., Mangiarini, L. and Bates, G. P. (1997). Formation of neuronal intranuclear inclusions underlies the neurological dysfunction in mice transgenic for the HD mutation. *Cell,* **90**(3): 537-548.

de Lau, L. M. and Breteler, M. M. (2006). Epidemiology of Parkinson's disease. *Lancet Neurol,* **5**(6): 525-535.

de Rijk, M. C., Breteler, M. M., Graveland, G. A., Ott, A., Grobbee, D. E., van der Meche, F. G. and Hofman, A. (1995). Prevalence of Parkinson's disease in the elderly: the Rotterdam Study. *Neurology,* **45**(12): 2143-2146.

de Rijk, M. C., Tzourio, C., Breteler, M. M., Dartigues, J. F., Amaducci, L., Lopez-Pousa, S., Manubens-Bertran, J. M., Alperovitch, A. and Rocca, W. A. (1997). Prevalence of parkinsonism and Parkinson's disease in Europe: the EUROPARKINSON Collaborative Study. European Community Concerted Action on the Epidemiology of Parkinson's disease. *J Neurol Neurosurg Psychiatry,* **62**(1): 10-15.

Dean, A., Ferlin, M. G., Brun, P., Castagliuolo, I., Yokel, R. A., Badocco, D., Pastore, P., Venzo, A., Bombi, G. G. and Di Marco, V. B. (2009). 1,6-Dimethyl-4-hydroxy-3-pyridinecarboxylic acid and 4-hydroxy-2-methyl-3-pyridinecarboxylic acid as new possible chelating agents for iron and aluminium. *Dalton Trans,* 10): 1815-1824.

Derewacz, D. K., Goodwin, C. R., McNees, C. R., McLean, J. A. and Bachmann, B. O. (2013). Antimicrobial drug resistance affects broad changes in metabolomic phenotype in addition to secondary metabolism. *Proc Natl Acad Sci U S A,* **110**(6): 2336-2341.

Dick, F. D., De Palma, G., Ahmadi, A., Osborne, A., Scott, N. W., Prescott, G. J., Bennett, J., Semple, S., Dick, S., Mozzoni, P., Haites, N., Wettinger, S. B., Mutti, A., Otelea, M., Seaton, A., Soderkvist, P., Felice, A. and group, G. s. (2007). Gene-environment interactions in parkinsonism and Parkinson's disease: the Geoparkinson study. *Occupational and Environmental Medicine,* **64**(10): 673-680.

DiFiglia, M., Sapp, E., Chase, K., Schwarz, C., Meloni, A., Young, C., Martin, E., Vonsattel, J. P., Carraway, R., Reeves, S. A. and et al. (1995). Huntingtin is a cytoplasmic protein associated with vesicles in human and rat brain neurons. *Neuron,* **14**(5): 1075-1081.

Dimos, J. T., Rodolfa, K. T., Niakan, K. K., Weisenthal, L. M., Mitsumoto, H., Chung, W., Croft, G. F., Saphier, G., Leibel, R., Goland, R., Wichterle, H., Henderson, C. E. and Eggan, K. (2008). Induced pluripotent stem cells generated from patients with ALS can be differentiated into motor neurons. *Science,* **321**(5893): 1218-1221.

Dobson, A. W., Erikson, K. M. and Aschner, M. (2004). Manganese neurotoxicity. *Ann N Y Acad Sci,* **1012**: 115-128.

Doi, A., Park, I.-H., Wen, B., Murakami, P., Aryee, M. J., Irizarry, R., Herb, B., Ladd-Acosta, C., Rho, J., Loewer, S., Miller, J., Schlaeger, T., Daley, G. Q. and Feinberg, A. P. (2009). Differential methylation of tissue- and cancer-specific CpG island shores distinguishes human induced pluripotent stem cells, embryonic stem cells and fibroblasts. *Nature Genetics,* **41**(12): 1350-1353.

Dolgin, E. (2010). Putting stem cells to the test. *Nat Med,* **16**(12): 1354-1357.

Dolmetsch, R. and Geschwind, D. H. (2011). The human brain in a dish: the promise of iPSC-derived neurons. *Cell,* **145**(6): 831-834.

Domaille, D. W., Que, E. L. and Chang, C. J. (2008). Synthetic fluorescent sensors for studying the cell biology of metals. *Nat Chem Biol,* **4**(3): 168-175.

Drewry, D. H., Willson, T. M. and Zuercher, W. J. (2014). Seeding collaborations to advance kinase science with the GSK Published Kinase Inhibitor Set (PKIS). *Curr Top Med Chem,* **14**(3): 340-342.

Dwight, D. K., Sarah, P. Y., Niels, G., Jerry, V., Wendy, E. S., Daniel Kelly, B., Yan, A., Susan, D. W., Shu, H. C., Deeksha, B., Marie, T. M., Priya, S. K., Chen, Y. T. and David, S. M. (2003). Rare Disorders of Metabolism with Elevated Butyryl- and Isobutyryl-Carnitine Detected by Tandem Mass Spectrometry Newborn Screening. *Pediatric Research,* **54**(2): 219-23.

Ebert, A. D., Yu, J., Rose, F. F., Mattis, V. B., Lorson, C. L., Thomson, J. A. and Svendsen, C. N. (2009). Induced pluripotent stem cells from a spinal muscular atrophy patient. *Nature,* **457**(7227): 277-280.

Eichler, G. S., Huang, S. and Ingber, D. E. (2003). Gene Expression Dynamics Inspector (GEDI): for integrative analysis of expression profiles. *Bioinformatics,* **19**(17): 2321-2322.

Elbaz, A. and Moisan, F. (2008). Update in the epidemiology of Parkinson's disease. *Curr Opin Neurol,* **21**(4): 454-460.

Ellis, J. and Bhatia, M. (2011). iPSC technology: platform for drug discovery. Point. *Clinical pharmacology and therapeutics,* **89**(5): 639-641.

Erikson, K., Thompson, K., Aschner, J. and Aschner, M. (2007). Manganese neurotoxicity: a focus on the neonate. *Pharmacology & therapeutics,* **113**(2): 369-377.

Erikson, K. M., Dorman, D. C., Fitsanakis, V., Lash, L. H. and Aschner, M. (2006). Alterations of oxidative stress biomarkers due to in utero and neonatal exposures of airborne manganese. *Biol Trace Elem Res,* **111**(1-3): 199-215.

Erikson, K. M., Shihabi, Z. K., Aschner, J. L. and Aschner, M. (2002). Manganese accumulates in iron-deficient rat brain regions in a heterogeneous fashion and is associated with neurochemical alterations. *Biol Trace Elem Res,* **87**(1-3): 143-156.

Esteban, M. A., Wang, T., Qin, B., Yang, J., Qin, D., Cai, J., Li, W., Weng, Z., Chen, J., Ni, S., Chen, K., Li, Y., Liu, X., Xu, J., Zhang, S., Li, F., He, W., Labuda, K., Song, Y., Peterbauer, A., Wolbank, S., Redl, H., Zhong, M., Cai, D., Zeng, L. and Pei, D. (2010). Vitamin C enhances the generation of mouse and human induced pluripotent stem cells. *Cell Stem Cell,* **6**(1): 71-79.

Fall, P. A., Axelson, O., Fredriksson, M., Hansson, G., Lindvall, B., Olsson, J. E. and Granerus, A. K. (1996). Age-standardized incidence and prevalence of Parkinson's disease in a Swedish community. *J Clin Epidemiol,* **49**(6): 637-641.

Farina, M., Rocha, J. B. T. and Aschner, M. (2011). Mechanisms of methylmercury-induced neurotoxicity: Evidence from experimental studies. *Life Sci,* **89**(15-16): 555-563.

Finkelstein, M. M. and Jerrett, M. (2007). A study of the relationships between Parkinson's disease and markers of traffic-derived and environmental manganese air pollution in two Canadian cities. *Environ Res,* **104**(3): 420-432.

Finkelstein, Y., Milatovic, D. and Aschner, M. (2007). Modulation of cholinergic systems by manganese. *Neurotoxicology,* **28**(5): 1003-1014.

Finney, L. A. and O'Halloran, T. V. (2003). Transition metal speciation in the cell: insights from the chemistry of metal ion receptors. *Science,* **300**(5621): 931-936.

Fitsanakis, V. A., Zhang, N., Anderson, J. G., Erikson, K. M., Avison, M. J., Gore, J. C. and Aschner, M. (2008). Measuring brain manganese and iron accumulation in rats following 14 weeks of low-dose manganese treatment using atomic absorption spectroscopy and magnetic resonance imaging. *Toxicol Sci,* **103**(1): 116-124.

Fragou, D., Fragou, A., Kouidou, S., Njau, S. and Kovatsi, L. (2011). Epigenetic mechanisms in metal toxicity. *Toxicology Mechanisms and Methods,* **21**(4): 343-352.

Friedman, J. H., Trieschmann, M. E., Myers, R. H. and Fernandez, H. H. (2005). Monozygotic twins discordant for Huntington disease after 7 years. *Arch Neurol,* **62**(6): 995-997.

Frigerio, R., Fujishiro, H., Maraganore, D. M., Klos, K. J., DelleDonne, A., Heckman, M. G., Crook, J. E., Josephs, K. A., Parisi, J. E., Boeve, B. F., Dickson, D. W. and Ahlskog, J. E. (2009). Comparison of risk factor profiles in incidental Lewy body disease and Parkinson disease. *Arch Neurol,* **66**(9): 1114-1119.

Frigerio, R., Sanft, K. R., Grossardt, B. R., Peterson, B. J., Elbaz, A., Bower, J. H., Ahlskog, J. E., de Andrade, M., Maraganore, D. M. and Rocca, W. A. (2006). Chemical exposures and Parkinson's disease: a population-based case-control study. *Mov Disord,* **21**(10): 1688-1692.

Fritsche, E., Cline, J. E., Nguyen, N.-H., Scanlan, T. S. and Abel, J. (2005). Polychlorinated biphenyls disturb differentiation of normal human neural progenitor cells: clue for involvement of thyroid hormone receptors. *Environmental Health Perspectives,* **113**(7): 871-876.

Fujishiro, H., Doi, M., Enomoto, S. and Himeno, S. (2011). High sensitivity of RBL-2H3 cells to cadmium and manganese: an implication of the role of ZIP8. *Metallomics,* **3**(7): 710-718.

Fujishiro, H., Kubota, K., Inoue, D., Inoue, A., Yanagiya, T., Enomoto, S. and Himeno, S. (2011). Cross-resistance of cadmium-resistant cells to manganese is associated with reduced accumulation of both cadmium and manganese. *Toxicology,* **280**(3): 118-125.

Fujishiro, H., Yano, Y., Takada, Y., Tanihara, M. and Himeno, S. (2012). Roles of ZIP8, ZIP14, and DMT1 in transport of cadmium and manganese in mouse kidney proximal tubule cells. *Metallomics,* **4**(7): 700-708.

Fukushima, T., Tan, X., Luo, Y. and Kanda, H. (2009). Relationship between Blood Levels of Heavy Metals and Parkinson's Disease in China. *Neuroepidemiology,* **34**(1): 18-24.

Garcia, S. J., Gellein, K., Syversen, T. and Aschner, M. (2007). Iron deficient and manganese supplemented diets alter metals and transporters in the developing rat brain. *Toxicol Sci,* **95**(1): 205-214.

Garrick, M. D., Dolan, K. G., Horbinski, C., Ghio, A. J., Higgins, D., Porubcin, M., Moore, E. G., Hainsworth, L. N., Umbreit, J. N., Conrad, M. E., Feng, L., Lis, A., Roth, J. A., Singleton, S. and Garrick, L. M. (2003). DMT1: a mammalian transporter for multiple metals. *Biometals,* **16**(1): 41-54.

Garrick, M. D., Singleton, S. T., Vargas, F., Kuo, H. C., Zhao, L., Knopfel, M., Davidson, T., Costa, M., Paradkar, P., Roth, J. A. and Garrick, L. M. (2006). DMT1: which metals does it transport? *Biol Res,* **39**(1): 79-85.

Genschow, E., Spielmann, H., Scholz, G., Pohl, I., Seiler, A., Clemann, N., Bremer, S. and Becker, K. (2004). Validation of the embryonic stem cell test in the international ECVAM validation study on three in vitro embryotoxicity tests. *Altern Lab Anim,* **32**(3): 209-244.

Georgiou, N., Bradshaw, J. L., Chiu, E., Tudor, A., O'Gorman, L. and Phillips, J. G. (1999). Differential clinical and motor control function in a pair of monozygotic twins with Huntington's disease. *Mov Disord,* **14**(2): 320-325.

Giorgini, F. (2013). A flexible polyglutamine hinge opens new doors for understanding huntingtin function. *Proc. Natl. Acad. Sci. U.S.A.,* **110**(36): 14516-14517.

Girijashanker, K., He, L., Soleimani, M., Reed, J. M., Li, H., Liu, Z., Wang, B., Dalton, T. P. and Nebert, D. W. (2008). Slc39a14 gene encodes ZIP14, a metal/bicarbonate symporter: similarities to the ZIP8 transporter. *Mol Pharmacol,* **73**(5): 1413-1423.

Gitler, A. D., Chesi, A., Geddie, M. L., Strathearn, K. E., Hamamichi, S., Hill, K. J., Caldwell, K. A., Caldwell, G. A., Cooper, A. A., Rochet, J. C. and Lindquist, S. (2009). Alpha-synuclein is part of a diverse and highly conserved interaction network that includes PARK9 and manganese toxicity. *Nat Genet,* **41**(3): 308-315.

Gomez-Esteban, J. C., Lezcano, E., Zarranz, J. J., Velasco, F., Garamendi, I., Perez, T. and Tijero, B. (2007). Monozygotic twins suffering from Huntington's disease show different cognitive and behavioural symptoms. *Eur Neurol,* **57**(1): 26-30.

Gomez-Tortosa, E., MacDonald, M. E., Friend, J. C., Taylor, S. A., Weiler, L. J., Cupples, L. A., Srinidhi, J., Gusella, J. F., Bird, E. D., Vonsattel, J. P. and Myers, R. H. (2001). Quantitative neuropathological changes in presymptomatic Huntington's disease. *Ann Neurol,* **49**(1): 29-34.

Gonzalez-Cuyar, L. F., Nelson, G., Criswell, S. R., Ho, P., Lonzanida, J. A., Checkoway, H., Seixas, N., Gelman, B. B., Evanoff, B. A., Murray, J., Zhang, J. and Racette, B. A. (2013). Quantitative neuropathology associated with chronic manganese exposure in South African mine workers. *Neurotoxicology,* doi: 10.1016/j.neuro.2013.12.008.

Goodwin, C. R., Sherrod, S. D., Marasco, C. C., Bachmann, B. O., Schramm-Sapyta, N., Wikswo, J. P. and McLean, J. A. (2014). Phenotypic Mapping of Metabolic Profiles Using Self-Organizing Maps of High-Dimensional Mass Spectrometry Data. *Analytical Chemistry,* **86**(13): 6563-6571.

Gore, A., Li, Z., Fung, H.-L., Young, J. E., Agarwal, S., Antosiewicz-Bourget, J., Canto, I., Giorgetti, A., Israel, M. A., Kiskinis, E., Lee, J.-H., Loh, Y.-H., Manos, P. D., Montserrat, N., Panopoulos, A. D., Ruiz, S., Wilbert,

M. L., Yu, J., Kirkness, E. F., Izpisua Belmonte, J. C., Rossi, D. J., Thomson, J. A., Eggan, K., Daley, G. Q., Goldstein, L. S. B. and Zhang, K. (2011). Somatic coding mutations in human induced pluripotent stem cells. *Nature,* **471**(7336): 63-67.

Gorell, J. M., Johnson, C. C., Rybicki, B. A., Peterson, E. L., Kortsha, G. X., Brown, G. G. and Richardson, R. J. (1999). Occupational exposure to manganese, copper, lead, iron, mercury and zinc and the risk of Parkinson's disease. *Neurotoxicology,* **20**(2-3): 239-247.

Gorell, J. M., Peterson, E. L., Rybicki, B. A. and Johnson, C. C. (2004). Multiple risk factors for Parkinson's disease. *J Neurol Sci,* **217**(2): 169-174.

Gospe, S. M., Jr., Caruso, R. D., Clegg, M. S., Keen, C. L., Pimstone, N. R., Ducore, J. M., Gettner, S. S. and Kreutzer, R. A. (2000). Paraparesis, hypermanganesaemia, and polycythaemia: a novel presentation of cirrhosis. *Arch Dis Child,* **83**(5): 439-442.

Greenamyre, J. T. and Hastings, T. G. (2004). Biomedicine. Parkinson's--divergent causes, convergent mechanisms. *Science,* **304**(5674): 1120-1122.

Grimm, C., Kraft, R., Sauerbruch, S., Schultz, G. and Harteneck, C. (2003). Molecular and functional characterization of the melastatin-related cation channel TRPM3. *J Biol Chem,* **278**(24): 21493-21501.

Guenther, M. G., Frampton, G. M., Soldner, F., Hockemeyer, D., Mitalipova, M., Jaenisch, R. and Young, R. A. (2010). Chromatin structure and gene expression programs of human embryonic and induced pluripotent stem cells. *Cell Stem Cell,* **7**(2): 249-257.

Guilarte, T. R. (2010). APLP1, Alzheimer's-like pathology and neurodegeneration in the frontal cortex of manganese-exposed non-human primates. *Neurotoxicology,* **31**(5): 572-574.

Guilarte, T. R. (2010). Manganese and Parkinson's disease: a critical review and new findings. *Environ Health Perspect,* **118**(8): 1071-1080.

Guilbert, A., Gautier, M., Dhennin-Duthille, I., Haren, N., Sevestre, H. and Ouadid-Ahidouch, H. (2009). Evidence that TRPM7 is required for breast cancer cell proliferation. *Am J Physiol Cell Physiol,* **297**(3): C493-502.

Gunshin, H., Mackenzie, B., Berger, U. V., Gunshin, Y., Romero, M. F., Boron, W. F., Nussberger, S., Gollan, J. L. and Hediger, M. A. (1997). Cloning and characterization of a mammalian proton-coupled metal-ion transporter. *Nature,* **388**(6641): 482-488.

Haidet-Phillips, A. M., Hester, M. E., Miranda, C. J., Meyer, K., Braun, L., Frakes, A., Song, S., Likhite, S., Murtha, M. J., Foust, K. D., Rao, M., Eagle, A., Kammesheidt, A., Christensen, A., Mendell, J. R., Burghes, A. H. and Kaspar, B. K. (2011). Astrocytes from familial and sporadic ALS patients are toxic to motor neurons. *Nat Biotechnol,* **29**(9): 824-828.

Hankowski, K. E., Hamazaki, T., Umezawa, A. and Terada, N. (2011). Induced pluripotent stem cells as a next-generation biomedical interface. *Lab Invest,* **91**(7): 972-977.

125

Hansen, S. L., Trakooljul, N., Liu, H. C., Moeser, A. J. and Spears, J. W. (2009). Iron transporters are differentially regulated by dietary iron, and modifications are associated with changes in manganese metabolism in young pigs. *J Nutr,* **139**(8): 1474-1479.

Harrill, J. A., Freudenrich, T. M., Machacek, D. W., Stice, S. L. and Mundy, W. R. (2010). Quantitative assessment of neurite outgrowth in human embryonic stem cell-derived hN2 cells using automated high-content image analysis. *Neurotoxicology,* **31**(3): 277-290.

Harrill, J. A., Freudenrich, T. M., Robinette, B. L. and Mundy, W. R. (2011). Comparative sensitivity of human and rat neural cultures to chemical-induced inhibition of neurite outgrowth. *Toxicol Appl Pharmacol,* **256**(3): 268-80.

Hayden, M. R. (1981). Huntington's chorea. Berlin ; New York, Springer-Verlag.

Hayflick, S. J., Westaway, S. K., Levinson, B., Zhou, B., Johnson, M. A., Ching, K. H. and Gitschier, J. (2003). Genetic, clinical, and radiographic delineation of Hallervorden-Spatz syndrome. *N Engl J Med,* **348**(1): 33-40.

He, L., Girijashanker, K., Dalton, T. P., Reed, J., Li, H., Soleimani, M. and Nebert, D. W. (2006). ZIP8, member of the solute-carrier-39 (SLC39) metal-transporter family: characterization of transporter properties. *Mol Pharmacol,* **70**(1): 171-180.

Heng, B. C., Richards, M., Shu, Y. and Gribbon, P. (2009). Induced pluripotent stem cells: a new tool for toxicology screening? *Archives of Toxicology,* **83**(7): 641-644.

Heuer, J., Bremer, S., Pohl, I. and Spielmann, H. (1993). Development of an in vitro embryotoxicity test using murine embryonic stem cell cultures. *Toxicol In Vitro,* **7**(4): 551-556.

Himeno, S., Yanagiya, T. and Fujishiro, H. (2009). The role of zinc transporters in cadmium and manganese transport in mammalian cells. *Biochimie,* **91**(10): 1218-1222.

Hirata, Y., Furuta, K., Miyazaki, S., Suzuki, M. and Kiuchi, K. (2004). Anti-apoptotic and pro-apoptotic effect of NEPP11 on manganese-induced apoptosis and JNK pathway activation in PC12 cells. *Brain research,* **1021**(2): 241-247.

Hong, H., Takahashi, K., Ichisaka, T., Aoi, T., Kanagawa, O., Nakagawa, M., Okita, K. and Yamanaka, S. (2009). Suppression of induced pluripotent stem cell generation by the p53-p21 pathway. *Nature,* **460**(7259): 1132-1135.

Hu, B. Y., Du, Z. W. and Zhang, S. C. (2009). Differentiation of human oligodendrocytes from pluripotent stem cells. *Nat Protoc,* **4**(11): 1614-1622.

Hu, B.Y., Weick, J. P., Yu, J., Ma, L.-X., Zhang, X.-Q., Thomson, J. A. and Zhang, S.-C. (2010). Neural differentiation of human induced pluripotent stem cells follows developmental principles but with variable potency. *Proc Natl Acad Sci USA,* **107**(9): 4335-4340.

Huang, E., Ong, W. Y. and Connor, J. R. (2004). Distribution of divalent metal transporter-1 in the monkey basal ganglia. *Neuroscience,* **128**(3): 487-496.

Huangfu, D., Maehr, R., Guo, W., Eijkelenboom, A., Snitow, M., Chen, A. E. and Melton, D. A. (2008). Induction of pluripotent stem cells by defined factors is greatly improved by small-molecule compounds. *Nat Biotechnol,* **26**(7): 795-797.

Hudnell, H. K. (1999). Effects from environmental Mn exposures: a review of the evidence from non-occupational exposure studies. *Neurotoxicology,* **20**(2-3): 379-397.

Hult, S., Schultz, K., Soylu, R. and Petersen, A. (2010). Hypothalamic and neuroendocrine changes in Huntington's disease. *Curr Drug Targets,* **11**(10): 1237-1249.

Hussein, S. M., Batada, N. N., Vuoristo, S., Ching, R. W., Autio, R., Närvä, E., Ng, S., Sourour, M., Hämäläinen, R., Olsson, C., Lundin, K., Mikkola, M., Trokovic, R., Peitz, M., Brüstle, O., Bazett-Jones, D. P., Alitalo, K., Lahesmaa, R., Nagy, A. and Otonkoski, T. (2011). Copy number variation and selection during reprogramming to pluripotency. *Nature,* **471**(7336): 58-62.

Inglese, J., Auld, D. S., Jadhav, A., Johnson, R. L., Simeonov, A., Yasgar, A., Zheng, W. and Austin, C. P. (2006). Quantitative high-throughput screening: a titration-based approach that efficiently identifies biological activities in large chemical libraries. *Proc Natl Acad Sci U S A,* **103**(31): 11473-11478.

Inglese, J., Johnson, R. L., Simeonov, A., Xia, M., Zheng, W., Austin, C. P. and Auld, D. S. (2007). High-throughput screening assays for the identification of chemical probes. *Nat Chem Biol,* **3**(8): 466-479.

Initiative, I. S. C., Adewumi, O., Aflatoonian, B., Ahrlund-Richter, L., Amit, M., Andrews, P. W., Beighton, G., Bello, P. A., Benvenisty, N., Berry, L. S., Bevan, S., Blum, B., Brooking, J., Chen, K. G., Choo, A. B. H., Churchill, G. A., Corbel, M., Damjanov, I., Draper, J. S., Dvorak, P., Emanuelsson, K., Fleck, R. A., Ford, A., Gertow, K., Gertsenstein, M., Gokhale, P. J., Hamilton, R. S., Hampl, A., Healy, L. E., Hovatta, O., Hyllner, J., Imreh, M. P., Itskovitz-Eldor, J., Jackson, J., Johnson, J. L., Jones, M., Kee, K., King, B. L., Knowles, B. B., Lako, M., Lebrin, F., Mallon, B. S., Manning, D., Mayshar, Y., McKay, R. D. G., Michalska, A. E., Mikkola, M., Mileikovsky, M., Minger, S. L., Moore, H. D., Mummery, C. L., Nagy, A., Nakatsuji, N., O'Brien, C. M., Oh, S. K. W., Olsson, C., Otonkoski, T., Park, K.-Y., Passier, R., Patel, H., Patel, M., Pedersen, R., Pera, M. F., Piekarczyk, M. S., Pera, R. A. R., Reubinoff, B. E., Robins, A. J., Rossant, J., Rugg-Gunn, P., Schulz, T. C., Semb, H., Sherrer, E. S., Siemen, H., Stacey, G. N., Stojkovic, M., Suemori, H., Szatkiewicz, J., Turetsky, T., Tuuri, T., van den Brink, S., Vintersten, K., Vuoristo, S., Ward, D., Weaver, T. A., Young, L. A. and Zhang, W. (2007). Characterization of human embryonic stem cell lines by the International Stem Cell Initiative. *Nat Biotechnol,* **25**(7): 803-816.

Inoue, H. and Yamanaka, S. (2011). The use of induced pluripotent stem cells in drug development. *Clinical pharmacology and therapeutics,* **89**(5): 655-661.

Iwami, O., Moon, C. S., Watanabe, T. and Ikeda, M. (1994). Association of metal concentrations in drinking water with the incidence of motor neuron disease in a focus on the Kii peninsula of Japan. *Bull Environ Contam Toxicol,* **52**(1): 109-116.

Iwami, O., Watanabe, T., Moon, C. S., Nakatsuka, H. and Ikeda, M. (1994). Motor neuron disease on the Kii Peninsula of Japan: excess manganese intake from food coupled with low magnesium in drinking water as a risk factor. *Sci Total Environ,* **149**(1-2): 121-135.

Jakes, R., Spillantini, M. G. and Goedert, M. (1994). Identification of two distinct synucleins from human brain. *FEBS Lett,* **345**(1): 27-32.

Jankovic, J. (2008). Parkinson's disease: clinical features and diagnosis. *J Neurol Neurosurg Psychiatry,* **79**(4): 368-376.

Jankovic, J. and Kapadia, A. S. (2001). Functional decline in Parkinson disease. *Arch Neurol,* **58**(10): 1611-1615.

Jardin, I., Gomez, L. J., Salido, G. M. and Rosado, J. A. (2009). Dynamic interaction of hTRPC6 with the Orai1-STIM1 complex or hTRPC3 mediates its role in capacitative or non-capacitative Ca(2+) entry pathways. *Biochem J,* **420**(2): 267-276.

Jaslove, S. W. (1992). The integrative properties of spiny distal dendrites. *Neuroscience,* **47**(3): 495-519.

Jeste, D. V., Barban, L. and Parisi, J. (1984). Reduced Purkinje cell density in Huntington's disease. *Exp Neurol,* **85**(1): 78-86.

Jin, Y. N., Hwang, W. Y., Jo, C. and Johnson, G. V. (2011). Metabolic state determines sensitivity to cellular stress in Huntington disease: normalization by activation of PPARγ. *PloS One,* **7**(1):

Jin, Y. N., Yu, Y. V., Gundemir, S., Jo, C., Cui, M., Tieu, K. and Johnson, G. V. (2012). Impaired mitochondrial dynamics and Nrf2 signaling contribute to compromised responses to oxidative stress in striatal cells expressing full-length mutant huntingtin. *PloS One,* **8**(3):

Johnston, P. A. and Johnston, P. A. (2002). Cellular platforms for HTS: three case studies. *Drug Discov Today,* **7**(6): 353-363.

Jones, L. L., McDonald, D. A. and Borum, P. R. (2010). Acylcarnitines: role in brain. *Prog Lipid Res,* **49**(1): 61-75.

Josephs, K. A., Ahlskog, J. E., Klos, K. J., Kumar, N., Fealey, R. D., Trenerry, M. R. and Cowl, C. T. (2005). Neurologic manifestations in welders with pallidal MRI T1 hyperintensity. *Neurology,* **64**(12): 2033-2039.

Josephson, R., Ording, C. J., Liu, Y., Shin, S., Lakshmipathy, U., Toumadje, A., Love, B., Chesnut, J. D., Andrews, P. W., Rao, M. S. and Auerbach, J. M. (2007). Qualification of embryonal carcinoma 2102Ep as a reference for human embryonic stem cell research. *Stem Cells,* **25**(2): 437-446.

Kamel, F., Tanner, C., Umbach, D., Hoppin, J., Alavanja, M., Blair, A., Comyns, K., Goldman, S., Korell, M., Langston, J., Ross, G. and Sandler, D. (2007). Pesticide exposure and self-reported Parkinson's disease in the agricultural health study. *Am J Epidemiol,* **165**(4): 364-374.

Kannurpatti, S. S., Joshi, P. G. and Joshi, N. B. (2000). Calcium sequestering ability of mitochondria modulates influx of calcium through glutamate receptor channel. *Neurochem Res,* **25**(12): 1527-1536.

Karumbayaram, S., Novitch, B. G., Patterson, M., Umbach, J. A., Richter, L., Lindgren, A., Conway, A. E., Clark, A. T., Goldman, S. A., Plath, K., Wiedau-Pazos, M., Kornblum, H. I. and Lowry, W. E. (2009). Directed differentiation of human-induced pluripotent stem cells generates active motor neurons. *Stem Cells,* **27**(4): 806-811.

Kaytor, M. D., Wilkinson, K. D. and Warren, S. T. (2004). Modulating huntingtin half-life alters polyglutamine-dependent aggregate formation and cell toxicity. *J Neurochem,* **89**(4): 962-973.

Kessner, D., Chambers, M., Burke, R., Agus, D. and Mallick, P. (2008). ProteoWizard: open source software for rapid proteomics tools development. *Bioinformatics,* **24**(21): 2534-2536.

Kim, D.-S., Lee, J. S., Leem, J. W., Huh, Y. J., Kim, J. Y., Kim, H.-S., Park, I.-H., Daley, G. Q., Hwang, D.-Y. and Kim, D.-W. (2010). Robust enhancement of neural differentiation from human ES and iPS cells regardless of their innate difference in differentiation propensity. *Stem Cell Reviews,* **6**(2): 270-281.

Kim, K., Doi, A., Wen, B., Ng, K., Zhao, R., Cahan, P., Kim, J., Aryee, M. J., Ji, H., Ehrlich, L. I. R., Yabuuchi, A., Takeuchi, A., Cunniff, K. C., Hongguang, H., McKinney-Freeman, S., Naveiras, O., Yoon, T. J., Irizarry, R. A., Jung, N., Seita, J., Hanna, J., Murakami, P., Jaenisch, R., Weissleder, R., Orkin, S. H., Weissman, I. L., Feinberg, A. P. and Daley, G. Q. (2010). Epigenetic memory in induced pluripotent stem cells. *Nature,* **467**(7313): 285-290.

Kim, Y., Kim, J. W., Ito, K., Lim, H. S., Cheong, H. K., Kim, J. Y., Shin, Y. C., Kim, K. S. and Moon, Y. (1999). Idiopathic parkinsonism with superimposed manganese exposure: utility of positron emission tomography. *Neurotoxicology,* **20**(2-3): 249-252.

Kokkinaki, M., Sahibzada, N. and Golestaneh, N. (2011). Human induced pluripotent stem-derived retinal pigment epithelium (RPE) cells exhibit ion transport, membrane potential, polarized vascular endothelial growth factor secretion, and gene expression pattern similar to native RPE. *Stem Cells,* **29**(5): 825-835.

Kotzbauer, P. T., Truax, A. C., Trojanowski, J. Q. and Lee, V. M. (2005). Altered neuronal mitochondrial coenzyme A synthesis in neurodegeneration with brain iron accumulation caused by abnormal processing, stability, and catalytic activity of mutant pantothenate kinase 2. *J Neurosci,* **25**(3): 689-698.

Kremer, H. P. (1992). The hypothalamic lateral tuberal nucleus: normal anatomy and changes in neurological diseases. *Prog Brain Res,* **93**: 249-261.

Kremer, H. P., Roos, R. A., Dingjan, G. M., Bots, G. T., Bruyn, G. W. and Hofman, M. A. (1991). The hypothalamic lateral tuberal nucleus and the characteristics of neuronal loss in Huntington's disease. *Neurosci Lett,* **132**(1): 101-104.

Krencik, R., Weick, J. P., Liu, Y., Zhang, Z. J. and Zhang, S. C. (2011). Specification of transplantable astroglial subtypes from human pluripotent stem cells. *Nat Biotechnol,* **29**(6): 528-534.

Kriks, S., Shim, J. W., Piao, J., Ganat, Y. M., Wakeman, D. R., Xie, Z., Carrillo-Reid, L., Auyeung, G., Antonacci, C., Buch, A., Yang, L., Beal, M. F., Surmeier, D. J., Kordower, J. H., Tabar, V. and Studer, L. (2011). Dopamine neurons derived from human ES cells efficiently engraft in animal models of Parkinson's disease. *Nature,* **480**(7378): 547-551.

Kuegler, P. B., Zimmer, B., Waldmann, T., Baudis, B., Ilmjarv, S., Hescheler, J., Gaughwin, P., Brundin, P., Mundy, W., Bal-Price, A. K., Schrattenholz, A., Krause, K. H., van Thriel, C., Rao, M. S., Kadereit, S. and Leist, M. (2010). Markers of murine embryonic and neural stem cells, neurons and astrocytes: reference points for developmental neurotoxicity testing. *ALTEX,* **27**(1): 17-42.

Kuhn, M., Szklarczyk, D., Pletscher-Frankild, S., Blicher, T. H., von Mering, C., Jensen, L. J. and Bork, P. (2014). STITCH 4: integration of protein-chemical interactions with user data. *Nucleic Acids Res,* **42**(Database issue): D401-407.

Kumar, K. K., Aboud, A. A. and Bowman, A. B. (2012). The potential of induced pluripotent stem cells as a translational model for neurotoxicological risk. *Neurotoxicology,* **33**(3): 518-529.

Kumar, K. K., Aboud, A. A., Patel, D. K., Aschner, M. and Bowman, A. B. (2013). Optimization of fluorescence assay of cellular manganese status for high throughput screening. *J Biochem Mol Toxicol,* **27**(1): 42-49.

Kwakye, G. F., Li, D. and Bowman, A. B. (2011). Novel high-throughput assay to assess cellular manganese levels in a striatal cell line model of Huntington's disease confirms a deficit in manganese accumulation. *Neurotoxicology,* **32**(5): 630-639.

Kwakye, G. F., Li, D., Kabobel, O. A. and Bowman, A. B. (2011). Cellular fura-2 manganese extraction assay (CFMEA). *Curr Protoc Toxicol,* **Chapter 12**: Unit 12-18.

Lang, A. E. (2007). The progression of Parkinson disease: a hypothesis. *Neurology,* **68**(12): 948-952.

Langston, J. W., Ballard, P., Tetrud, J. W. and Irwin, I. (1983). Chronic Parkinsonism in humans due to a product of meperidine-analog synthesis. *Science,* **219**(4587): 979-980.

Laustriat, D., Gide, J. and Peschanski, M. (2010). Human pluripotent stem cells in drug discovery and predictive toxicology. *Biochem Soc Trans,* **38**(4): 1051-1057.

LeBaron, M. J., Rasoulpour, R. J., Klapacz, J., Ellis-Hutchings, R. G., Hollnagel, H. M. and Gollapudi, B. B. (2010). Epigenetics and chemical safety assessment. *Mutation Research,* **705**(2): 83-95.

Lechpammer, M., Clegg, M. S., Muzar, Z., Huebner, P. A., Jin, L. W. and Gospe, S. M., Jr. (2014). Pathology of inherited manganese transporter deficiency. *Ann Neurol,* **75**(4): 608-612.

Leist, M., Bremer, S., Brundin, P., Hescheler, J., Kirkeby, A., Krause, K.-H., Poerzgen, P., Puceat, M., Schmidt, M., Schrattenholz, A., Zak, N. B. and Hentze, H. (2008). The biological and ethical basis of the use of human embryonic stem cells for in vitro test systems or cell therapy. *ALTEX,* **25**(3): 163-190.

Lemonnier, T., Blanchard, S., Toli, D., Roy, E., Bigou, S., Froissart, R., Rouvet, I., Vitry, S., Heard, J. M. and Bohl, D. (2011). Modeling neuronal defects associated with a lysosomal disorder using patient-derived induced pluripotent stem cells. *Human Molecular Genetics,* **20**(18): 3653-3666.

Levin, J., Bertsch, U., Kretzschmar, H. and Giese, A. (2005). Single particle analysis of manganese-induced prion protein aggregates. *Biochem Biophys Res Commun,* **329**(4): 1200-1207.

Li, H., Collado, M., Villasante, A., Strati, K., Ortega, S., Cañamero, M., Blasco, M. A. and Serrano, M. (2009). The Ink4/Arf locus is a barrier for iPS cell reprogramming. *Nature,* **460**(7259): 1136-1139.

Li, X. J., Du, Z. W., Zarnowska, E. D., Pankratz, M., Hansen, L. O., Pearce, R. A. and Zhang, S. C. (2005). Specification of motoneurons from human embryonic stem cells. *Nat Biotechnol,* **23**(2): 215-221.

Li, X. J., Hu, B. Y., Jones, S. A., Zhang, Y. S., Lavaute, T., Du, Z. W. and Zhang, S. C. (2008). Directed differentiation of ventral spinal progenitors and motor neurons from human embryonic stem cells by small molecules. *Stem Cells,* **26**(4): 886-893.

Li, S. C., Schoenberg, B. S., Wang, C. C., Cheng, X. M., Rui, D. Y., Bolis, C. L. and Schoenberg, D. G. (1985). A prevalence survey of Parkinson's disease and other movement disorders in the People's Republic of China. *Arch Neurol,* **42**(7): 655-657.

Li, W., Sun, W., Zhang, Y., Wei, W., Ambasudhan, R., Xia, P., Talantova, M., Lin, T., Kim, J., Wang, X., Kim, W. R., Lipton, S. A., Zhang, K. and Ding, S. (2011). Rapid induction and long-term self-renewal of primitive neural precursors from human embryonic stem cells by small molecule inhibitors. *Proc Natl Acad Sci USA,* **108**(20): 8299-8304.

Li, X.-J., Zhang, X., Johnson, M. A., Wang, Z.-B., Lavaute, T. and Zhang, S.-C. (2009). Coordination of sonic hedgehog and Wnt signaling determines ventral and dorsal telencephalic neuron types from human embryonic stem cells. *Development,* **136**(23): 4055-4063.

Lilienfeld, D. E. and Perl, D. P. (1993). Projected neurodegenerative disease mortality in the United States, 1990-2040. *Neuroepidemiology,* **12**(4): 219-228.

Lin, M. T. and Beal, F. M. (2006). Mitochondrial dysfunction and oxidative stress in neurodegenerative diseases. *Nature,* **443**(7113): 787-795.

Lin, T., Ambasudhan, R., Yuan, X., Li, W., Hilcove, S., Abujarour, R., Lin, X., Hahm, H. S., Hao, E., Hayek, A. and Ding, S. (2009). A chemical platform for improved induction of human iPSCs. *Nat Methods,* **6**(11): 805-808.

Lister, R., Pelizzola, M., Kida, Y. S., Hawkins, R. D., Nery, J. R., Hon, G., Antosiewicz-Bourget, J., O'Malley, R., Castanon, R., Klugman, S., Downes, M., Yu, R., Stewart, R., Ren, B., Thomson, J. A., Evans, R. M. and Ecker, J. R. (2011). Hotspots of aberrant epigenomic reprogramming in human induced pluripotent stem cells. *Nature,* **471**(7336): 68-73.

Litvan, I., Bhatia, K. P., Burn, D. J., Goetz, C. G., Lang, A. E., McKeith, I., Quinn, N., Sethi, K. D., Shults, C. and Wenning, G. K. (2003). Movement Disorders Society Scientific Issues Committee report: SIC Task Force appraisal of clinical diagnostic criteria for Parkinsonian disorders. *Mov Disord,* **18**(5): 467-486.

Liu, A. and Niswander, L. A. (2005). Bone morphogenetic protein signalling and vertebrate nervous system development. *Nat Rev Neurosci,* **6**(12): 945-954.

Liu, H. and Zhang, S.-C. (2011). Specification of neuronal and glial subtypes from human pluripotent stem cells. *Cell Mol Life Sci,* **68**(24): 3995-4008.

Liu, X., Sullivan, K. A., Madl, J. E., Legare, M. and Tjalkens, R. B. (2006). Manganese-induced neurotoxicity: the role of astroglial-derived nitric oxide in striatal interneuron degeneration. *Toxicol Sci,* **91**(2): 521-531.

Liuzzi, J. P., Aydemir, F., Nam, H., Knutson, M. D. and Cousins, R. J. (2006). Zip14 (Slc39a14) mediates non-transferrin-bound iron uptake into cells. *Proc Natl Acad Sci U S A,* **103**(37): 13612-13617.

Loutzenhiser, K. and Loutzenhiser, R. (2000). Angiotensin II-induced Ca(2+) influx in renal afferent and efferent arterioles: differing roles of voltage-gated and store-operated Ca(2+) entry. *Circ Res,* **87**(7): 551-557.

Lucaciu, C. M., Dragu, C., Copaescu, L. and Morariu, V. V. (1997). Manganese transport through human erythrocyte membranes. An EPR study. *Biochim Biophys Acta,* **1328**(2): 90-98.

Lucchini, R. G., Albini, E., Benedetti, L., Borghesi, S., Coccaglio, R., Malara, E. C., Parrinello, G., Garattini, S., Resola, S. and Alessio, L. (2007). High prevalence of Parkinsonian disorders associated to manganese exposure in the vicinities of ferroalloy industries. *Am J Ind Med,* **50**(11): 788-800.

Lucchini, R. G., Martin, C. J. and Doney, B. C. (2009). From manganism to manganese-induced parkinsonism: a conceptual model based on the evolution of exposure. *Neuromolecular Med,* **11**(4): 311-321.

Luong, M. X., Auerbach, J., Crook, J. M., Daheron, L., Hei, D., Lomax, G., Loring, J. F., Ludwig, T., Schlaeger, T. M., Smith, K. P., Stacey, G., Xu, R.-H. and Zeng, F. (2011). A call for standardized naming and reporting of human ESC and iPSC lines. *Cell Stem Cell,* **8**(4): 357-359.

Macarron, R., Banks, M. N., Bojanic, D., Burns, D. J., Cirovic, D. A., Garyantes, T., Green, D. V., Hertzberg, R. P., Janzen, W. P., Paslay, J. W., Schopfer, U. and Sittampalam, G. S. (2011). Impact of high-throughput screening in biomedical research. *Nat Rev Drug Discov,* **10**(3): 188-195.

Macdonald, V. and Halliday, G. (2002). Pyramidal cell loss in motor cortices in Huntington's disease. *Neurobiol Dis,* **10**(3): 378-386.

Macdonald, V., Halliday, G. M., Trent, R. J. and McCusker, E. A. (1997). Significant loss of pyramidal neurons in the angular gyrus of patients with Huntington's disease. *Neuropathol Appl Neurobiol,* **23**(6): 492-495.

Mackenzie, B., Takanaga, H., Hubert, N., Rolfs, A. and Hediger, M. A. (2007). Functional properties of multiple isoforms of human divalent metal-ion transporter 1 (DMT1). *Biochem J,* **403**(1): 59-69.

Madison, J. L., Wegrzynowicz, M., Aschner, M. and Bowman, A. B. (2012). Disease-toxicant interactions in manganese exposed Huntington disease mice: early changes in striatal neuron morphology and dopamine metabolism. *PLoS One,* **7**(2): e31024.

Maggiora, G., Vogt, M., Stumpfe, D. and Bajorath, J. (2014). Molecular similarity in medicinal chemistry. *J Med Chem,* **57**(8): 3186-3204.

Magistretti, P. J. and Allaman, I. (2013). Brain energy metabolism, Springer.

Mainen, Z. F. and Sejnowski, T. J. (1996). Influence of dendritic structure on firing pattern in model neocortical neurons. *Nature,* **382**(6589): 363-366.

Marchetto, M. C., Brennand, K. J., Boyer, L. F. and Gage, F. H. (2011). Induced pluripotent stem cells (iPSCs) and neurological disease modeling: progress and promises. *Human Molecular Genetics,* **20**(R2): R109-115.

Marchetto, M. C. N., Carromeu, C., Acab, A., Yu, D., Yeo, G. W., Mu, Y., Chen, G., Gage, F. H. and Muotri, A. R. (2010). A model for neural development and treatment of Rett syndrome using human induced pluripotent stem cells. *Cell,* **143**(4): 527-539.

Marchetto, M. C. N., Winner, B. and Gage, F. H. (2010). Pluripotent stem cells in neurodegenerative and neurodevelopmental diseases. *Human Molecular Genetics,* **19**(R1): R71-6.

Mayeux, R., Marder, K., Cote, L. J., Denaro, J., Hemenegildo, N., Mejia, H., Tang, M. X., Lantigua, R., Wilder, D., Gurland, B. and et al. (1995). The frequency of idiopathic Parkinson's disease by age, ethnic group, and sex in northern Manhattan, 1988-1993. *Am J Epidemiol,* **142**(8): 820-827.

McNeil, S. M., Novelletto, A., Srinidhi, J., Barnes, G., Kornbluth, I., Altherr, M. R., Wasmuth, J. J., Gusella, J. F., MacDonald, M. E. and Myers, R. H. (1997). Reduced penetrance of the Huntington's disease mutation. *Hum Mol Genet,* **6**(5): 775-779.

Meisner, L. F. and Johnson, J. A. (2008). Protocols for cytogenetic studies of human embryonic stem cells. *Methods,* **45**(2): 133-141.

Menendez, L., Yatskievych, T. A., Antin, P. B. and Dalton, S. (2011). Wnt signaling and a Smad pathway blockade direct the differentiation of human pluripotent stem cells to multipotent neural crest cells. *Proc Natl Acad Sci U S A,* **108**(48): 19240-19245.

Menezes-Filho, J.A., Novaes, Cde O., Moreira, J.C., Sarcinelli, P.N., Mergler, D. (2011). Elevated manganese and cognitive performance in school-aged children and their mothers. *Environ Res.* **111**(1): 156-63.

Mikkelsen, T. S., Hanna, J., Zhang, X., Ku, M., Wernig, M., Schorderet, P., Bernstein, B. E., Jaenisch, R., Lander, E. S. and Meissner, A. (2008). Dissecting direct reprogramming through integrative genomic analysis. *Nature,* **454**(7200): 49-55.

Milosevic, J., Storch, A. and Schwarz, J. (2005). Cryopreservation does not affect proliferation and multipotency of murine neural precursor cells. *Stem Cells,* **23**(5): 681-688.

Moors, M., Rockel, T. D., Abel, J., Cline, J. E., Gassmann, K., Schreiber, T., Schuwald, J., Weinmann, N. and Fritsche, E. (2009). Human neurospheres as three-dimensional cellular systems for developmental neurotoxicity testing. *Environ Health Perspect,* **117**(7): 1131-1138.

Moos, T. and Rosengren Nielsen, T. (2006). Ferroportin in the postnatal rat brain: implications for axonal transport and neuronal export of iron. *Semin Pediatr Neurol,* **13**(3): 149-157.

Morgante, L., Rocca, W. A., Di Rosa, A. E., De Domenico, P., Grigoletto, F., Meneghini, F., Reggio, A., Savettieri, G., Castiglione, M. G., Patti, F. and et al. (1992). Prevalence of Parkinson's disease and other types of parkinsonism: a door-to-door survey in three Sicilian municipalities. The Sicilian Neuro-Epidemiologic Study (SNES) Group. *Neurology,* **42**(10): 1901-1907.

Mori, F., Tanji, K., Yoshimoto, M., Takahashi, H. and Wakabayashi, K. (2002). Demonstration of alpha-synuclein immunoreactivity in neuronal and glial cytoplasm in normal human brain tissue using proteinase K and formic acid pretreatment. *Exp Neurol,* **176**(1): 98-104.

Morizane, A., Doi, D., Kikuchi, T., Nishimura, K. and Takahashi, J. (2011). Small-molecule inhibitors of bone morphogenic protein and activin/nodal signals promote highly efficient neural induction from human pluripotent stem cells. *J Neurosci Res,* **89**(2): 117-126.

Mukai, H., Isagawa, T., Goyama, E., Tanaka, S., Bence, N. F., Tamura, A., Ono, Y. and Kopito, R. R. (2005). Formation of morphologically similar globular aggregates from diverse aggregation-prone proteins in mammalian cells. *Proc Natl Acad Sci U S A,* **102**(31): 10887-10892.

Mukhopadhyay, S. and Linstedt, A. D. (2011). Identification of a gain-of-function mutation in a Golgi P-type ATPase that enhances Mn2+ efflux and protects against toxicity. *Proc Natl Acad Sci U S A,* **108**(2): 858-863.

Müller, F.J., Goldmann, J., Löser, P. and Loring, J. F. (2010). A call to standardize teratoma assays used to define human pluripotent cell lines. *Cell Stem Cell,* **6**(5): 412-414.

Muller, F. J., Schuldt, B. M., Williams, R., Mason, D., Altun, G., Papapetrou, E. P., Danner, S., Goldmann, J. E., Herbst, A., Schmidt, N. O., Aldenhoff, J. B., Laurent, L. C. and Loring, J. F. (2011). A bioinformatic assay for pluripotency in human cells. *Nat Methods,* **8**(4): 315-317.

Muñoz-Sanjuán, I. and Brivanlou, A. H. (2002). Neural induction, the default model and embryonic stem cells. *Nat Rev Neurosci,* **3**(4): 271-280.

Murphy, V. A., Wadhwani, K. C., Smith, Q. R. and Rapoport, S. I. (1991). Saturable transport of manganese(II) across the rat blood-brain barrier. *J Neurochem,* **57**(3): 948-954.

Nakagawa, M., Koyanagi, M., Tanabe, K., Takahashi, K., Ichisaka, T., Aoi, T., Okita, K., Mochiduki, Y., Takizawa, N. and Yamanaka, S. (2008). Generation of induced pluripotent stem cells without Myc from mouse and human fibroblasts. *Nat Biotechnol,* **26**(1): 101-106.

Neely, M., Tidball, A., Aboud, A., Ess, K. and Bowman, A. (2011). Induced pluripotent stem cells (iPSCs) - an emerging model system for the study of human neurotoxicology. Neuromethods - Springer Protocols: Cell Culture Techniques. M. Aschner, C. Sunol and A. Price. New York, NY., Humana Press. **56**.

Neely, M. D., Litt, M. J., Tidball, A. M., Li, G. G., Aboud, A. A., Hopkins, C. R., Chamberlin, R., Hong, C. C., Ess, K. C. and Bowman, A. B. (2012). DMH1, a highly selective small molecule BMP inhibitor promotes neurogenesis of hiPSCs: comparison of PAX6 and SOX1 expression during neural induction. *ACS Chem Neurosci,* **3**(6): 482-491.

Newland, M. C., Ceckler, T. L., Kordower, J. H. and Weiss, B. (1989). Visualizing manganese in the primate basal ganglia with magnetic resonance imaging. *Exp Neurol,* **106**(3): 251-258.

Ni, M., Li, X., Yin, Z., Sidoryk-Węgrzynowicz, M., Jiang, H., Farina, M., Rocha, J. B. T., Syversen, T. and Aschner, M. (2011). Comparative study on the response of rat primary astrocytes and microglia to methylmercury toxicity. *Glia,* **59**(5): 810-820.

Nies, A. T. and Keppler, D. (2007). The apical conjugate efflux pump ABCC2 (MRP2). *Pflugers Arch,* **453**(5): 643-659.

Nishino, K., Toyoda, M., Yamazaki-Inoue, M., Fukawatase, Y., Chikazawa, E., Sakaguchi, H., Akutsu, H. and Umezawa, A. (2011). DNA methylation dynamics in human induced pluripotent stem cells over time. *PLoS Genetics,* **7**(5): e1002085.

Nunez, M. T., Tapia, V., Rojas, A., Aguirre, P., Gomez, F. and Nualart, F. (2010). Iron supply determines apical/basolateral membrane distribution of intestinal iron transporters DMT1 and ferroportin 1. *Am J Physiol Cell Physiol,* **298**(3): C477-485.

Nussbaum, R. L. and Ellis, C. E. (2003). Alzheimer's disease and Parkinson's disease. *N Engl J Med,* **348**(14): 1356-1364.

Nuytemans, K., Theuns, J., Cruts, M. and Van Broeckhoven, C. (2010). Genetic etiology of Parkinson disease associated with mutations in the SNCA, PARK2, PINK1, PARK7, and LRRK2 genes: a mutation update. *Hum Mutat,* **31**(7): 763-780.

Okita, K., Matsumura, Y., Sato, Y., Okada, A., Morizane, A., Okamoto, S., Hong, H., Nakagawa, M., Tanabe, K., Tezuka, K.-I., Shibata, T., Kunisada, T., Takahashi, M., Takahashi, J., Saji, H. and Yamanaka, S. (2011). A more efficient method to generate integration-free human iPS cells. *Nature Methods,* **8**(5): 409-412.

Okita, K., Nakagawa, M., Hyenjong, H., Ichisaka, T. and Yamanaka, S. (2008). Generation of mouse induced pluripotent stem cells without viral vectors. *Science,* **322**(5903): 949-953.

Olanow, C. W. (2004). Manganese-induced parkinsonism and Parkinson's disease. *Ann N Y Acad Sci,* **1012**: 209-223.

Ortiz, A. N., Kurth, B. J., Osterhaus, G. L. and Johnson, M. A. (2011). Impaired dopamine release and uptake in R6/1 Huntington's disease model mice. *Neurosci Lett,* **492**(1): 11-14.

Pal, R., Mamidi, M. K., Das, A. K. and Bhonde, R. (2011). Human embryonic stem cell proliferation and differentiation as parameters to evaluate developmental toxicity. *J Cell Physiol,* **226**(6): 1583-1595.

Papapetrou, E. P., Tomishima, M. J., Chambers, S. M., Mica, Y., Reed, E., Menon, J., Tabar, V., Mo, Q., Studer, L. and Sadelain, M. (2009). Stoichiometric and temporal requirements of Oct4, Sox2, Klf4, and c-Myc expression for efficient human iPSC induction and differentiation. *Proc. Natl. Acad. Sci. U.S.A.,* **106**(31): 12759-12764.

Park, I.-H., Zhao, R., West, J. A., Yabuuchi, A., Huo, H., Ince, T. A., Lerou, P. H., Lensch, M. W. and Daley, G. Q. (2008). Reprogramming of human somatic cells to pluripotency with defined factors. *Nature,* **451**(7175): 141-146.

Patrawala, L., Calhoun, T., Schneider-Broussard, R., Zhou, J., Claypool, K. and Tang, D. G. (2005). Side population is enriched in tumorigenic, stem-like cancer cells, whereas ABCG2+ and ABCG2- cancer cells are similarly tumorigenic. *Cancer Res,* **65**(14): 6207-6219.

Paulsen, J. S., Hoth, K. F., Nehl, C., Stierman, L. and Grp, H. S. (2005). Critical periods of suicide risk in Huntington's disease. *American Journal of Psychiatry,* **162**(4): 725-731.

Perera, F. and Herbstman, J. (2011). Prenatal environmental exposures, epigenetics, and disease. *Reproductive Toxicology,* **31**(3): 363-373.

Pfisterer, U., Kirkeby, A., Torper, O., Wood, J., Nelander, J., Dufour, A., Bjorklund, A., Lindvall, O., Jakobsson, J. and Parmar, M. (2011). Direct conversion of human fibroblasts to dopaminergic neurons. *Proc Natl Acad Sci U S A,* **108**(25): 10343-10348.

Pinilla-Tenas, J. J., Sparkman, B. K., Shawki, A., Illing, A. C., Mitchell, C. J., Zhao, N., Liuzzi, J. P., Cousins, R. J., Knutson, M. D. and Mackenzie, B. (2011). Zip14 is a complex broad-scope metal-ion transporter whose functional properties support roles in the cellular uptake of zinc and nontransferrin-bound iron. *Am J Physiol Cell Physiol,* **301**(4): C862-871.

Post, B., Merkus, M. P., de Haan, R. J. and Speelman, J. D. (2007). Prognostic factors for the progression of Parkinson's disease: a systematic review. *Mov Disord,* **22**(13): 1839-1851.

Pridmore, S. A. (1990). The large Huntington's disease family of Tasmania. *Med J Aust,* **153**(10): 593-595.

Pringsheim, T., Wiltshire, K., Day, L., Dykeman, J., Steeves, T., Jette, N. (2012). The incidence and prevalence of Huntington's disease: A systematic review and meta−analysis. *Mov Disord.* **27**(9): 1083-91.

Qiang, L., Fujita, R., Yamashita, T., Angulo, S., Rhinn, H., Rhee, D., Doege, C., Chau, L., Aubry, L., Vanti, W. B., Moreno, H. and Abeliovich, A. (2011). Directed conversion of Alzheimer's disease patient skin fibroblasts into functional neurons. *Cell,* **146**(3): 359-371.

Quadri, M., Federico, A., Zhao, T., Breedveld, G. J., Battisti, C., Delnooz, C., Severijnen, L. A., Di Toro Mammarella, L., Mignarri, A., Monti, L., Sanna, A., Lu, P., Punzo, F., Cossu, G., Willemsen, R., Rasi, F., Oostra, B. A., van de Warrenburg, B. P. and Bonifati, V. (2012). Mutations in SLC30A10 cause parkinsonism and dystonia with hypermanganesemia, polycythemia, and chronic liver disease. *Am J Hum Genet,* **90**(3): 467-477.

Rabin, O., Hegedus, L., Bourre, J. M. and Smith, Q. R. (1993). Rapid brain uptake of manganese(II) across the blood-brain barrier. *J Neurochem,* **61**(2): 509-517.

Racette, B. A., McGee-Minnich, L., Moerlein, S. M., Mink, J. W., Videen, T. O. and Perlmutter, J. S. (2001). Welding-related parkinsonism: clinical features, treatment, and pathophysiology. *Neurology,* **56**(1): 8-13.

Rada-Iglesias, A. and Wysocka, J. (2011). Epigenomics of human embryonic stem cells and induced pluripotent stem cells: insights into pluripotency and implications for disease. *Genome Med,* **3**(6): 36.

Radio, N. M. and Mundy, W. R. (2008). Developmental neurotoxicity testing in vitro: models for assessing chemical effects on neurite outgrowth. *Neurotoxicology,* **29**(3): 361-376.

Riccio, A., Mattei, C., Kelsell, R. E., Medhurst, A. D., Calver, A. R., Randall, A. D., Davis, J. B., Benham, C. D. and Pangalos, M. N. (2002). Cloning and functional expression of human short TRP7, a candidate protein for store-operated Ca2+ influx. *J Biol Chem,* **277**(14): 12302-12309.

Robinson, J. F., Theunissen, P. T., van Dartel, D. A., Pennings, J. L., Faustman, E. M. and Piersma, A. H. (2011). Comparison of MeHg-induced toxicogenomic responses across in vivo and in vitro models used in developmental toxicology. *Reprod Toxicol,* **32**(2): 180-188.

Rollin, H., Mathee, A., Levin, J., Theodorou, P. and Wewers, F. (2005). Blood manganese concentrations among first-grade schoolchildren in two South African cities. *Environ Res,* **97**(1): 93-99.

Roth, J., Ponzoni, S. and Aschner, M. (2013). Manganese homeostasis and transport. *Met Ions Life Sci,* **12**(169-201.

Roth, J. A. and Garrick, M. D. (2003). Iron interactions and other biological reactions mediating the physiological and toxic actions of manganese. *Biochem Pharmacol,* **66**(1): 1-13.

Rousseeuw, P. J. and Verboven, S. (2002). Robust estimation in very small samples. *Computational Statistics & Data Analysis,* **40**(4): 741-758.

Rubinsztein, D. C. and Carmichael, J. (2003). Huntington's disease: molecular basis of neurodegeneration. *Expert Rev Mol Med,* **5**(20): 1-21.

Rubinsztein, D. C., Leggo, J., Coles, R., Almqvist, E., Biancalana, V., Cassiman, J. J., Chotai, K., Connarty, M., Crauford, D., Curtis, A., Curtis, D., Davidson, M. J., Differ, A. M., Dode, C., Dodge, A., Frontali, M., Ranen, N. G., Stine, O. C., Sherr, M., Abbott, M. H., Franz, M. L., Graham, C. A., Harper, P. S., Hedreen, J. C., Hayden, M. R. and et al. (1996). Phenotypic characterization of individuals with 30-40 CAG repeats in the Huntington disease (HD) gene reveals HD cases with 36 repeats and apparently normal elderly individuals with 36-39 repeats. *Am J Hum Genet,* **59**(1): 16-22.

Sadowski, J. and Gasteiger, J. (1993). From atoms and bonds to three-dimensional atomic coordinates: automatic model builders. *Chemical Reviews,* **93**: 2567-2581.

Saha, K. and Jaenisch, R. (2009). Technical challenges in using human induced pluripotent stem cells to model disease. *Cell Stem Cell,* **5**(6): 584-595.

Samii, A., Nutt, J. G. and Ransom, B. R. (2004). Parkinson's disease. *Lancet,* **363**(9423): 1783-1793.

Santos, D., Milatovic, D., Andrade, V., Batoreu, M., Aschner, M. and Marreilha dos Santos, A. (2012). The inhibitory effect of manganese on acetylcholinesterase activity enhances oxidative stress and neuroinflammation in the rat brain. *Toxicology,* **292**(2-3): 90-98.

Schmidt-Hieber, C., Jonas, P. and Bischofberger, J. (2007). Subthreshold dendritic signal processing and coincidence detection in dentate gyrus granule cells. *J Neurosci,* **27**(31): 8430-8441.

Schoenberg, B. S., Osuntokun, B. O., Adeuja, A. O., Bademosi, O., Nottidge, V., Anderson, D. W. and Haerer, A. F. (1988). Comparison of the prevalence of Parkinson's disease in black populations in the rural United States and in rural Nigeria: door-to-door community studies. *Neurology,* **38**(4): 645-646.

Scholz, G., Pohl, I., Genschow, E., Klemm, M. and Spielmann, H. (1999). Embryotoxicity screening using embryonic stem cells in vitro: correlation to in vivo teratogenicity. *Cells Tissues Organs,* **165**(3-4): 203-211.

Schreiber, T., Gassmann, K., Götz, C., Hübenthal, U., Moors, M., Krause, G., Merk, H. F., Nguyen, N.-H., Scanlan, T. S., Abel, J., Rose, C. R. and Fritsche, E. (2010). Polybrominated diphenyl ethers induce developmental neurotoxicity in a human in vitro model: evidence for endocrine disruption. *Environ Health Perspect,* **118**(4): 572-578.

Schuler, P., Oyanguren, H., Maturana, V., Valenzuela, A., Cruz, E., Plaza, V., Schmidt, E. and Haddad, R. (1957). [Manganese poisoning; clinical & environmental study in a manganese mine]. *Rev Med Chil,* **85**(11): 623-630.

Seibler, P., Graziotto, J., Jeong, H., Simunovic, F., Klein, C. and Krainc, D. (2011). Mitochondrial Parkin recruitment is impaired in neurons derived from mutant PINK1 induced pluripotent stem cells. *J Neurosci,* **31**(16): 5970-5976.

Seiler, A. E. and Spielmann, H. (2011). The validated embryonic stem cell test to predict embryotoxicity in vitro. *Nat Protoc,* **6**(7): 961-978.

Sepulveda, M. R., Berrocal, M., Marcos, D., Wuytack, F. and Mata, A. M. (2007). Functional and immunocytochemical evidence for the expression and localization of the secretory pathway Ca2+-ATPase isoform 1 (SPCA1) in cerebellum relative to other Ca2+ pumps. *J Neurochem,* **103**(3): 1009-1018.

Seth, P. K. and Chandra, S. V. (1984). Neurotransmitters and neurotransmitter receptors in developing and adult rats during manganese poisoning. *Neurotoxicology,* **5**(1): 67-76.

Shafa, M., Sjonnesen, K., Yamashita, A., Liu, S., Michalak, M., Kallos, M. S. and Rancourt, D. E. (2011). Expansion and long-term maintenance of induced pluripotent stem cells in stirred suspension bioreactors. *J Tissue Eng Regen Med,* **6**(6): 462-72.

Shutoh, Y., Takeda, M., Ohtsuka, R., Haishima, A., Yamaguchi, S., Fujie, H., Komatsu, Y., Maita, K. and Harada, T. (2009). Low dose effects of dichlorodiphenyltrichloroethane (DDT) on gene transcription and DNA methylation in the hypothalamus of young male rats: implication of hormesis-like effects. *J Toxicol Sci.,* **34**(5): 469-482.

Sinha, S. and Chen, J. K. (2006). Purmorphamine activates the Hedgehog pathway by targeting Smoothened. *Nat Chem Biol,* **2**(1): 29-30.

Slow, E. J., van Raamsdonk, J., Rogers, D., Coleman, S. H., Graham, R. K., Deng, Y., Oh, R., Bissada, N., Hossain, S. M., Yang, Y. Z., Li, X. J., Simpson, E. M., Gutekunst, C. A., Leavitt, B. R. and Hayden, M. R. (2003). Selective striatal neuronal loss in a YAC128 mouse model of Huntington disease. *Hum Mol Genet,* **12**(13): 1555-1567.

Slyshenkov, V. S., Dymkowska, D. and Wojtczak, L. (2004). Pantothenic acid and pantothenol increase biosynthesis of glutathione by boosting cell energetics. *FEBS Lett,* **569**(1-3): 169-172.

Smith, C. A., Elizabeth, J., O'Maille, G., Abagyan, R. and Siuzdak, G. (2006). XCMS: processing mass spectrometry data for metabolite profiling using nonlinear peak alignment, matching, and identification. *Analytical Chemistry,* **78**(3): 779-787.

Snowden, J. S., Craufurd, D., Griffiths, H. L. and Neary, D. (1998). Awareness of involuntary movements in Huntington disease. *Archives of neurology,* **55**(6): 801-805.

Spargo, E., Everall, I. P. and Lantos, P. L. (1993). Neuronal loss in the hippocampus in Huntington's disease: a comparison with HIV infection. *J Neurol Neurosurg Psychiatry,* **56**(5): 487-491.

Spielmann, H., Pohl, I., Doering, B., Liebsch, M. and Moldenhauer, F. (1997). The embryonic stem cell test, an in vitro embryotoxicity test using two permanent mouse cell lines: 3T3 fibroblasts and embryonic stem cells. *Toxicol In Vitro,* **10**: 119–127.

Stadtfeld, M., Apostolou, E., Akutsu, H., Fukuda, A., Follett, P., Natesan, S., Kono, T., Shioda, T. and Hochedlinger, K. (2010). Aberrant silencing of imprinted genes on chromosome 12qF1 in mouse induced pluripotent stem cells. *Nature,* **465**(7295): 175-181.

Stadtfeld, M., Nagaya, M., Utikal, J., Weir, G. and Hochedlinger, K. (2008). Induced pluripotent stem cells generated without viral integration. *Science,* **322**(5903): 945-949.

Stamelou, M., Tuschl, K., Chong, W. K., Burroughs, A. K., Mills, P. B., Bhatia, K. P. and Clayton, P. T. (2012). Dystonia with brain manganese accumulation resulting from SLC30A10 mutations: a new treatable disorder. *Mov Disord,* **27**(10): 1317-1322.

Stredrick, D. L., Stokes, A. H., Worst, T. J., Freeman, W. M., Johnson, E. A., Lash, L. H., Aschner, M. and Vrana, K. E. (2004). Manganese-induced cytotoxicity in dopamine-producing cells. *Neurotoxicology,* **25**(4): 543-553.

Street, J. O., Carroll, R. J. and Ruppert, D. (1988). A Note on Computing Robust Regression Estimates Via Iteratively Reweighted Least-Squares. *American Statistician,* **42**(2): 152-154.

Stummann, T., Hareng, L. and Bremer, S. (2009). Hazard assessment of methylmercury toxicity to neuronal induction in embryogenesis using human embryonic stem cells. *Toxicology,* **257**(3): 117-126.

Suhr, S. T., Chang, E. A., Tjong, J., Alcasid, N., Perkins, G. A., Goissis, M. D., Ellisman, M. H., Perez, G. I. and Cibelli, J. B. (2010). Mitochondrial rejuvenation after induced pluripotency. *PLoS ONE,* **5**(11): e14095.

Sumner, L. W., Amberg, A., Barrett, D., Beale, M. H., Beger, R., Daykin, C. A., Fan, T. W. M., Fiehn, O., Goodacre, R. and Griffin, J. L. (2007). Proposed minimum reporting standards for chemical analysis. *Metabolomics,* **3**(3): 211-221.

Swaiman, K. F. (1991). Hallervorden-Spatz syndrome and brain iron metabolism. *Arch Neurol,* **48**(12): 1285-1293.

Swistowski, A., Peng, J., Liu, Q., Mali, P., Rao, M. S., Cheng, L. and Zeng, X. (2010). Efficient generation of functional dopaminergic neurons from human induced pluripotent stem cells under defined conditions. *Stem Cells,* **28**(10): 1893-1904.

Takahashi, K., Tanabe, K., Ohnuki, M., Narita, M., Ichisaka, T., Tomoda, K. and Yamanaka, S. (2007). Induction of pluripotent stem cells from adult human fibroblasts by defined factors. *Cell,* **131**(5): 861-872.

Takano, H., Cancel, G., Ikeuchi, T., Lorenzetti, D., Mawad, R., Stevanin, G., Didierjean, O., Durr, A., Oyake, M., Shimohata, T., Sasaki, R., Koide, R., Igarashi, S., Hayashi, S., Takiyama, Y., Nishizawa, M., Tanaka, H., Zoghbi, H., Brice, A. and Tsuji, S. (1998). Close associations between prevalences of dominantly inherited spinocerebellar ataxias with CAG-repeat expansions and frequencies of large normal CAG alleles in Japanese and Caucasian populations. *Am J Hum Genet,* **63**(4): 1060-1066.

Takeda, A. (2003). Manganese action in brain function. *Brain Res Brain Res Rev,* **41**(1): 79-87.

Takser, L., Mergler, D., Hellier, G., Sahuquillo, J. and Huel, G. (2003). Manganese, monoamine metabolite levels at birth, and child psychomotor development. *Neurotoxicology,* **24**(4-5): 667-674.

Tamm, C., Duckworth, J., Hermanson, O. and Ceccatelli, S. (2006). High susceptibility of neural stem cells to methylmercury toxicity: effects on cell survival and neuronal differentiation. *Journal of Neurochemistry,* **97**(1): 69-78.

Tang, T. S., Chen, X., Liu, J. and Bezprozvanny, I. (2007). Dopaminergic signaling and striatal neurodegeneration in Huntington's disease. *J Neurosci,* **27**(30): 7899-7910.

Tateno, M., Ukai, W., Ozawa, H., Yamamoto, M., Toki, S., Ikeda, H. and Saito, T. (2004). Ethanol inhibition of neural stem cell differentiation is reduced by neurotrophic factors. *Alcoholism, Clinical and Experimental Research,* **28**(8 Suppl Proceedings): 134S-138S.

Theunissen, P. T., Pennings, J. L. A., Robinson, J. F., Claessen, S. M. H., Kleinjans, J. C. S. and Piersma, A. H. (2011). Time-response evaluation by transcriptomics of methylmercury effects on neural differentiation of murine embryonic stem cells. *Toxicol Sci,* **122**(2): 437-447.

Thompson, K., Molina, R. M., Donaghey, T., Schwob, J. E., Brain, J. D. and Wessling-Resnick, M. (2007). Olfactory uptake of manganese requires DMT1 and is enhanced by anemia. *FASEB J,* **21**(1): 223-230.

Tison, F., Dartigues, J. F., Dubes, L., Zuber, M., Alperovitch, A. and Henry, P. (1994). Prevalence of Parkinson's disease in the elderly: a population study in Gironde, France. *Acta Neurol Scand,* **90**(2): 111-115.

Tofighi, R., Moors, M., Bose, R., Ibrahim, W. N. W. and Ceccatelli, S. (2011). Neural stem cells for developmental neurotoxicity studies. *Methods Mol Biol,* **758**: 67-80.

Tofighi, R., Wan Ibrahim, W. N., Rebellato, P., Andersson, P. L., Uhlen, P. and Ceccatelli, S. (2011). Non-dioxin like polychlorinated biphenyls interfere with neuronal differentiation of embryonic neural stem cells. *Toxicol Sci,* 192-201.

Tolosa, E., Borght, T. V. and Moreno, E. (2007). Accuracy of DaTSCAN (123I-Ioflupane) SPECT in diagnosis of patients with clinically uncertain parkinsonism: 2-year follow-up of an open-label study. *Mov Disord,* **22**(16): 2346-2351.

Trettel, F., Rigamonti, D., Hilditch-Maguire, P., Wheeler, V. C., Sharp, A. H., Persichetti, F., Cattaneo, E. and MacDonald, M. E. (2000). Dominant phenotypes produced by the HD mutation in STHdh(Q111) striatal cells. *Hum Mol Genet,* **9**(19): 2799-2809.

Tsay, D. and Yuste, R. (2004). On the electrical function of dendritic spines. *Trends Neurosci,* **27**(2): 77-83.

Tuschl, K., Clayton, P. T., Gospe, S. M., Jr., Gulab, S., Ibrahim, S., Singhi, P., Aulakh, R., Ribeiro, R. T., Barsottini, O. G., Zaki, M. S., Del Rosario, M. L., Dyack, S., Price, V., Rideout, A., Gordon, K., Wevers, R. A., Chong, W. K. and Mills, P. B. (2012). Syndrome of hepatic cirrhosis, dystonia, polycythemia, and hypermanganesemia caused by mutations in SLC30A10, a manganese transporter in man. *Am J Hum Genet,* **90**(3): 457-466.

Tuschl, K., Mills, P. B. and Clayton, P. T. (2013). Manganese and the brain. *Int Rev Neurobiol,* **110**: 277-312.

Utikal, J., Polo, J. M., Stadtfeld, M., Maherali, N., Kulalert, W., Walsh, R. M., Khalil, A., Rheinwald, J. G. and Hochedlinger, K. (2009). Immortalization eliminates a roadblock during cellular reprogramming into iPS cells. *Nature,* **460**(7259): 1145-1148.

van Dellen, A., Grote, H. E. and Hannan, A. J. (2005). Gene-environment interactions, neuronal dysfunction and pathological plasticity in Huntington's disease. *Clin Exp Pharmacol Physiol,* **32**(12): 1007-1019.

Van Raamsdonk, J. M., Pearson, J., Slow, E. J., Hossain, S. M., Leavitt, B. R. and Hayden, M. R. (2005). Cognitive dysfunction precedes neuropathology and motor abnormalities in the YAC128 mouse model of Huntington's disease. *J Neurosci,* **25**(16): 4169-4180.

Vescovi, A., Gebbia, M., Cappelletti, G., Parati, E. A. and Santagostino, A. (1989). Interactions of manganese with human brain glutathione-S-transferase. *Toxicology,* **57**(2): 183-191.

Vierbuchen, T., Ostermeier, A., Pang, Z. P., Kokubu, Y., Südhof, T. C. and Wernig, M. (2010). Direct conversion of fibroblasts to functional neurons by defined factors. *Nature,* **463**(7284): 1035-1041.

Vinayavekhin, N., Homan, E. A. and Saghatelian, A. (2010). Exploring disease through metabolomics. *ACS Chem Biol,* **5**(1): 91-103.

Vojnits, K. and Bremer, S. (2010). Challenges of using pluripotent stem cells for safety assessments of substances. *Toxicology,* **270**(1): 10-17.

Vonsattel, J. P. and DiFiglia, M. (1998). Huntington disease. *J Neuropathol Exp Neurol,* **57**(5): 369-384.

Walker, F. O. (2007). Huntington's disease. *Lancet,* **369**(9557): 218-228.

Wang, J. D., Huang, C. C., Hwang, Y. H., Chiang, J. R., Lin, J. M. and Chen, J. S. (1989). Manganese induced parkinsonism: an outbreak due to an unrepaired ventilation control system in a ferromanganese smelter. *Br J Ind Med,* **46**(12): 856-859.

Wasserman, G. A., Liu, X., Parvez, F., Ahsan, H., Levy, D., Factor-Litvak, P., Kline, J., van Geen, A., Slavkovich, V., LoIacono, N. J., Cheng, Z., Zheng, Y. and Graziano, J. H. (2006). Water manganese exposure and children's intellectual function in Araihazar, Bangladesh. *Environ Health Perspect,* **114**(1): 124-129.

Weiss, B., Clarkson, T. W. and Simon, W. (2002). Silent latency periods in methylmercury poisoning and in neurodegenerative disease. *Environ Health Perspect,* **110:** 851-854.

Weisskopf, M. G., Weuve, J., Nie, H., Saint-Hilaire, M. H., Sudarsky, L., Simon, D. K., Hersh, B., Schwartz, J., Wright, R. O. and Hu, H. (2010). Association of cumulative lead exposure with Parkinson's disease. *Environ Health Perspect,* **118**(11): 1609-1613.

Wexler, N. S., Lorimer, J., Porter, J., Gomez, F., Moskowitz, C., Shackell, E., Marder, K., Penchaszadeh, G., Roberts, S. A., Gayan, J., Brocklebank, D., Cherny, S. S., Cardon, L. R., Gray, J., Dlouhy, S. R., Wiktorski, S., Hodes, M. E., Conneally, P. M., Penney, J. B., Gusella, J., Cha, J. H., Irizarry, M., Rosas, D., Hersch, S., Hollingsworth, Z., MacDonald, M., Young, A. B., Andresen, J. M., Housman, D. E., De Young, M. M., Bonilla, E., Stillings, T., Negrette, A., Snodgrass, S. R., Martinez-Jaurrieta, M. D., Ramos-Arroyo, M. A., Bickham, J., Ramos, J. S., Marshall, F., Shoulson, I., Rey, G. J., Feigin, A., Arnheim, N., Acevedo-Cruz, A., Acosta, L., Alvir, J., Fischbeck, K., Thompson, L. M., Young, A., Dure, L., O'Brien, C. J., Paulsen, J., Brickman, A., Krch, D., Peery, S., Hogarth, P., Higgins, D. S., Jr., Landwehrmeyer, B. and Project, U. S.-V. C. R. (2004). Venezuelan kindreds reveal that genetic and environmental factors modulate Huntington's disease age of onset. *Proc Natl Acad Sci U S A,* **101**(10): 3498-3503.

Wichterle, H. and Przedborski, S. (2010). What can pluripotent stem cells teach us about neurodegenerative diseases? *Nature Neuroscience,* **13**(7): 800-804.

Williams, B. B., Kwakye, G. F., Wegrzynowicz, M., Li, D., Aschner, M., Erikson, K. M. and Bowman, A. B. (2010). Altered manganese homeostasis and manganese toxicity in a Huntington's disease striatal cell model are not explained by defects in the iron transport system. *Toxicol Sci,* **117**(1): 169-179.

Williams, B. B., Li, D., Wegrzynowicz, M., Vadodaria, B. K., Anderson, J. G., Kwakye, G. F., Aschner, M., Erikson, K. M. and Bowman, A. B. (2010). Disease-toxicant screen reveals a neuroprotective interaction between Huntington's disease and manganese exposure. *J Neurochem,* **112**(1): 227-237.

Williams, R., Schuldt, B. and Müller, F.-J. (2011). A guide to stem cell identification: Progress and challenges in system-wide predictive testing with complex biomarkers. *BioEssays,* **33**(11): 880-890.

Willis, A. W., Evanoff, B. A., Lian, M., Galarza, A., Wegrzyn, A., Schootman, M. and Racette, B. A. (2010). Metal emissions and urban incident Parkinson disease: a community health study of Medicare beneficiaries by using geographic information systems. *Am J Epidemiol,* **172**(12): 1357-1363.

Willis, A. W., Schootman, M., Tran, R., Kung, N., Evanoff, B. A., Perlmutter, J. S. and Racette, B. A. (2012). Neurologist-associated reduction in PD-related hospitalizations and health care expenditures. *Neurology,* **79**(17): 1774-1780.

Winkler, J., Sotiriadou, I., Chen, S., Hescheler, J. and Sachinidis, A. (2009). The potential of embryonic stem cells combined with -omics technologies as model systems for toxicology. *Curr Med Chem,* **16**(36): 4814-4827.

Wobus, A. M. and Loser, P. (2011). Present state and future perspectives of using pluripotent stem cells in toxicology research. *Arch Toxicol,* **85**(2): 79-117.

Wood-Kaczmar, A., Gandhi, S. and Wood, N. W. (2006). Understanding the molecular causes of Parkinson's disease. *Trends Mol Med,* **12**(11): 521-528.

Woolley, C. S., Weiland, N. G., McEwen, B. S. and Schwartzkroin, P. A. (1997). Estradiol increases the sensitivity of hippocampal CA1 pyramidal cells to NMDA receptor-mediated synaptic input: correlation with dendritic spine density. *J Neurosci,* **17**(5): 1848-1859.

Wright, H. H., Still, C. N. and Abramson, R. K. (1981). Huntington's disease in black kindreds in South Carolina. *Arch Neurol,* **38**(7): 412-414.

Yagi, T., Ito, D., Okada, Y., Akamatsu, W., Nihei, Y., Yoshizaki, T., Yamanaka, S., Okano, H. and Suzuki, N. (2011). Modeling familial Alzheimer's disease with induced pluripotent stem cells. *Human Molecular Genetics,* **20**(23): 4530-4539.

Yan, Y., Yang, D., Zarnowska, E. D., Du, Z., Werbel, B., Valliere, C., Pearce, R. A., Thomson, J. A. and Zhang, S.-C. (2005). Directed differentiation of dopaminergic neuronal subtypes from human embryonic stem cells. *Stem Cells,* **23**(6): 781-790.

Yin, Z., Jiang, H., Lee, E. S., Ni, M., Erikson, K. M., Milatovic, D., Bowman, A. B. and Aschner, M. (2010). Ferroportin is a manganese-responsive protein that decreases manganese cytotoxicity and accumulation. *J Neurochem,* **112**(5): 1190-1198.

Yokel, R. A. (2009). Manganese flux across the blood-brain barrier. *Neuromolecular Med,* **11**(4): 297-310.

Yokel, R. A. and Crossgrove, J. S. (2004). Manganese toxicokinetics at the blood-brain barrier. *Res Rep Health Eff Inst,* 119: 7-73.

Yoshida, Y., Takahashi, K., Okita, K., Ichisaka, T. and Yamanaka, S. (2009). Hypoxia enhances the generation of induced pluripotent stem cells. *Cell Stem Cell,* **5**(3): 237-241.

Yu, J., Vodyanik, M. A., Smuga-Otto, K., Antosiewicz-Bourget, J., Frane, J. L., Tian, S., Nie, J., Jonsdottir, G. A., Ruotti, V., Stewart, R., Slukvin, II and Thomson, J. A. (2007). Induced pluripotent stem cell lines derived from human somatic cells. *Science,* **318**(5858): 1917-1920.

Yusa, K., Rad, R., Takeda, J. and Bradley, A. (2009). Generation of transgene-free induced pluripotent mouse stem cells by the piggyBac transposon. *Nat Methods,* **6**(5): 363-369.

Zecca, L., Youdim, M. B., Riederer, P., Connor, J. R. and Crichton, R. R. (2004). Iron, brain ageing and neurodegenerative disorders. *Nat Rev Neurosci,* **5**(11): 863-873.

Zeng, H., Guo, M., Martins-Taylor, K., Wang, X., Zhang, Z., Park, J. W., Zhan, S., Kronenberg, M. S., Lichtler, A., Liu, H. X., Chen, F. P., Yue, L., Li, X. J. and Xu, R. H. (2010). Specification of region-specific neurons including forebrain glutamatergic neurons from human induced pluripotent stem cells. *PLoS One,* **5**(7): e11853.

Zhang, J. H., Chung, T. D. and Oldenburg, K. R. (1999). A Simple Statistical Parameter for Use in Evaluation and Validation of High Throughput Screening Assays. *J Biomol Screen,* **4**(2): 67-73.

Zhang, P., Hatter, A. and Liu, B. (2007). Manganese chloride stimulates rat microglia to release hydrogen peroxide. *Toxicology letters,* **173**(2): 88-100.

Zhou, W. and Freed, C. R. (2009). Adenoviral gene delivery can reprogram human fibroblasts to induced pluripotent stem cells. *Stem Cells,* **27**(11): 2667-2674.